AERODYNAMIC FEASIBILITY STUDY OF AN INTEGRATED WING-IN-GROUND-EFFECT HOVERCRAFT.

DD Agbada

MPhil

2022

AERODYNAMIC FEASIBILITY STUDY OF AN INTEGRATED WING-IN-GROUND-EFFECT HOVERCRAFT.

Darius Dafe Agbada

A thesis submitted in partial fulfilment of the requirements of the award of Master of Philosophy of the University of Northumbria at Newcastle

Research Undertaken in the Faculty of Engineering and Environment, Department of Mechanical and Construction Engineering

August 2022

Keywords

Aerofoil, Angle of Attack, Coefficient of Lift and Drag, Height to Chord Ratio, Hovercraft, Lift to Drag Ratio, Wing-in-Ground effect, NACA 0012, NACA 4412.

Abstract

Wings operating close to a boundary surface are referred to as (WIGs) Wing in Ground Effect Vehicle, and this type of flight has been recognised to be more aerodynamically efficient than freestream flight from the literature. This has led to the design and construction of craft specifically intended to operate close to the ground and fly 'in ground effect'. A wide variety of Wing in Ground effect vehicle (WIGs) have been manufactured ranging from 2 seat recreational vehicles to ekranoplan. This paper investigates if WIG technology is a viable solution to improve the aerodynamic performance of an amphibious hovercraft which can be used in maritime search and rescue operations to save lives more quickly. As WIGs cruise over the surface of a boundary at height up to 7m, using the wings to generate lift. They operate over flat areas and rely on the aerodynamic interaction between the wings and a boundary surface.

A parametric study was conducted by using computational fluid dynamic analysis (CFD) to determine the feasibility of using an aerodynamic wing mounted on a hovercraft. The effects at various operating conditions such as the height above the ground ‘h’, the angle of attack, and the effect of the aerofoil geometry were studied in order to attain whether the ground effect provides significant performance gains. A computational strategy was developed and validated for the numerical investigation of aerofoils in ground effect. The detailed design of the integrated wing and hovercraft was analysed, and the flow characteristics were observed. Based on the feasibility assessment of the current study, the WIG hovercraft was found to improve the aerodynamic performance by increasing the lift coefficient of a WIG hovercraft due to it flying in ground effect.

This study provides a detailed procedure for the preliminary design of a wing-in-ground effect hovercraft and explores the performance that can be obtained by improving a marine search and rescue hovercraft with WIG technology. As a result, combining the ground effect phenomena with a search and rescue hovercraft would save lives more quickly.

Table of Contents

List of Figures

List of Tables

List of Abbreviations

- Air Cushion Vehicle (ACV)
- Angle of Attack (AOA)
- Aspect ratio (AR)
- Centre of Lift (COL)
- Centre of Gravity (COG)
- Chord Dominated Ground Effect (CDGE)
- Computational Fluid Dynamics (CFD)
- Department of Hydro-Mechanics of the Marine Technical University (DHMTU)
- Height to Chord ratio (h/c)
- National Advisory Committee on Aeronautics (NACA)
- Royal National Lifeboat Institution (RNLI)
- Span Dominated Ground Effect (SDGE)
- University of Illinois Urbana-Champaign (UIUC)
- Universal Hovercraft (UH)
- World Health Organisation (WHO)
- World Meteorological Organization (WMO)

List of Nomenclature

Symbol	Definition	SI Unit
A	Area	m^2
C_D	Drag coefficient	Dimensionless
C_L	Lift coefficient	Dimensionless
C_M	Moment coefficient	Dimensionless
D	Drag force	N
L	Lift force	N
M	Moment	Nm
p	Pressure	N/m^2
V	Velocity	m/s^2
Φ	Mass flux rate	$kg/ m^2/s$
ρ	Density	Kg/m^3

Declaration

I declare the work contained in this thesis has not been previously submitted to meet requirements for an award at this or any other higher education institution. To the best of my knowledge and belief, the thesis contains no material previously published or written by another person except where due reference is made.

Any ethical clearance for the research presented in this thesis has been approved. Approval has been sought and granted by the Northumbria University Ethics Committee on [24/10/2019].

I declare that the word count of this Thesis is 21,068 words.

Name: Darius Dafe Agbada

Date: 20/08/2022

Acknowledgements

I'd like to thank my patient and supportive supervisors, Dr. Ken Leung, Dr. Madeleine Combrinck, and Prof. Robert Dominy, for their assistance throughout this research study. I am appreciative of our friendly conversations at the end of our meetings, as well as your support in my academic endeavours. I am also grateful to the School of Engineering and Environment staff members for their thoughtful guidance. Finally, I must express my gratitude to my family and friends for their unwavering support throughout this very intense academic year.

Chapter 1: Introduction

1.1 BACKGROUND

According to a 2019 study by the world health organisation (WHO), maritime accidents have been a severe and underappreciated public health threat, claiming the lives of 372,000 people worldwide each year [1]. Rivers, swamps, seashores, and beaches account for more than 90% of fatalities. For example, drowning is the third most significant cause of unintentional injury mortality worldwide, accounting for 7% of all injury-related deaths [1]. This death toll is approximately two-thirds that of hunger and more than half that of malaria. However, unlike these public health challenges, there are no large-scale preventative efforts targeting drowning [1].

The current study investigates the feasibility of incorporating wing-in-ground effect technology on a hovercraft by performing computational fluid dynamic analysis (CFD) and examining the lift and drag coefficients of the integrated wing and hovercraft in ground effect, as well as displaying the flow characteristics for this application. In this study, the RNLI search and rescue hovercraft is used because it is a versatile vehicle capable of transporting people and equipment on land and water, as well as loading and unloading on land, and is used in search and rescue operations to save drowning victims, survivors of downed aircraft, sailors, and passengers in distress due to a defective engine [2]. Figure 1 shows the orientating images of a search and rescue hovercraft and a wing-in-ground effect hovercraft.

(a) (b)

Figure 1: Orientating figures of (a) Search and Rescue Hovercraft [2] (b) Wing-in-ground effect hovercraft

The wing-in-ground (WIG) effect refers to increased lift and reduced drag experienced by a wing operating near a ground surface. WIG craft employs the ground effect to attain quicker travel speeds by hovering close to the ground. A WIG vehicle is a multimodal craft that exploits this benefit by being designed to maintain a small and constant gap between the ground's surface and the wing's trailing edge in cruising flight. Due to the craft flying under the ground effect, the power required to fly the vehicle is considerably less than a ship that

might be used in its case. Furthermore, the speed attained by this vehicle is comparable to that of some planes [3].

To generate lift, compressed air is formed between the hull above, the water or ground below, and a flexible skirt around the edge of the hovercraft. It is sometimes called an Air Cushion Vehicle (ACV) due to its ability to move by cushion or skirt filled with air and causes the board to hover above the ground, and it moves by a thrust engine forward fills up the cushion by the lift engine. As a result, combining Wing-In-Ground (WIG) effect technology with a hovercraft base considerably reduces a hovercraft's drag force as it travels over the ground on an air cushion, allowing the vehicle to glide easily over the flat surface below, and reducing friction.

The use of wing-in-ground effect technology improves aerodynamic performance by boosting the craft speed and reducing the power required for ground effect flight, according to research from the literature review. In a range of industries, such as recreation, commerce, and transportation, the use of a Wing-In-Ground (WIG) hovercraft is noticeable. Such a vehicle might be utilised to reach inaccessible locations for search and rescue, the discovery of new transportation routes, and environmental conservation in challenging areas such as swamps, rocks, beaches, mud, ice, lakes, and so on that other rescue vehicles like a rib, airboats, and helicopters cannot. This is a niche market, but it has the potential to be incredibly valuable in search and rescue operations because it allows for more lives to be saved at a faster rate.

1.2 CONTEXT

The project examines the integration of wing-in-ground effect (WIG) technology to an amphibious hovercraft for the current generation of inshore lifeboat services used for search and rescue operations at conditions of sea state 2 and below for low altitude flight. The versatility and speed of integrating a wing into a hovercraft will have a significant impact on marine search and rescue efficiency, allowing more lives to be saved at a faster rate across various terrains, particularly big bodies of water.

It has been investigated from relevant literature studies that the use of wing-in-ground effect technology will improve hovercraft efficiency [3]. It will increase the lift force generated by the wings, reducing the amount of pumped air required to hover and the power consumed by the vehicle. In an aerodynamic application, the usual demands are a reduction in overall drag and an increase in lift, which poses a significant challenge in any aerodynamic application or study. The ground effect principle increases the wing's lifting capability, resulting in a more efficient and quicker vehicle.

1.3 PURPOSES

The distinctiveness of this project lies in the systematic implementation of Wing-In-Ground effect (WIG) technology in a hovercraft. To build a model as well as accurately validate the results, which will generate insights about the improved performance of a hovercraft. This study will yield an understanding of the interaction between the air cushion and the wing.

This study aims to investigate if wing-in-ground effect technology is a viable solution to improve the aerodynamic performance of amphibious hovercraft in search and rescue operations.

The objectives of this study are as follow:

- Develop and validate a computational strategy for the numerical investigation of aerofoils in ground effect.
- Determine the aerodynamic performance and characteristics of different types of wing geometries in ground effect.
- Conduct a parametric study to determine the optimal configuration for integrating of a wing and a hovercraft hull.
- Analyse the detailed design for the wing in ground effect hovercraft.

1.4 SIGNIFICANCE, SCOPE AND DEFINITIONS

According to WHO research, integrating WIG technology into a hovercraft could improve maritime search and rescue efforts [1]. The benefits of ground effect include increased lift and speed, allowing the WIG hovercraft to fly higher and faster. The advantages of ground effect are also affected by the surface on which the vehicle is hovering. When flying over water, tall grass, or boulders, for example, the aerodynamic performance is reduced when compared to flying over a flat surface.

Furthermore, previous studies indicate that ground effect aerofoils at specific speed ranges can assist types of vehicles [3]. Nevertheless, the aerofoils theory of ground effects on the other vehicles has still not been fully grasped. The types of ground effect vehicles studied are limited. Since the Russian ground effect vehicle ekranoplan has been restricted to certain craft speeds. Appendix A shows the Gap in Literature.

1.5 THESIS OUTLINE

Chapter 2 is the literature review chapter where in-depth discussion is carried out on hovercraft, aerofoil, wing-in-ground effect, rescue vehicles, and sea state, outlining the findings from previous researchers.

Chapter 3 details the methodology adopted in this research, describing the largely qualitative phase. Solidworks was used to design the WIG hovercraft, while Ansys workbench was used to generate and execute the computational domain. The main values of interest are lift, drag, moment coefficients, and lift-to-drag ratio acting on the WIG hovercraft. Fluent can easily obtain these values, which is why a CFD study using fluent is carried out. Fluent can also display contour and vector plots, giving excellent flow visualisation of the ground effect. Chapter 3.2 simulated the different classes of aerofoils, and the NACA 4412 wing was chosen due to its favourable aerodynamic efficiency. In chapter 3.3, the wing is integrated into the hovercraft hull, the wing's position was determined to have a WIG hovercraft that provides the required lift and is aerodynamically stable. In chapter 3.4, the detailed design of the WIG hovercraft is simulated, and the flow characteristics are observed.

Chapter 4 contains the results and discussion section. This evaluates and describes the significance of the research study findings, as well as demonstrating the interaction between the air cushion and the wing and provides insight into the possibility of implementing WIG technology on a hovercraft.

Chapter 5 concludes the thesis by summarising the study’s key findings and results from chapters 4 to 5. Recommendations are made in terms of opportunities for future research.

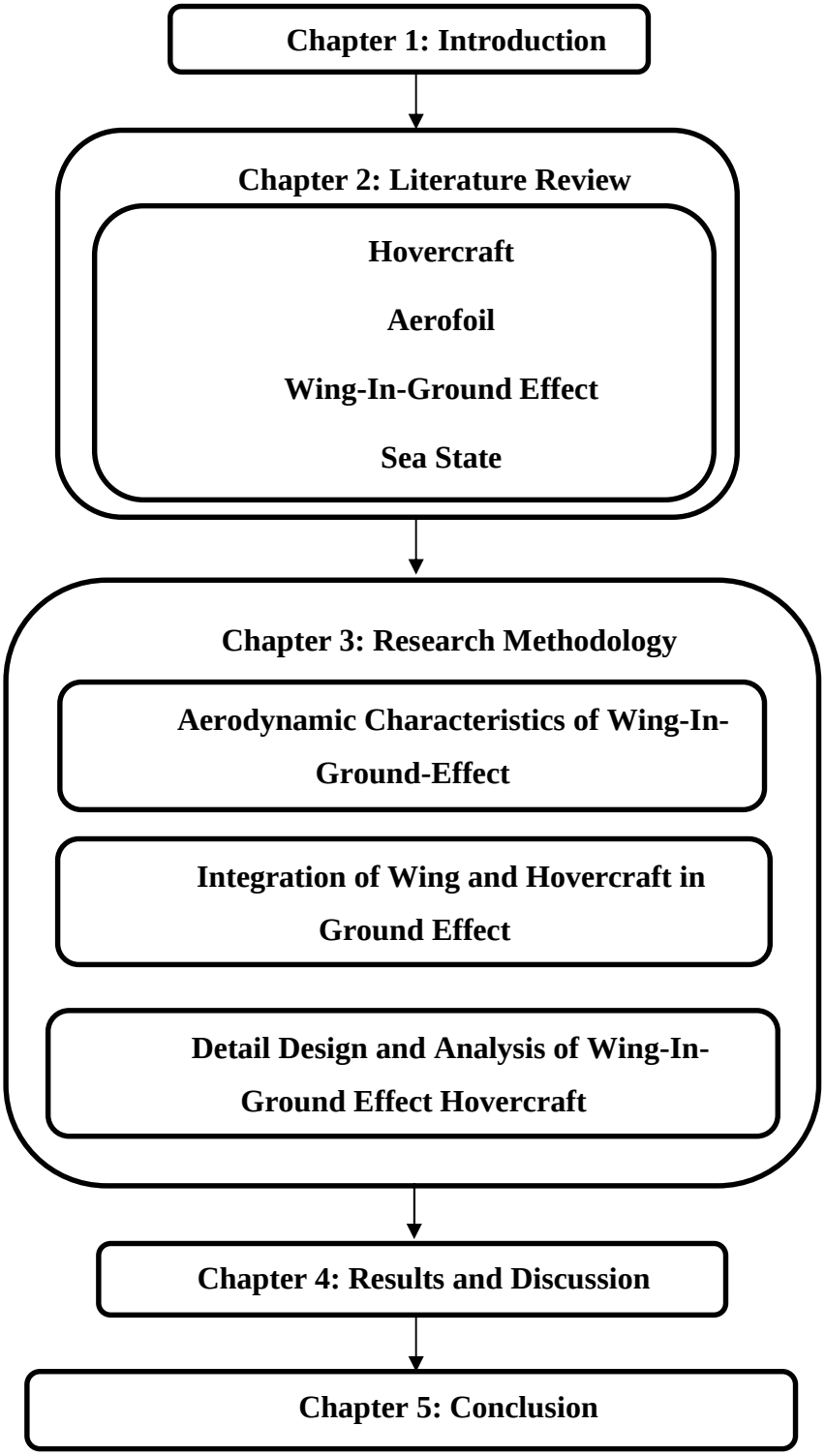

Figure 2: Thesis Outline

Chapter 2: Literature Review

2.1 HISTORICAL BACKGROUND

A WIG craft is a high-speed aerodynamic surface/marine vehicle. The majority of WIG crafts have evolved from analytical theory, model testing and building prototypes. WIG craft theory and technology covers wide range of possible craft configurations. WIG craft size and speed ranges from single passenger prototypes operating at 13m/s to large military craft at 138m/s. The largest WIG craft build to-date is KM with a length of 106.07m and wingspan of 40m, KM is able to transport 550 tons (498,952kg) of cargo. The KM is also known as the Caspian Sea Monster because of its massive size as seen in figure 3 [4].

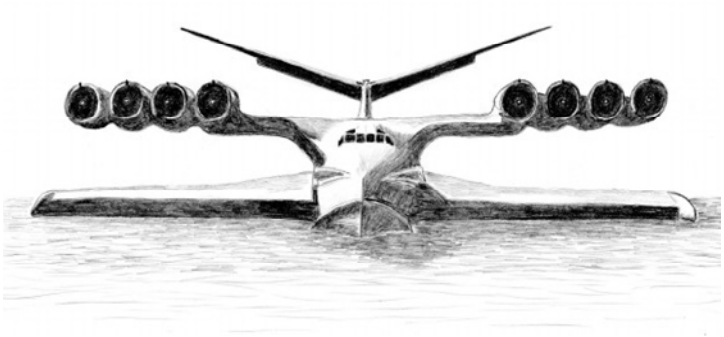

Figure 3: Caspian Sea Monster [4]

2.1.1 Technology and research

The development of WIG vehicles has seen a number of different approaches. The result of substantial testing has not seen the emergence of one generic configuration. This is attributable to the difficulties in optimising the design for different operational considerations. Depending on the craft's intended application, each configuration type offers pros and cons of its own. This led to the prototyping of numerous distinct WIG craft planform variants [4]. The more notable of these configurations are summarised below.

i. Ram Wing

The term "ram wing" refers to a wing that is in contact with the ground at the trailing edge. The air is rammed into the closed cavity increasing the pressure. This influence on lift is caused by the wing and ground plane and is known as ram pressure. This principle is used by a number of WIG craft to take off [4]. The ram wing planform is made up of a small span wing with a low aspect ratio. This wing is typically straight with zero taper. For stability a tail surface is needed which is positioned out of ground effect. Due to the inherent instability of the wing the tail area is large, typically 50% of the main wing and of similar span. This large tail surface helps to stabilise the craft at various altitudes above the ground plane [4].

Other criteria that are typical to this sort of design include optimal cruise heights above the surface that equate to about 10 to 25% of the wing chord. The usage of S-shaped wing sections is a recent innovation for improving stability and reducing necessary tail area. Experiments with end plates have been carried out in an attempt to reduce induced drag even more while increasing the effective aspect ratio. The ram wing configuration has been favoured by Russian designers. It is widely used on a variety of big Ekranoplanes and smaller WIG craft developed in Russia [4].

ii. Ekranoplan

The Lun-class ekranoplan is the only ground effect vehicle (GEV) that has ever been operationally deployed as a warship. It was designed by Rostislav Alexeyev in 1975 and was used by the Soviet and Russian militaries from 1987 until the late 1990s [].

It flew using lift generated by the ground effect acting on its large wings when within about 4m (13ft) above the surface of the water. Despite its resemblance to typical aircraft, ekranoplans such as the Lun are not classified as aircraft, seaplanes, hovercraft, or hydrofoils. Rather, the International Maritime Organization classifies craft like the Lun-class ekranoplan as maritime ships due to its utilization of the ground effect, in which the craft glides just above the surface of the water [4].

The Soviet Union designers have acknowledged that the first generation of the craft represents the preliminary design. They state that there is potential for further development resulting in greater efficiencies [4]. Figure 4 shows the Lun Ekranoplan.

Figure 4: Lun Ekranoplan [4]

iii. Lippisch

In 1963, Alexander Lippisch created the X-l12, one of the first WIG craft. The X-112 was distinguished by its reversed delta wing with a low aspect ratio, known as the Lippisch planform. The reversed delta wing is very stable, which results in requiring only a small stabilizer compared to the ram wing craft. Figure 5 shows the X-114, which is one of the Lippisch planform [4].

The craft designed on this planform have been tested for military applications and developed for recreational use. These craft have not reached the high displacement weights of the Russian Ekranoplans however designs using a similar planform and utilising a flying wing have been mooted by a US company Aerocon [4].

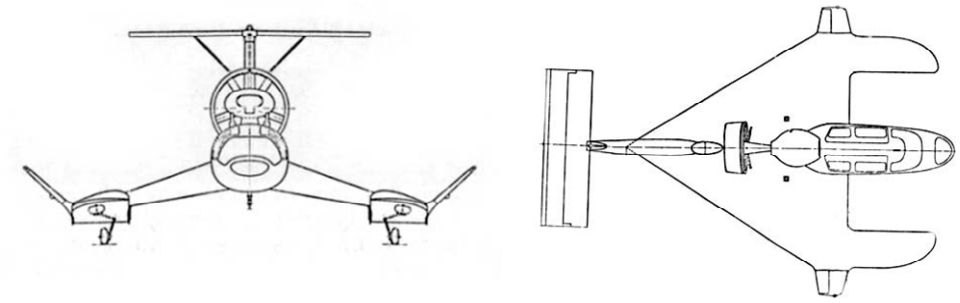

Figure 5: Lippisch planform (X-114) [4]

iv. Tandem

Tandem wings were invented in the Soviet Union in 1960. It utilizes two small wings in a row. Despite various issues such as restricted stability, low seaworthiness, and high take-off speeds, the Tandem type WIG craft was created in Germany as a leisure river craft. In Germany, Jörg has used the tandem wing configuration to design a number of small WIG craft. These craft are incapable of flight out of ground effect and have limited seaworthiness however they are stable over their operating range. Jörg has manufactured a number of craft as recreational river craft [4]. Figure 6 shows a tandem type of WIG Craft (Jörg VI)

Figure 6: A Tandem type of WIG Craft (Jörg VI) [4]

WIG craft have been suggested as the solution to a number of possible operational activities. The increased lift is one of the most appealing WIG craft features.. As an alternative to the relatively large aircraft required to achieve these transit objectives, WIG vessels have been proposed [4].

On the other hand, smaller WIG craft have been created for recreational and non-military purposes since the 1980s. Table 1 displays the prototype WIG crafts that have been

comparatively late in development. Additionally, numerous nations, including Australia, China, Germany, Japan, Korea, Russia, Taiwan, and the United States, have continued to conduct research and development on WIG craft. Although there are active debates, research, and development efforts for WIG craft around the world, real-world commercialization of WIG craft has not yet been accomplished.

Table 1: Prototype WIG craft /hovercraft [4,5]

Name	Country/manufacturer	Year	Weight/seat	Speed	Purpose
Amphistar	Russia/MAC.	-	1900 kg/4 seat	41 m/s	Recreational
Volga 2	Russia/SDPP	1986	2700 kg/10 seat	30.8 m/s	Small Ferry
Jorg 6	Germany/Jorg	1991	3150 kg/7 seat	41 m/s	Small Ferry
Airfish 3	Germany/F.F	1990	650 kg/2 seat	33.4 m/s	Recreational
Hoverwing	Germany/T.T	1997	915 kg/2 seat	33.4 m/s	-
X-114	Germany/RFB	1977	1500 kg/6 seat	51.4 m/s	Military
L-325	USA/Flarecraft	-	1550 kg	33.4 m/s	Commercial
Ram 902	China/CSSRC	1984	385 kg/1 seat	33.4 m/s	Test
A18 WIG	Russia	2015	1800kg/21 seat	22 m/s	Recreational
UH-18SP	USA	-	383kg/6 seat	33m/s	Recreational

Theoretical studies into the aerodynamics, ground effect, and stability of WIG craft have been conducted. On prototypes and with model tests, performance improvement of take-off and landing distances as well as strategies to raise sea state constraints have been analysed. The best configuration of the planform is still being determined by research.

Wing in ground effect is a novel approach to designing fast ships with various applications in fields such as cargo transport, tourism, rescue operations, and military missions. The blade segments used for aircraft wings and propeller blade segments are geometrically configured to produce high lift and low drag values. This situation is possible with lifting vanes that include bodies such as a kite, aerofoil, hydrofoil, and propeller blade. When wings operate near the ground, their normal pressure distribution changes. The trapped air and pressure create a high level under the wing, which adds to the lift of the aerofoil. The ground effect refers to the additional trapped air pressure on the wing's bottom side. The ground effect is a phenomenon that occurs when a body cruises very close to the water or ground surface, and its lift-to-drag ratio increases [5]. The Wright brothers first noticed the ground effect in 1904, when they could fly at a short height above the ground but discovered problems obtaining enough thrust to launch into full flight due to ground

effect [6]. The ground effect occurs within one chord line of the ground at low clearances. The effect on the airflow below the aerofoil increases the static pressure below the wing, which improves the lift and reduces the drag.

2.1.2 Rescue Operation

A rescue operation is defined by maritime law and convention as assisting persons in distress at sea, regardless of their nationality or status, or the circumstances under which they are found [7].

The first airborne lifeboat was British, a 32-foot (10 m) reinforced wooden canoe-shaped boat constructed in 1943 by Uffa Fox to be dropped by Avro Lancaster heavy bombers for the rescue of fallen aircrew in the English Channel [8]. Since the late 1800s, fast, durable, and powerful motorised lifeboats or rescue boats have been employed to undertake maritime rescues [8].

Germany created the ideas of coordinating small surface boat rescue missions with direction and help from air units in the 1930s, and other nations followed suit in the 1940s. However, both the airborne lifeboat and the rescue boat have a speed limitation. As a result, it will take a longer time to reach the location of the accident site. Since their introduction in the 1940s, helicopters have played a critical role in air-sea rescue [9]. Helicopters also have limited range and endurance, cannot land at sea, and have a high operating cost [10].

2.2 HOVERCRAFT

A Hovercraft is a hybrid vehicle operated by a pilot as an aircraft rather than a captain as a marine vessel. They typically hover between 0.2m and 0.6m above any surface and can operate at speeds above 15.6m/s (35mph) [11].

The vehicle typically operates over gentle terrain, although they can climb slopes up to 20%, depending upon surface characteristics. They are best suited for locations inaccessible by landed vehicles due to natural phenomena such as swamps, mud, ice lakes, and beaches. Hovercraft can be used for various purposes, ranging from toys to passenger and cargo transportation to spraying plants with seeds, fertilisers, insecticides, and so on. They are now commonly used for specialised transport in disaster relief, coast ground military and survey applications, and sports and passenger services. Large versions have been used in hostile environments and terrain to transport tanks, soldiers, and large equipment. There was a great need in riverine areas for a transportation system that is fast, efficient, and safe, as transferring a load from a landed vehicle to a boat takes time. The British invented the first practical hovercraft design between 1950 and 1960. Sir Christopher Cockerel demonstrated the scientific principle behind hovercraft for the first time in 1955.

It is capable of transporting people and equipment over different terrains. As a result, it can be used in military organisations. It can be used instead of boats in water transport to carry many passengers [12].

A hovercraft works on the principle of lifting the craft with an air cushion and propelling it with propellers/fans. The desire to increase the speed of a boat by feeding air beneath it inspired the idea of supporting the vehicle on an air cushion. The air beneath the hull would lubricate the surface of a boat and reduce water drag, allowing it to travel faster through the water. Large lifting fans attached to the primary structure of the craft draw in air through a port. They are either propelled by a gas turbine or a diesel engine. The air is pushed to the bottom part of the craft. When the pressure equals the craft's weight, the craft lifts, and air escapes around the skirt's edges. As a result, a constant supply of air is required to lift the craft and compensate for the losses. Thus, the craft is elevated. After that, the propellers mounted on the hovercraft provide propulsion. The air from the propellers passes over rudders, which are used to steer the craft in the same way that an aircraft does [13].

One or more engines can drive hovercraft; small craft typically has one engine with the drive split through a gearbox. On vehicles with several engines, one usually is responsible for moving the fan (or impeller), which is responsible for lifting the vehicle by forcing high-pressure air under the craft. The air inflates the skirt beneath the vehicle, raising it above the surface. Additional engines produce thrust to propel the craft. Some hovercraft use ducting to allow a single engine to perform both functions by diverting some of the air to the skirt and the rest of the air to push the craft forward [14]. As figure 7 shows the main parts of a hovercraft.

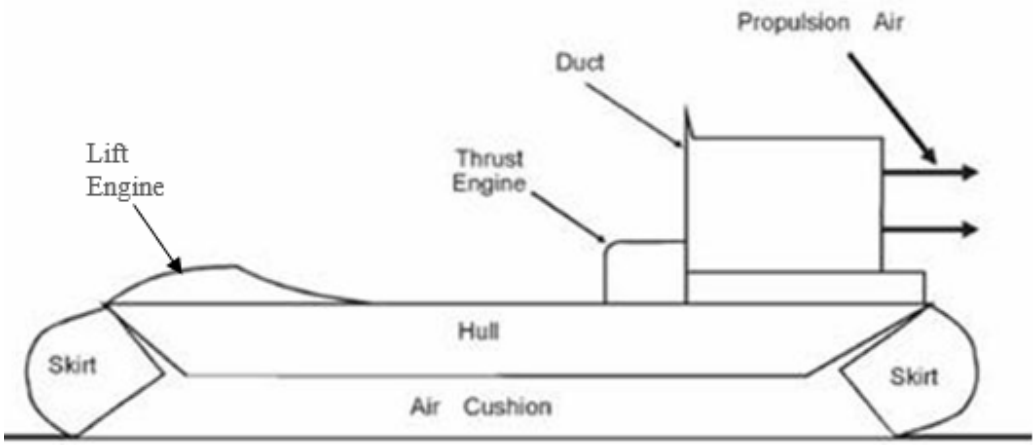

Figure 7: Main part of a Hovercraft [15].

2.3 AEROFOIL

An aerofoil is a cross-sectional shape of a wing that produces an aerodynamic force. When air flows past an aerofoil, the pressure on the top surface of the aerofoil reduces while

the pressure underneath the aerofoil significantly increases. This pressure differential creates a force that pushes the aerofoil upwards and is slightly tilted backward. They are typically used on aircraft as lift wings or propeller blades to generate thrust. Both forces are perpendicular to the direction of airflow. Drag is a function of lift/thrust output and operates in the same direction as the airflow. Figure 8 shows the pressure difference around an aerofoil, which typically associates a higher velocity and lower static pressure with the suction surface (upper surface). The pressure surface (lower surface) has a higher static pressure than the suction point. The pressure gradient between these two surfaces contributes to the lifting force produced by a given aerofoil. A traditional aerofoil generates lift due to the wing's shape causing airflow at different pressures on the upper and lower parts of the wing. The increased pressure on the lower part of the wing generates upward lift. The ground effect occurs due to the increase in static pressure below the wing at low ground clearances, within one chord length of the ground, which improves lift and reduces drag. A 2D aerofoil is equivalent to an infinite wing, whereas a 3D wing is equivalent to a finite wing. As trailing vortices are an unavoidable by-product of finite-span lifting wings, they can be formed by air travelling up and around the wingtip. Pressure differences between the upper and lower surfaces of the wings produce spinning vortices as the Wing-in-ground effect (WIG) vehicle flies through the air [16, 17].

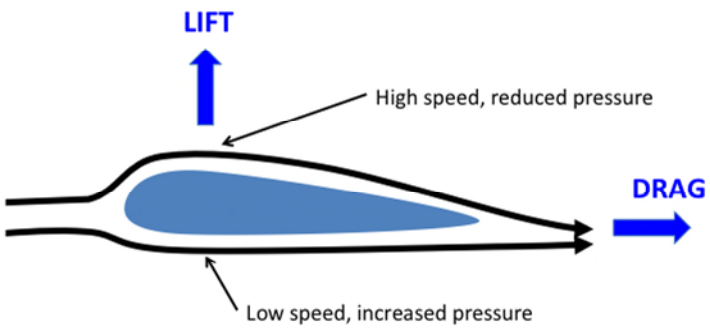

Figure 8: Pressure differential of an aerofoil [17].

The physical geometry of an aerofoil also has a significant impact on the craft's performance. Different aerofoil cross-sections have other aerodynamic properties, such as lift and drag, depending on the angle of attack. As a result, aircraft with varying operational requirements have different aerofoil cross-sections. Aircraft flying at low speeds have relatively thick cross-sections, whereas aircraft flying at high speeds have relatively thin cross-sections. The aspect ratio of an aerofoil affects its performance as well. The aspect ratio compares the chord length to the wings' span (tip to tip). Due to the losses in the lift being greatest at the wingtips, the higher the aspect ratio (i.e., the greater the span compared to the chord), the more efficient the wing. In theory, the most efficient wing is one with an infinite length. In practice, this is tempered by the structural inefficiencies of long

cantilevered wings [18]. Although the aerofoil is more of a subsystem of the wing, it is an essential component that deserves a brief mention in the section on wing design. Aerofoils are classified into four types: symmetrical, semi-symmetrical, flat bottomed, and under-cambered. As figure 9 shows the diagram of the four main aerofoil designs. The symmetrical and semi-symmetrical aerofoils will provide higher levels of manoeuvrability and are usually used for planes that are required to perform acrobatic manoeuvres, whereas under-cambered and flat-bottomed aerofoils provide significant lift and are useful for load carrying or long-distance flying [19].

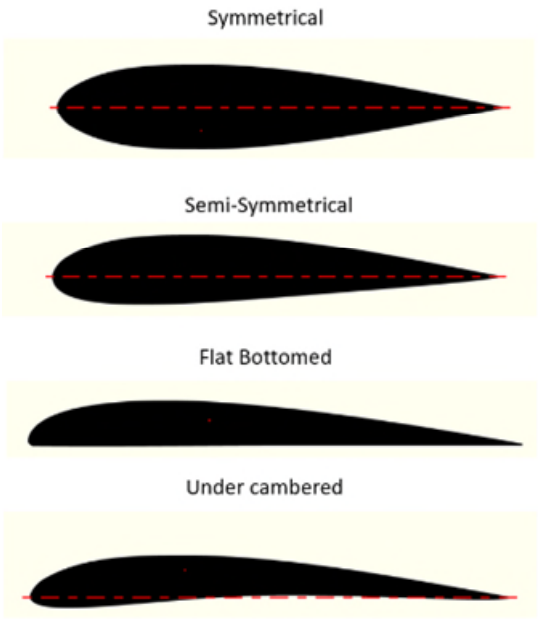

Figure 9: Four main aerofoil design [20].

The interaction of a fluid with an aerofoil produces two forces: lift and drag, which are often represented by the two aerodynamic coefficients. Lift is the force that keeps aircraft in the sky. Drag, on the other hand, acts in the same direction as the airflow. For example, in an aeroplane, extra fuel must be used to overcome the drag forces. Drag forces arise mainly from airflow, leading edge, average camber line, chord, trailing edge, thickness, and angle of attack (AOA). Appendix B shows the aerofoil terminology. When comparing different aerofoils, lift and drag coefficients are often more useful than total lift and drag forces acting on the aerofoil. Lift and drag coefficients are non-dimensional numbers that quantify the amount of lift or drag on a given aerofoil under a given set of flow conditions, such as Reynold's number and Angle of Attack [21].

• **Lift Coefficient (C_l):** It is a dimensionless quantity that relates the lift produced by an aerofoil to the fluid density surrounding the body, the fluid velocity, and an associated reference area [21].

$$C_l = \frac{F_l}{1/2\,\rho V^2 A} \quad (1)$$

Where;

- F_l is the lift force,
- ρ is the density of air (kg/m^3)
- V is inlet velocity of air (m/s)
- A is the area of aerofoil (m^2)

• **Drag Coefficient (C_d):** It is a dimensional quantity used to quantify an object's drag or resistance in a fluid environment [19].

$$C_d = \frac{F_d}{1/2\,\rho V^2 A} \quad \text{Equation (2)}$$

Where;

- F_d is the lift force,
- ρ is the density of air (kg/m^3)
- V is inlet velocity of air (m/s)
- A is the area of aerofoil (m^2)

Aircraft frequently fly near the ground surface, taking advantage of the ground effect for efficient flight. The wing experiences increased lift and decreased drag as a result of two mechanisms:

- An increase in static pressure beneath the aerofoil is due to the finite distance between the aerofoil and the ground (chord-dominated ground effect), which increases lift.
- The disruption in wingtip vortex formation is caused by the proximity of the ground (span-dominated ground effect), which reduces induced drag. The combined effect of the two phenomena is an increase in the lift-drag ratio (L/D) ratio.

The L/D ratio is a common way to express a vehicle's efficiency. When a vehicle is stationary, its weight equals its lift, and its propulsive thrust equals its drag. As a result, the L/D ratio expresses the importance that can be carried with a given amount of thrust. The higher this ratio, the more efficient it is and the less fuel it consumes (for a given weight). As a result, the Lift to Drag (L/D) ratio increases significantly compared to free flight, as

shown in Figure 10. The ground effect would thus be experienced by any aircraft operating close to the ground [22].

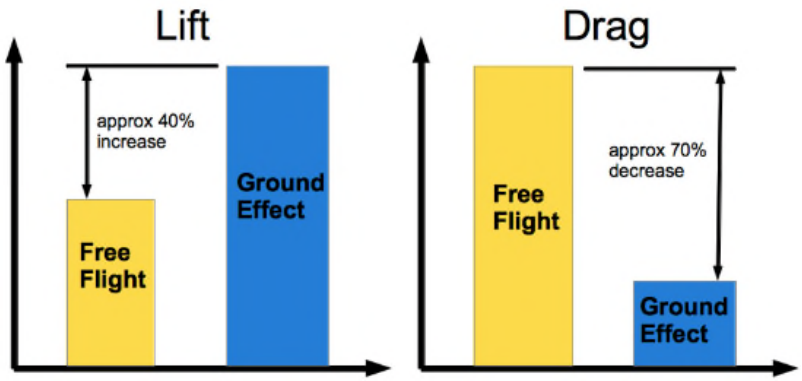

Figure 10**:** Comparison of ground effect with free flight condition [21].

2.4 TURBULENCE MODEL

Turbulence is a state of fluid flow in which the fluid travels irregularly. The Navier-Stoke (NS) equations describe fluid motion as a closed system of equations, and direct numerical simulation requires enormous computational resources and is challenging to apply in practice. The Reynolds-averaged Navier-Stokes equations (RANS) method is widely used to average the time term of turbulence fluctuation. The primary challenge of numerical simulation is to choose a suitable model to describe turbulence. For most numerical simulation applications involving aerofoils, Spalart-Allmaras (SA), k-epsilon (k-ε), and SST k-omega (k-ω) are widely accepted and investigated in this study [23].

2.4.1 Turbulence Model

i. Spalart-Allmaras (SA): The Spalart-Allmaras turbulence models solve a single transport equation determining the turbulent viscosity. It is explicitly designed for wall-bounded flow applications in aeronautics and aerospace. It has shown to be relatively stable, to have good convergence, and to produce good results for boundary layers subjected to unfavourable pressure gradients. The turbulence model has the drawback of not accurately computing fields that exhibit shear flow, separated flow, or decaying turbulence [24].

ii. Standard k-epsilon (k-ε) model: In general, k-ε models offer a reasonable balance of robustness, computational cost, and accuracy. The k-ε turbulence model is a two-equation model in which transport equations for turbulent kinetic energy and dissipation rate are solved. It has traditionally been one of industrial CFD's most often used turbulence models. The disadvantage of k-ε models is their insensitivity to adverse pressure gradients and boundary layer

separation, which typically predicts a delayed and reduced separation relative to observations [25].

iii. Shear stress k-omega (SST k-ω) model: The SST k-ω model is a hybrid of the k-ε model in the free stream zone and the k-ω model near the walls. The SST k-ω turbulence model is a two-equation model in which the transport equations for turbulent kinetic energy and a specified dissipation rate are solved. This model provides a better prediction of flow separation than most RANS models and accounts for its good behaviour in adverse pressure gradients. It can account for the transport of the principal shear stress in adverse pressure gradient boundary layers. On the negative side, the SST k-ω model generates some large turbulence levels in regions with large normal strain, like stagnation regions and regions with strong acceleration [25, 26].

The selection of the correct turbulence model is essential to correctly model the ground effect problem and model the flow over a wing. Jung et al. conducted an error rate analysis on the turbulence model, comparing the numerical and experimental data. Two models of SST and omega Reynolds stress show negligible errors being in good agreement with experimental data. The common point of these two models is the omega base, but other models, such as the k-ε and k-ε RNG models, produce a higher error rate than experimental data. Table 2 represents the aerodynamic coefficients of lift, drag, and lift-to-drag ratio. The SST k-ω model shows the lowest error rate, in which the lift and drag error rate is lower than other models. That is because this model combines the exact formulation of the k-ω standard model near the wall with the k-ε model away from the wall in the free flow [27].

Table 2: Aerodynamic coefficients of lift, drag and lift to drag ratio for NACA 6409 [27]

Coefficients	**SST k-ω**	**k-ε**	**k-ω**	**ω RS**	**k-ε RNG**	**Experimental (Jung et al., 2008)**
C_L	0.335	0.348	0.347	0.336	0.346	0.314
Error (C_L)	6.843	10.966	10.385	7.052	10.196	
C_d	0.038	0.039	0.040	0.038	0.038	0.037
Error (C_d)	1.372	5.713	8.938	2.918	2.591	
L/D	8.905	8.869	8.561	8.788	9.075	8.449
Error (L/D)	5.396	4.969	1.328	4.016	7.412	
Notes: h/c=0.1; AOA=2°						

Table 3 shows the lift and drag coefficient table obtained from a wind tunnel test (experimental) result taken from Abbott's books "theory of wing section." The table also contains the lift and drag coefficients obtained from two turbulence models (SST k-ω and Spalart-Allmaras model) [28].

By comparing the fluent results with the wind tunnel results at different angles of attack ranging from 0°-18°, the SST k-ω model is well predicted at the stall region at an angle of attack of roughly 12°-14°, the flow on the upper surface of the aerofoil began to separate. A condition known as stall began to develop. Hence, from the observation of the preliminary modelling of this current study, the most accurate model is the SST k-ω model second came the Spalart-Allmaras, and the latest in precision was the Realisable k-ε. As a result, the SST k-ω turbulence model for the main analysis.

Table 3: Lift and Drag coefficient for NACA 4412 aerofoil [29]

Wind Tunnel Test Data			**SST k-ω model with transition**		**Spalart-Allmaras**	
AOA, Degrees	C_L	C_d	C_L	C_d	C_L	C_d
0	0.4	0.008	0.53	0.007	0.51	0.008
2	0.6	0.008	0.72	0.0075	0.67	0.008
4	0.8	0.079	0.96	0.008	0.90	0.0085
6	1.0	0.0078	1.15	0.0076	1.11	0.009
8	1.18	0.008	1.35	0.0078	1.23	0.012
10	1.32	0.009	1.4	0.0085	1.29	0.015
12	1.41	0.0125	1.48	0.014	1.36	0.018
14	1.5	0.019	1.52	0.02	1.58	0.03
16	1.4	0.023	1.78	0.028	1.59	0.035
18	1.3	0.029	1.69	0.033	1.51	0.04

2.4.2 Reynolds Number

Reynold's Number describes the relationship between inertial and viscous forces within a fluid subjected to relative internal movement due to different fluid velocities. It can be used to describe flow types: for example, laminar flow occurs at low Reynolds numbers and is characterised by smooth, continuous fluid motion, whereas turbulent flow occurs at high Reynolds numbers and is dominated by inertial forces, resulting in unpredictable eddies, vortices, and other flow instabilities [30]. It is possible to calculate it as follows:

$$Re = \frac{Inertial\ Forces}{Viscous\ Forces} = \frac{\rho V^2 L^2}{\mu VL} = \frac{\rho VL}{\mu} \qquad \text{Equation (3)}$$

- Re = Reynold's number (dimensionless)
- ρ = Fluid density (kg/m^3)
- V = Fluid velocity (m/s)
- L = Characteristic length (m), e.g., aerofoil chord length
- μ = Dynamic viscosity (kg/ms)

2.4.3 Boundary Layers

The boundary layer is a thin layer of fluid that forms around the surface of an aerodynamic body due to friction between the body's surface and the viscous fluid that flows around it. The flow over an aerofoil usually begins laminar before transitioning to turbulent as it moves away from the leading edge. Reynold's number and the localised flow conditions determine the transition point's location. Figure 11 shows the development of the boundary layer around an aerofoil [31].

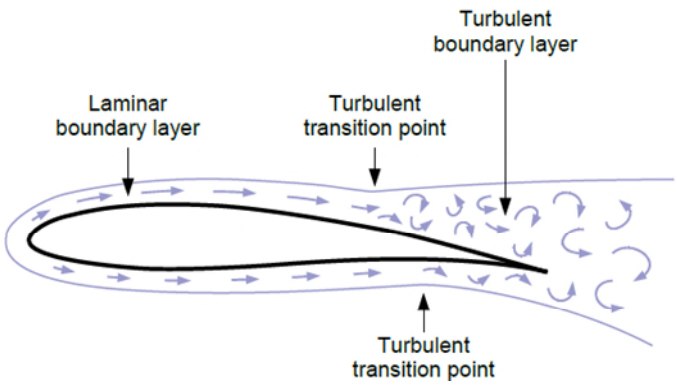

Figure 11: The development of the boundary layer around an aerofoil [32].

2.5 WING-IN-GROUND EFFECT

The most common explanation for ground effect is that the Air Cushion Vehicle (ACV) is riding on an "air cushion." When an aircraft approaches the ground, it rides on a cushion of air that squeezes between the wing and the ground. This is primarily due to the ground interfering with the formation of wingtip vortices and interfering with downwash behind the wing. The wings generate lift by moving air across the top and bottom surfaces. The thrust propels the craft through the air. This provides the necessary speed for the wing to generate lift. Hence, the term "Ground Effect" refers to the positive influence on the lifting properties of an aerofoil's horizontal surfaces when it is close to the ground. When an aerofoil produces lift, induced drag occurs, and wingtip vortices form. When a wing is in ground effect, an improved lift/drag ratio means that a given amount of lift can be produced at a lower angle of attack than required in free air [33, 34].

Ground-effect vehicles or crafts use a propeller or air source to create an air cushion beneath the craft's body, allowing it to float. Using the aerodynamic lift generated by lifting the vehicle from the ground to reduce hydrodynamic drag is one of the advantages of ground effect in the design of a hovercraft. The ground effect is similar to a magnetic levitation train (Maglev). The goal in both cases is to keep the vehicle from making contact with the ground. It is accomplished using a Maglev train powered by magnetism, a ground effect train powered by an air cushion, either in a hovercraft or the Wing-in-ground design. The ground effect was primarily used to improve the Russian Ekranoplan aircraft. This type of vehicle

is also known as a Wing-in-Ground (WIG) craft. These distinct vehicles fly at very low altitudes to the ground, benefiting from a favourable aerodynamic relationship between the wing and the ground, increasing the lift-to-drag ratios. The Soviets were the first to use this trend, designing and building the first WIG craft to transport their soldiers and goods during the Cold War [35 - 37].

Figure 12 depicts the relationship between the Ground effect and its impact on trailing vortices. This means that as the wing gets closer to the ground, the wingtip vortices decrease as they spin around the tip of the wing, hitting the ground and dissipating the impact as a decrease in downwash [38].

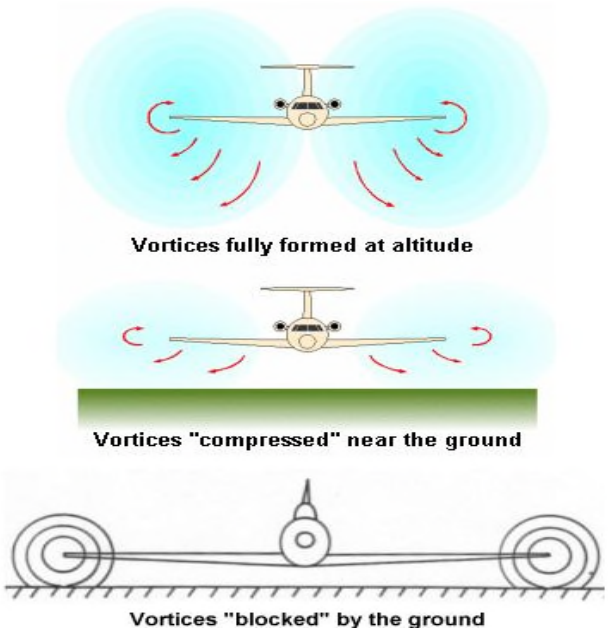

Figure 12: Ground effect and its influence on trailing vortices [39].

Ground effects consist of two phenomena: chord-dominated ground effect and span-dominated ground effect. As illustrated in Figure 13, the height to chord (h/c) ratio is commonly used to define the chord-dominated ground effect. In contrast, the height to span (h/b) ratio defines the span-dominated ground effect. The combination of the two increases the lift-to-drag (L/D) ratio of the wing-in-ground effect, making it more efficient [40].

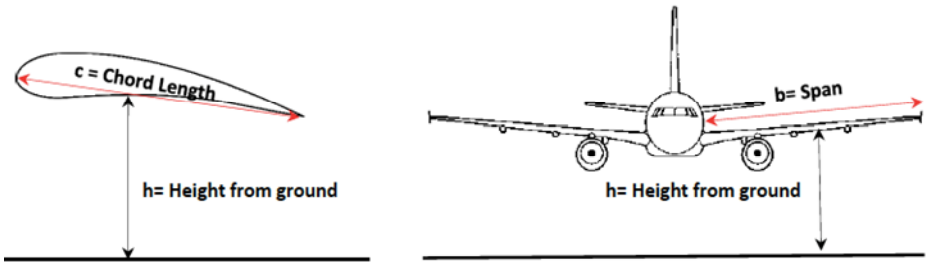

Figure 13: Definition of Chord and Span Dominated Ground effect (L to R) [41].

The Chord Dominated Ground Effect (CDGE) is caused primarily by the increase in static pressure on the wing's lower side, creating an air cushion as ground clearance decreases. Because of the increased pressure, the wing can generate more lift while requiring a smaller angle of attack. In the Span Dominated Ground Effect (SDGE), as the wing moves closer to the ground, the wingtip vortices are suppressed due to the presence of the ground and thus are not allowed to develop fully. This reduces induced drag by limiting the amount of downwash produced. Furthermore, the wingtip vortices are pushed outwards, resulting in an effective increase in the wingspan. The former is associated with an increase in lift, while the latter is related to a decrease in drag. As a result, the combination of SDGE and CDGE increases a wing's lift-to-drag ratio, making it more efficient [41]. Three critical factors determine what happens in the ground effect, namely.

- Having more vertical lift, which works against weight.
- Having less rear lift, which works against drag.
- Having smaller vortices and less downwash, resulting in less drag

A thorough investigation of the flow characteristics over the wings and other lifting surfaces is required to develop a Wing-In-Ground effect (WIG) hovercraft vehicle that will be used in both overwater and overland transport. The effect of different wing designs on aerodynamic characteristics has been investigated experimentally and analytically. Previous research has demonstrated that experimental examination of a WIG hovercraft has limitations, such as the 2011 study from San Jose State University that investigated the cargo capacity and cost of a WIG hovercraft as a faster and less expensive mode of transportation in coastal locations [42].

A few commercially produced WIG hovercraft, such as Universal Hovercraft's UH-18SPW Hoverwing, are primarily intended for recreational purposes. Table 4 contrasts a traditional hovercraft used for search and rescue by the Royal National Lifeboat Institution (RNLI) with a WIG hovercraft used for recreational activities by Universal Hovercraft (UH). According to table 4, the hovering travels faster than a traditional hovercraft and at a higher altitude, allowing it to travel over difficult terrains quicker for search and rescue operations. The vehicle's versatility and speed will have a significant impact on the efficiency and effectiveness of search and rescue services, especially in drowning cases, allowing more lives to be rescued at a faster pace near large bodies of water.

Table 4: Comparison between a conventional hovercraft and a WIG hovercraft [43, 44].

Specification	Griffon 380TD (RNLI)	18SPW Hoverwing (UH)
Capacity	3 to 4 Persons (838lbs/380kg)	2 to 3 Persons (550lbs/250kg)
Max Speed	35 Mph (15m/s)	75 Mph (33m/s)
Hover height	0.2 m	0.2 m
Max Altitude	0.5 m	3m
Length	6.8m	7m
Empty weight	551lbs (300kg)	844lbs (383kg)

A traditional hovercraft cannot operate on slopes steeper than 9 inches (0.2m) as the waves are high and rough. High winds and higher sea states have a negative impact on the performance of smaller vehicles. Incorporating wing-in-ground effect technology into a hovercraft would allow it to cover a large area in a short amount of time (flying higher and faster), allowing it to reach victims more quickly. It can go places traditional rescue boats cannot, such as swamps, ice, and thick grass [45]. This study's analysis focuses on the vehicle's aerodynamic efficiency and speed.

Table 5 compares the performance of various rescue vehicles to that of a wing-in-ground effect hovercraft (WIG). The WIG hovercraft outperformed the other rescue vehicles.

Table 5: Comparison of Other rescue vehicles and a WIG hovercraft [46, 47]

Features	Airboats	Boats	Helicopter	WIG Hovercraft
Safety	Medium	Low	Low	High
Speed	High	High	High	High
Low Power consumption	High	Medium	Medium	Low
Use in Overhead Obstructions	Medium	Low	High	High
Multipurpose craft	High	Low	Low	High
Response time	Medium	Medium	Medium	High
Low Cost	Low	Low	High	Medium
Low Weight	High	Medium	Medium	Low

A WIG hovercraft, unlike an airboat, is an amphibious flying machine that travels on a cushion of air with no wake and uses ground effect to fly faster. This allows for a quick response, which helps to reduce body recovery rescue operations while still carrying a payload suitable for water rescue. Unlike airboats, hovercraft do not require a boat dock to launch.

Airboats/inshore rescue boats are limited to relatively smooth water due to their hulls' low gunwales that can slam into the water or ground. Unlike a WIG hovercraft, an amphibious craft can travel through any terrain (dry, wet, ice, mud, grass, etc.)

Helicopters are expensive to buy and operate, and they generate a large downdraft that can obstruct rescue efforts. Since a WIG hovercraft is amphibious, it aids in rescue efforts by approaching victims directly, keeping rescuers out of the water [47].

2.5.1 Comparison of WIG Craft technology with other means of transportation

I. Transport Productivity

Payload ratio means the ratio of the payload to the full weight of the vehicle. The payload weight fraction (W_p/W) of ships is higher than that of WIG craft and aircraft. On the contrary, the speed of ships is comparatively lower than that of the others. Indeed, the payload ratio of WIG craft is higher to that of aircraft as seen on figure 14 [48]. In relation with the payload ratio, although some vehicles have a high payload ratio, with a low speed, such as ships, whilst other vehicles have a low payload ratio but a high speed, such as WIG craft and aeroplanes.

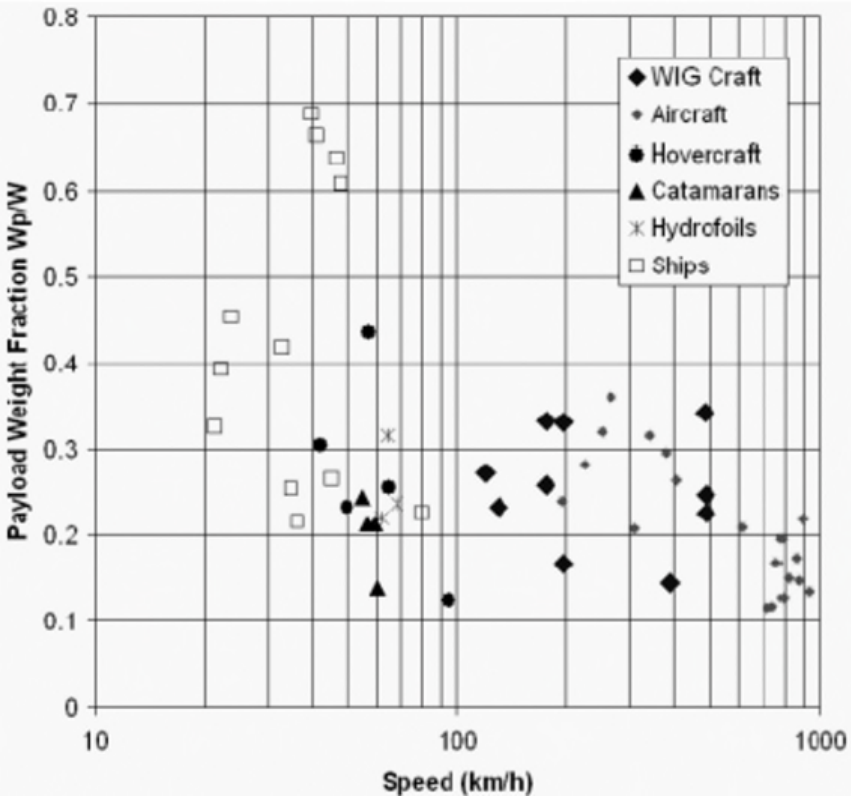

Figure 14: Payload efficiency comparison [49]

II. Initial capital investment and maintains of support infrastructure.

When compared to other modes of transportation, the initial capital required is insignificant, as ships require the construction and maintenance of a port or jetty, and aeroplanes require an airstrip or a helipad, as well as air traffic control management, which frequently requires costly equipment and highly skilled employees for radar and lighting operations [49].

III. Cost analysis

The cost of a trip in WIG would be far cheaper than that of an aircraft or a helicopter, and it would require no facilities at the destination, significantly lowering the cost. WIGs are classified as boats by the International Maritime Organization, which results in significantly lower commercial operation costs as compared to an aircraft, which requires multiple clearances and timely inspections for each flight [50].

A WIG hovercraft has great potential as privately-owned vehicles for luxurious, fast and safe mode of transportation at low cost between coastal cities or to water locked bodies or island cut off from the mainland. As the WIG hovercraft will not require any costly support infrastructure like airstrips or ports/jetty it can be used in areas which are not easily accessible or the terrain does not support their construction. The craft instead of sailing flies thus eliminating the other effects of sea travel like rolling, pitching, and heaving or the effects of waves making the journey a more comfortable one [51].

Using WIG technology in a hovercraft for the purpose of sea rescue as the crafts can attain speeds as high as 30m/s using the ground effect to reach the sight of accident and come in close proximity of the causality resulting in better rescuing capabilities.

2.6 SEA STATE

The benefits of ground effect in the design of a hovercraft include the use of increased speed to reach drowning victims, people stuck at sea due to a faulty engine at a faster pace, exploring more travel routes, and saving energy. The WIG hovercraft concept is aimed at medium/short-range applications such as a river, coastal, inter-island, delta/estuary transport in areas where sea-state two is permitted, as seen in figure 15. The typical operating environment includes critical air and sea parameters that can be used to assess the reliability of a hovercraft and specify the capabilities required of any new design. Some of the most important environmental factors and their implications are as follows: Wind velocity and Sea level [52].

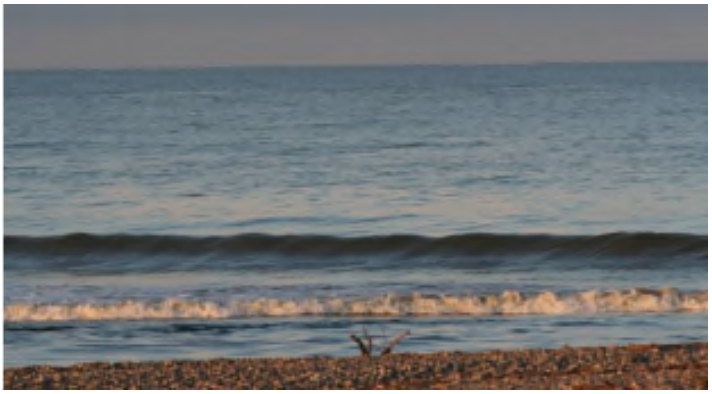

Figure 15 : Sea State 2, Conditions: Small wavelets all over (smooth), Wind Speed: 2 - 3m/s [52]

Sea state is a function of wave height. The term "sea state" refers to the general condition of a large body of water's free surface in relation to wind waves and swell at a specific location and time and is usually measured on a scale of 0 to 9 depending on the average wave height. Larger vehicles, such as seaplanes, ekranoplans, and wingships, will have greater sea state capabilities than smaller vehicles, such as airboats, hovercraft, canoes, etc. The World Meteorological Organization (WMO) sea state code primarily uses the 'wind sea' definition from the Douglas Sea Scale. The Douglas Sea Scale is a scale for determining the height of waves and the amount of swell in the sea that refers to waves that develop over a longer period of time and a larger area than locally generated wind waves [52].

Table 6 describes the swell characteristics, and table 7 depicts a simple scale that can describe sea state conditions in an approximate yet concise manner. Previous researchers used the Sea State Code as their beach watch protocol [52]. The sea state must be recorded during shore watch because it influences the likelihood of a sighting. Each increase in sea level reduces the possibility of seeing animals when they are present. Cetacean mammals' detection becomes extremely unlikely in high sea states, limiting the value of the data collected. As a result, shore watch is not conducted when the sea state exceeds 4 [53]. At this stage of the project, the WIG hovercraft is designed for sea states two and below in other to study the effect of the WIG hovercraft in calm sea conditions.

Table 6: Swell Characteristics [53]

Sea State	Description (Swell)
0	No swell
1	Very Low (short or average and low wave)
2	Low (long and low wave)
3	Light (short and moderate wave)
4	Moderate (average and moderate wave)
5	Moderate rough (long and moderate wave)
6	Rough (short and high wave)
7	High (average and high wave)
8	Very high (long and high wave)
9	Confused (wavelength and height indefinable)

Table 7: World Meteorological Organization (WMO) sea state code [52, 53]

WMO Sea State	Wave height (m)	Wind Speed (m/s)	Characteristics	Wind Description
0	0m	<0.5m/s	Calm (glassy), Sea surface smooth and mirror-like.	Calm, light air
1	0m to 0.1m	0.5m/s to 1.5m/s	Calm (ripples), Scaly ripples, no foam crests.	Light Breeze
2	0.1m to 0.5 m	2m/s to 3m/s	Smooth (wavelets), Small wavelets, Crests glassy, no breaking.	Gentle Breeze
3	0.5m to 1.25m	3.4m/s to 5.5 m/s	Slight, Large wavelets, crests begin to break, scattered white caps.	Moderate Breeze
4	1.25m to 2.5m	5.7m/s to 8.2m/s	Moderate, Small waves, becoming longer numerous white caps.	Fresh Breeze
5	2.5m to 4m	8.7m/s to 10.8m/s	Rough, Moderate waves, taking longer form, many white caps, some spray.	Strong Breeze
6	4 to 6 m	11.3m/s to 14m/s	Very rough, large waves with white foam crests, more spray.	Gale
7	6 to 9m	17.2m/s to 24.4m/s	High waves, heavy rolling, lowered visibility.	Storm
8	9 to 14m	28.5m/s to 32.6m/s	Very high waves, foam patches cover sea, visibility more reduced.	Violent storm
9	> 14m	>32.7m/s	Phenomenal, Air filled with foam, sea completely white with driving spray, visibility greatly reduced.	Hurricane

2.7 SUMMARY AND IMPLICATIONS

Ground-effect operations do not require a pilot's licence, and the vehicle is typically registered as a boat in most locations, opening up a slew of new opportunities. Several researchers have investigated the phenomenon of ground effect through numerous experimental and numerical simulations. Jung et al. investigated the wing in an experimental setting using the NACA 6409 aerofoil section. Three distinct types of endplates were investigated in those studies at varying ground clearances, angle of attacks, and aspect ratios. Endplates improve wing performance by shifting the centre of pressure to the leading edge. It was also discovered that the freestream velocity does not affect the aerodynamic coefficients of the wings [54].

M.R. Ahmed investigated the flow characteristics of symmetrical aerofoils in ground effect at various angles of attack and discovered significant high-pressure coefficient values

at low ground clearances, which extended over almost the entire bottom section at a high angle of attack. M.R. Ahmed also found that the geometry of the aerofoil played a role in the behaviour of the ground effect. At very small ground clearances of 0.05 h/c (h denotes the height of the aerofoil from the ground), a strong suction effect was observed, which was attributed to the formation of a convergent, divergent passage between the aerofoil and ground [55].

Moore et al. used a wind tunnel to compare the ground effect performance of a NACA 0012 and a DHTMU 12. Although the individual design characteristics of an aerofoil are not investigated, it has been discovered that the DHMTU aerofoil outperforms the NACA 0012 aerofoil in ground effect. However, the findings are not directly applicable to supercritical aerofoils due to the use of relatively simple aerofoils. Certain aerofoils outperform others in terms of ground effect [56].

S. Saradaet. al used the FLUENT code to conduct 2D and 3D CFD analysis for the NACA 64618 subsonic aerofoil, concluding that 2D simulations using the K-epsilon model do not produce reasonable results in the stalling region, while 3D CFD simulations predict reasonable results in the stalling region [57].

Douvi applied various turbulence models to experimental data to determine the best model for the ground effect problem. The k-ω SST model was found to be slightly more accurate than the Spalart-Allmaras [58].

Vance Dippold. investigated various near-wall flow modelling methods available in the WIND CFD code and concluded that both two-equation turbulence models worked well in the presence of a neutral or favourable pressure gradient. However, when an adverse pressure gradient was present, the SST model performed better [58].

S.D. Sharma conducted a comparison study of NACA 0012, NACA 6409, and DHMTU 12 aerofoils specifically designed for WIG aircraft. When flying close to the ground, the CFD simulation results showed a decrease in drag coefficient and an increase in lift coefficient, resulting in an overall increase in the lift to drag ratio of the aerofoils. Furthermore, DHMTU aerofoils demonstrated greater consistency in CL behaviour as the height-to-chord (h/c) ratio decreased [59].

Park and Lee investigated the effect of endplates on the aerodynamic characteristics of a small aspect ratio (AR) wing. According to their research, reducing the tip vortex will significantly increase the lift and lift-to-drag ratio, which the endplate can develop. They claimed endplates also made a small deviation of height stability at different ground clearances and angles of attacks, reducing the height stability [60].

Yang et al. demonstrated that end plates improve three-dimensional wing height stability at low ground clearance [61]. Kornev and Matveev discovered that the profiles of the tail and main wings are the most critical factors in static height stability. They suggested that for the acceptable stability of a WIG craft, the centre of gravity should be close to the height of the aerodynamic centre (X_h), and it should be between the heights of the aerodynamic centre and pitch aerodynamic centre (X_a) [62].

BE Okafor performed a detailed design analysis of a hovercraft prototype to determine the size of components in accordance with relevant standard requirements as applicable in the air cushion model. The test performance resulted in a design efficiency of 69 percent, resulting in a good performance in the propulsion and lifting systems. However, it was suggested that more research be conducted to improve the craft's efficiency [63].

Nawaf H. Saeid conducted a CFD analysis to optimise the shape of a hovercraft hull and cabin, as well as the location and size of the lifting fans. The CFD results show that the semi-circular front with a rectangular shape has less drag force than the other two for the same flow condition. It has been discovered that the best location for the intake of the lifting fan should be on the inclined front surface near the hovercraft platform's stagnation point [64].

Siva Nagaraju Dasari carried out a structural analysis of a hovercraft assembly on the entire analysis requirement, thrust and lift formulas, drag component calculation, and other important parameters to realise the design of the working model hovercraft. The normal stress along the interface layer was discovered to be non-uniform across the width of the hybrid joint (structural component between the hull and the superstructure in the hovercraft). It was suggested that the more refined FE mesh model be examined in other to gain a better understanding of the stresses that lead to failure [65].

The term “hoverwing” can refer to a variety of novel flying machines/concepts:

- The Hoverwing (rc), a small radio-controlled aircraft being developed in the United Kingdom.
- The Fischer Flugmechanik Hoverwing (FF), an experimental German Ground effect vehicle.
- The Universal Hovercraft Hoverwing (UH) ground effect light hovercraft.

Some theories explain how Wing In ground effect craft can be employed for search and rescue operations. According to Jonathan Quah Yong Seng's 2005 research, the possible benefits of Wing In Ground craft are:

- Wing In Ground craft can fulfil the need for increased speed of marine transport and may thus fill the gap between shipping and aviation,
- WIG boats achieve high speeds while still maintaining high efficiency, especially when compared to other high speed marine craft,
- WIG boats achieve high speeds while still maintaining high efficiency,
- Wing In Ground boats have lower operational costs than aircraft due to their marine nature [66].

Previous research has shown that experimental examination of a WIG craft has limitations, such as a May 2011 study from San Jose State University that investigated the cargo capacity and cost of a WIG craft as a faster and less expensive mode of transportation in coastal locations. A few commercially produced WIG hovercraft, such as Universal Hovercraft's UH-18SPW Hoverwing, are primarily intended for recreational purposes. According to the literature review, improving the aerodynamic characteristics of the wing as it approaches close to the ground using various techniques such as endplates and different wing configurations is one of the most important aspects of developing a WIG vehicle. Improved wings can increase a craft's range and endurance while decreasing fuel consumption and CO^2 emissions [67].

As a result, several research articles on the wing-in-ground effect have been written. However, most of these articles have concentrated solely on the aerodynamic characteristics of the wing rather than the overall WIG vehicle. Even though the WIG hovercraft research and development is still a new technology, there is no domestic consumption of this technology. This project examines the aerodynamic efficiency of an integrated wing and hovercraft in ground effect using computational fluid dynamics (CFD).

Chapter 3: Methodology

3.1 COMPUTATIONAL STRATEGY

The first stage in this study is to identify a CFD scheme that produces reasonably accurate results for the intended application. This is done by reproducing the results of research data available for validation. For this purpose, various papers have been used to establish a working scheme. The aerofoil geometry was picked up as arranging vertices, i.e., writings, content, records, and imported into the ANSYS Fluent. The X & Y coordinates for the profile were taken from the NACA database to prepare the model. The reproduction of the paper's results was followed closely for the different aerofoils, and the following parameters were established with the chosen CFD software (Fluent®). ANSYS Fluent uses CFD for analysis and mainly for simulation of fluid mechanics and thermodynamics problems. CFD analysis and study of results are carried out in 3 steps: Pre-processing, Solving, and Post-processing by using FLUENT solver in ANSYS workbench. Figure 16 shows the flowchart of the Computational Fluid Dynamics (CFD) methodology from the ANSYS workbench 20 [68].

i. Pre-processor: This is the initial phase in the CFD simulation process, and it aids in accurately defining the geometry by identifying the fluid domain of interest. Using CFD-GEOM, the domain of interest is then further divided into smaller segments, which is known as the mesh generation stage.

ii. Solver: Once the physics of the problem has been determined, the fluid material properties, flow physics model, and boundary conditions are established to solve using ANSYS FLUENT on a computer.

iii. Post-processor: After receiving the data, the next step is to analyse them using various methods such as contour plots, vector plots, streamlines, and so on for appropriate graphical representations and reports using ANSYS CFD-Post [69].

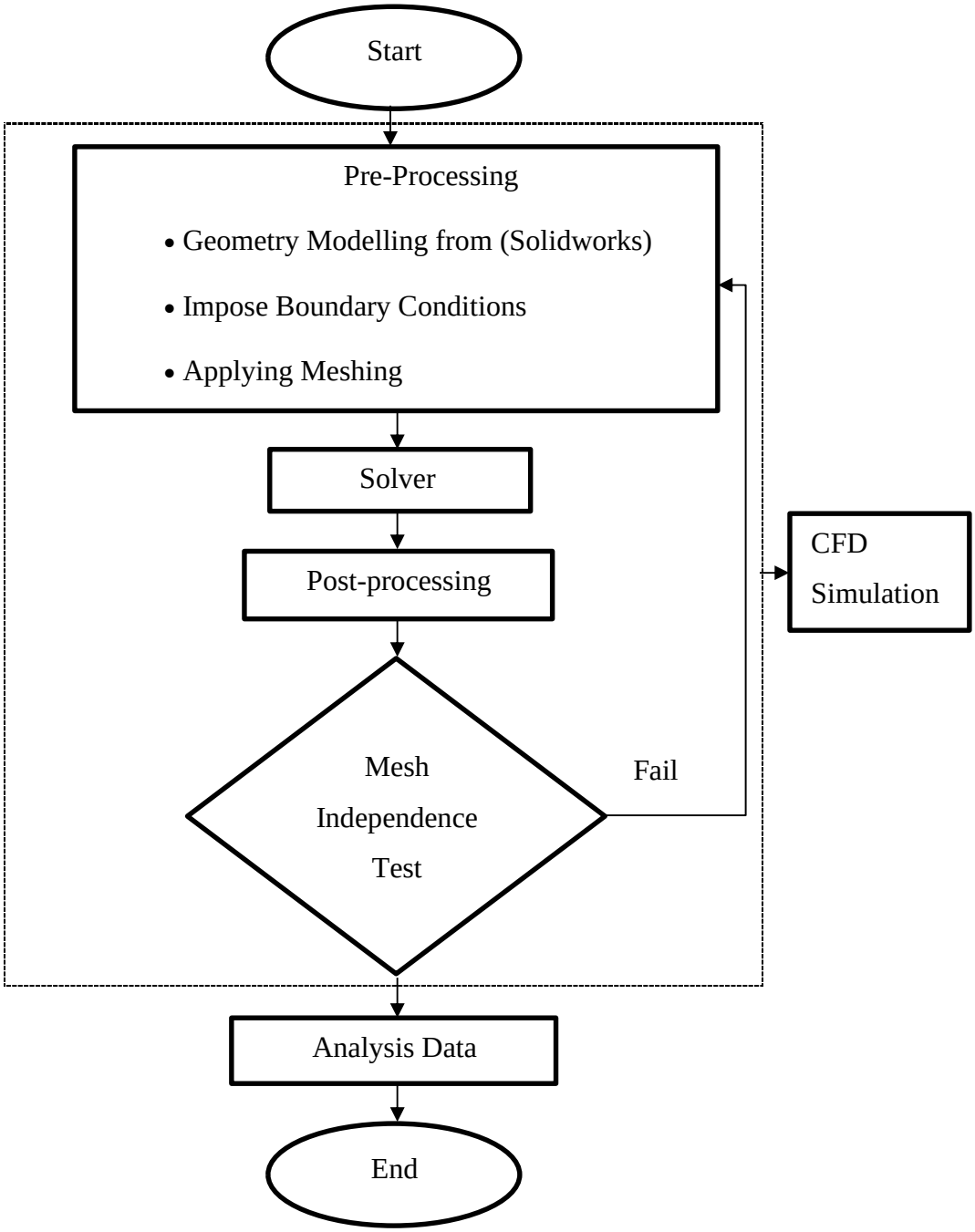

Figure 16: Flowchart of CFD Methodology

3.1.1 Domain and Boundary Condition

The flow around the aerofoil has been simulated by solving the equations for conservation of mass and momentum. The finite volume-based method was used to convert the governing equations of flow into algebraic equations that can be solved numerically. More details about these equations and the finite volume method can be found in Ref. [70].

In the present study, flow in the ground effect region is simulated by solving the incompressible Reynolds-averaged Navier-Stokes equations (RANS) with the SST k-ω model based on the features described in the previous section, which makes the SST k-ω

model more accurate and reliable for external flow fields of aerofoils. Therefore, the SST k-ω turbulence model was adopted in this study at the Reynolds number of $2x10^6$. It was assumed that the flow around the aerofoil is treated as steady, incompressible, and turbulent. The 3D RANS equations with the SST k-ω turbulence model are solved using the high-resolution advection scheme once the meshes are created. By finding Y^+, the turbulence model SST k-ω is capable of automatic near-wall treatment to capture turbulence closure. For flow separation under an adverse pressure gradient, the SST k-ω turbulence model is used, which accounts for the transport of turbulent shear stress.

The boundary conditions were defined as follows: The general boundary condition at the ground has been chosen as a no-slip wall moving at the free stream velocity of 30m/s. This condition provides a realistic WIG flight model without introducing a ground boundary layer as on a stationary no-slip wall. The inlet was assumed to use a uniform boundary condition with the inflow velocity of 30m/s [71] as the operating condition for an aerofoil near the ground, and the assumed 5% turbulence intensity; the outlet used a prescribed pressure boundary condition of P_0 = 1 atm; the aerofoil surface, top, bottom, and back domains used the no-slip wall boundary conditions. The boundary conditions, as seen in table 8, are used in all simulations unless specified otherwise.

Table 8: Boundary Conditions

Boundary Condition	**Description**
Moving Wall	No-slip wall moving at the free stream velocity of 30m/s in +ve x-direction
Aerofoil surface	Stationary wall with no slip condition
Top and Side walls	Symmetry
Velocity inlet	Inflow velocity of 30 m/s
Pressure Outlet	Absolute static pressure

Operating Conditions:

- $Re = 2.0 \times 10^6$
- Pressure based
- Model: SST k-ω
- Solution control gauss-seidel method

Ground clearance (h) is the distance between the aerofoil's chord length and the ground. Ground proximity causes higher pressure levels on the lower surface of the aerofoil at higher angles of attack, resulting in increased lift. The flow is considered steady and turbulent with constant free stream velocity, and the fluid flow is considered Newtonian; finally, the solution domain is three-dimensional. Then a meshing comparison and

turbulence model comparison was undertaken to ensure the quality of the mesh was sufficiently accurate, and the correct turbulence model was chosen for this purpose.

To acquire a dimension-independent numerical solution, domain dimensions and boundary conditions are considered, as shown in figure 17. A rectangular flow domain was created with a distance of the aerofoil from the top surface of the domain wall taken as 10m, and the inlet and outlet distance set as 5m and 15m from the leading and trailing edges, respectively as it was observed that this dimension does not affect the simulation. The aerofoil boundary was subtracted using Boolean, and the rectangular flow domain was obtained.

An investigation has been carried out to determine the domain size required for optimum results. This domain is chosen since it captures all-important physical phenomena, and it is similar, if not larger, than domains used in other WIG studies [72]. The aspect ratio is taken to be 1, with the chord and span of the aerofoil assumed to be 1m, respectively, as this gives a standard approach in the 3D simulation.

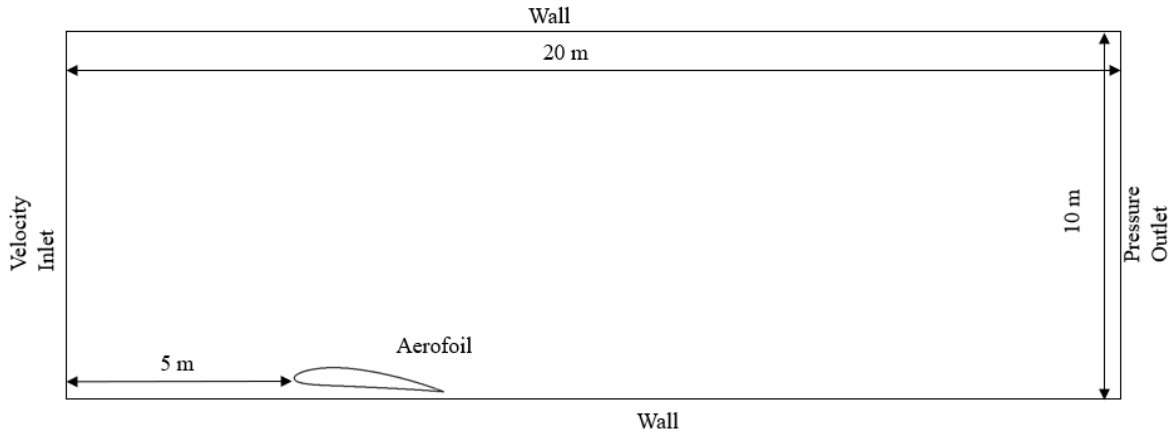

Figure 17: Boundary condition

The proximity and curvature advance size function is set at the default setting on ANSYS 20 to generate the mesh. This function automatically refines the mesh in the areas that would typically have higher gradients. The computational mesh consists of tetrahedron cells with five layers of inflations near the solid walls. The near wall inflation layers are important to implement the near wall corrections in the turbulence model, as shown in figure 18 for one of the cases. A mesh independence study was carried out to ensure the mesh converged to a steady value. Otherwise, that would have a different result even if the simulation runs for additional iterations. To establish the accuracy of the CFD solution, the wing was analysed using: the standard SST k-ω model, at uniform V_{in} = 30m/s and AOA = 5^{o}. The study was performed by developing five different meshes to predict the lift coefficient (C_L) on normalised mesh cells to determine how the mesh quality affects CFD simulation results.

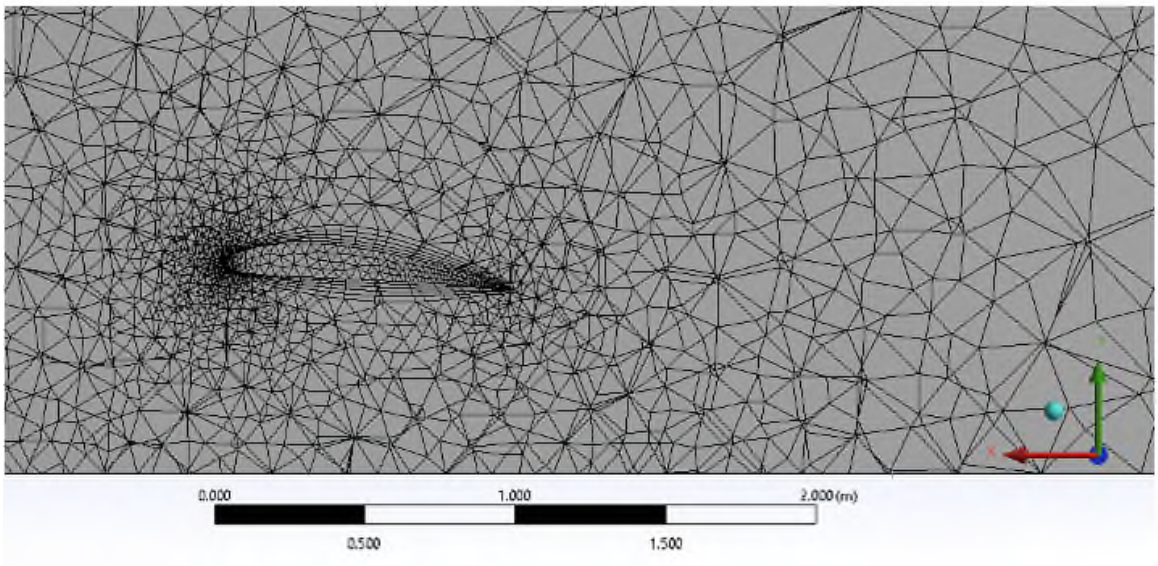

Figure 18: Mesh details near the walls of the NACA 4412 Aerofoil (AR=1).

3.1.2 Solution

Analysis setup of all cases is carried out in ANSYS FLUENT Solver. The result for analysis is done using ANSYS Post Processor. Velocity and pressure plots are plotted for all the cases of study. The investigated aerofoils are DHMTU 12, NACA 0012, and NACA 4412 with different angles of attack (-10° to 20°) and altitudes from the ground (h/c = 0.05, 0.1, 0.5, and 1) where the values of Coefficient of Lift and Drag were observed. A freestream velocity of 30 m/s and 1m chord are assumed across the solution.

The double-precision solver is selected, and the solver type is set to pressure-based. The turbulent model is selected, and the air is chosen as the flow material. All the reference values were computed from the inlet. The Coupled pressure velocity scheme was used as it will converge faster than the simple scheme, and monitors were set up to monitor the values of C_L and C_D. The convergence criteria selected for continuity were set at $1x10^{-6}$ as the values obtained from this would be sufficiently accurate. The initialization method is chosen as the hybrid. First order upwind scheme was employed on momentum, turbulence kinetic energy, and turbulence dissipation rate special discretization for one hundred iterations. It is then changed to the second order upwind on the next number of iterations for more accurate results. The pressure and velocity contours were plotted to analyse the flow of the aerofoil.

Y^+ is a dimensionless quantity representing the distance from the wall in viscous lengths. It is frequently used to characterise the coarseness or fineness of a mesh for a specific flow pattern. In turbulence modelling, determining the right size of cells near domain barriers is critical [73]. To achieve sufficient boundary-layer resolution, the Y^+ values on the aerofoil's surface and in relevant regions of the viscous wall were kept below 1. The minimum amount of Y^+ is taken to be 0.9. Table 9 summarises the key characteristics

of the meshes, and it is clear that CFD simulation time is highly dependent on the number of mesh nodes considered. The five meshes generated have near-wall resolution, i.e., $y^+ < 1$.

Table 9: Mesh Independence study [73]

Case	Element Size	Nodes	Cells	C_L
1	1.5	58109	185228	0.4265
2	1	206203	664736	0.5283
3	0.8	373056	1506002	0.6415
4	0.4	409341	1719410	0.6453
5	0.2	951759	4950206	0.6453

It is important to note that mesh resolution plays a pivotal role in the final CFD results. The mesh nodes need to be small to resolve the boundary layer on the wing surfaces. The parameters monitored for convergence were lift coefficient. The mesh converged at 4950206 cells, and this mesh size was used for the simulation. The final CFD simulation time required for convergence of the two meshes is significantly different from the conventional mesh independency method. It is clear from the simulation that the size of the element is highly dependent on the number of cells. The 5th case leads to the reasonable prediction of the lift coefficient, as seen in Figure 19, where it converges from this region. Inflation mesh is used for meshing purposes to capture the boundary layer region accurately. The mesh refinement is done near the wing area as it is the focus of interest.

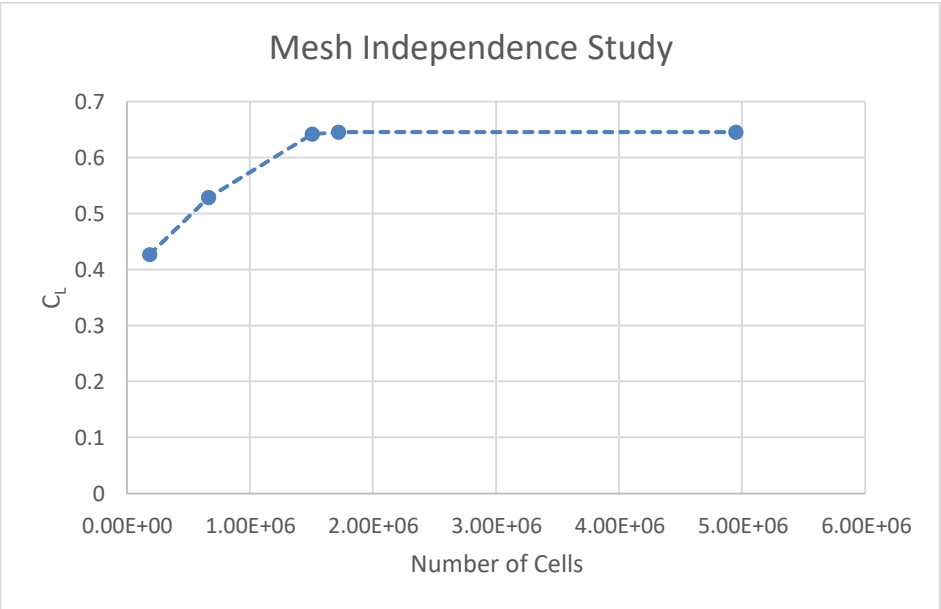

Figure 19: Graph of Mesh Independence study for 3D NACA0012 (AR=3)

A fine mesh with a mesh number of more than 1 million was chosen for the simulation as it gives close prediction to data from the literature as seen in table 10. The quality of the mesh is also validated through performing orthogonality and skewness checks which are well within the limit which were 0.97 and 0.22 respectively.

Table 10: Mesh comparison Validation

	University of Southampton [74]	NACA 0012 3D CFD
Reynolds number	$2x10^6$	$2x10^6$
Angle of Attack	5°	5°
Height to Chord ratio (h/c)	0.05	0.05
Aspect Ratio	3	3
Lift Coefficient	0.6	0.6453

3.1.3 Aerofoil Research Design

The next step in the design of a wing-in-ground effect (WIG) hovercraft is to choose an appropriate aerofoil to achieve the desired amount of lift generated for the WIG hovercraft under specified boundary conditions. The most important values to consider for the proper aerodynamic design of an aerofoil are the lift-to-drag ratio and coefficient of lift. Fluent has been widely used by previous researchers for analysis involving aerofoil, as it can display contour and vector plots, which gives excellent flow visualisation of the ground effect [75].

The UIUC Aerofoil Database and aerofoil tools were used to obtain the coordinate files for the three aerofoil shapes used in this investigation [76, 77]. Figure 20 shows the chosen symmetric aerofoil, Figure 21 shows the Asymmetric aerofoil to be a NACA 4412, and Figure 22 shows the chosen unconventional aerofoil to be a DHMTU 12. These aerofoils were selected due to their relative similarities in amount of camber, thickness, and shape. The aerofoils were investigated for AOA (Angle of Attack) ranging from -10° to 20° at different ground clearances. The 3D models of the aerofoils were then developed using the coordinate points in the Ansys design modeller.

Figure 20: NACA 0012 (Chord= 1m and Span=1m)

Figure 21: NACA 4412 (Chord= 1m and Span=1m)

The National Advisory Committee for Aeronautics (NACA) is a U.S. federal agency which undertakes, promote, and institutionalise aeronautical research. This NACA aerofoil series is controlled by four digits NACA MPXX

- M is the maximum camber divided by 100.
- P is the position of the maximum camber divided by10.

- XX is the thickness divided by 100

For example, the NACA 4412 aerofoil has a maximum camber of 4% located 40% (0.4 chords) from the leading edge with a maximum thickness of 12% of the chord.

The NACA 0012 aerofoil is symmetrical, the 00 indicating that it has no camber. The 15 indicates that the aerofoil has a 12% thickness to chord length ratio: it is 12% as thick as it is long [78].

Figure 22: DHMTU 12 (Chord= 1m and Span=1m)

Department of Hydro-Mechanics of the Marine Technical University (DHMTU) in Saint Petersburg, Russia is the family of a flat bottom aerofoil. Like the NACA 4-digit series, the aerofoil shape is composed of polynomial segments and a straight lower surface. Their camber line is slightly reflexed, and the outline between points 2 and 3 is a straight-line segment. A DHMTU section is described by eight numbers which define the geometry of the upper and lower surface. The format being DHMTU a-b-c-d-e-f-g-h. The section analysed is the DHMTU 12-35-3-10-2-80-12-2 for reasons of brevity. It is known throughout this paper as DHMTU 12 [79]. Table 11 shows the nomenclature of DHMTU.

Table 11: Nomenclature of Dhmtu Aerofoil [79]

Prefix	Definition	Value
A	Maximum ordinate of upper surface(%C)	12
B	Position of maximum ordinate(%C)	35
C	Ordinate of start of the flat section (%C, below the horizontal is positive)	3
D	Position of start of flat section(%C)	10
E	Ordinate of the end of flat section (%C, below the horizontal is positive)	2
F	Position of end of flat section(%C)	80
G	Slope parameter of the upper trailing edge	12
H	Nose radius parameter	2

The DHMTU 12-35-3-10-2-80-12-2 is characterised by a flat undersurface and an S-shaped mean line, as shown in Figure 22. The relatively slender wing has a 12% maximum thickness ratio (t/c) at a chordwise station from the leading edge, x/c = 35%.

3.2 AERODYNAMIC CHARACTERISTICS OF WING-IN-GROUND-EFFECT

The 2D and 3D study of different classes of aerofoils (NACA 4412, NACA 0012, and DHMTU 12) in ground effect was investigated due to their similar thickness. Simulations were done at various angles of attack to assess the accuracy of different turbulence models' results and then validated using existing experimental data from the literature survey.

Data from Abbott and Doenhoff showed similar tendencies in terms of aerodynamic efficiency to that of the present computational analysis that was evaluated. This was used to validate the 2D analysis of the NACA 4412. As shown in Figure 23, the dimensionless lift coefficient increased linearly with the angle of attack. Throughout this period, the flow was linked to the aerofoil. The flow on the upper surface of the aerofoil began to separate at a 15° angle of attack, and a situation known as stall began to develop.

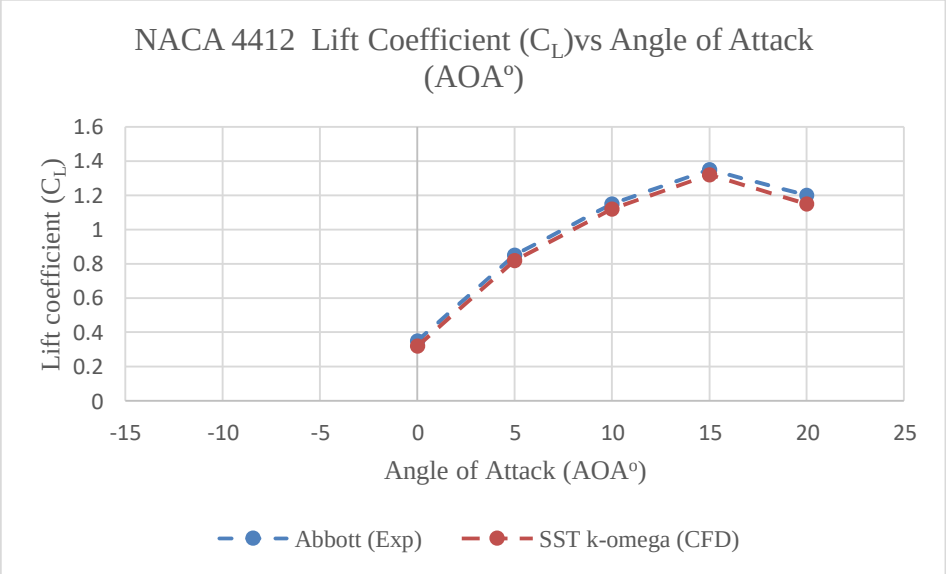

Figure 23: 2D Validation of the Literature Lift Coefficient (C_L) vs Angle of Attack (AOAº) NACA 4412 (AR=1) [80]

The model could accurately predict Abbott's results to within 3% accuracy, but the essential part of the model was that it efficiently followed the trends of the comparison investigated. A comparison of Abbott & Doenhoff's wind tunnel experimental data from table 12 with the CFD analysis of a NACA 4412 aerofoil. The experimental data are compared to the lift coefficient for computational model NACA 4412 in unbounded flow for the angle of attacks ranging from 0° to 20°. The results demonstrate good agreement across all attack angles and validate the computational method's adaptation. As this was the only data that gave a consistent result without optimising, the Reynolds number ranged from $2x10^6$ to $10x10^6$. As a result, further simulation was conducted, with each experiment matched to the previous Reynolds number to increase repeatability and compare data accuracy.

Table 12: Validation comparison of NACA4412 (Experimental vs Computational)

	Abbott and Doenhoff [80]	**NACA 4412 2D SST k-ω (CFD)**
Reynolds number	$2x10^6$ to $10x10^6$	$2x10^6$
Angle of Attack	5°	5°
Aspect Ratio	1	1
Lift Coefficient	0.85	0.82

On an aerofoil, the resultant forces are usually resolved into two forces and one moment. The net force acting normal to the incoming flow stream is known as the lift force, and the component of the net force acting parallel to the incoming flow stream is known as the drag force. The obtained C_L and C_D exhibited similar trends with the published experimental data at all angles of attack until stall at 15°, as shown in Figures 24 & 25. The SST k-ω turbulence model was a suitable fit for the simulations since it provides near predictions and follows the C_L and C_D trends in the literature.

The NACA 0012 was utilised to validate the mesh of the 3D analysis using available experimental data from Landson and the University of Southampton [81, 82], as there was not enough information on the experimental data of the NACA 4412 for the validation of the 3D analysis. Aerofoils working in ground effect have been shown to have various features that affect their aerodynamic characteristics. The influence of aspect ratio (AR), angle of attack (AOA), and height to chord ratio (h/c) on the ground effect region was explored, where an optimal wing shape was obtained. The NACA 4412 was the most appropriate aerofoil used for ground effect based on the CFD analysis as it had superior lift performance compared to other aerofoils operating in the ground effect region. The profile having a flat lower surface makes it beneficial for ground effect situations where a venturi effect can be set up by convergent-divergent flow under a more highly curved surface.

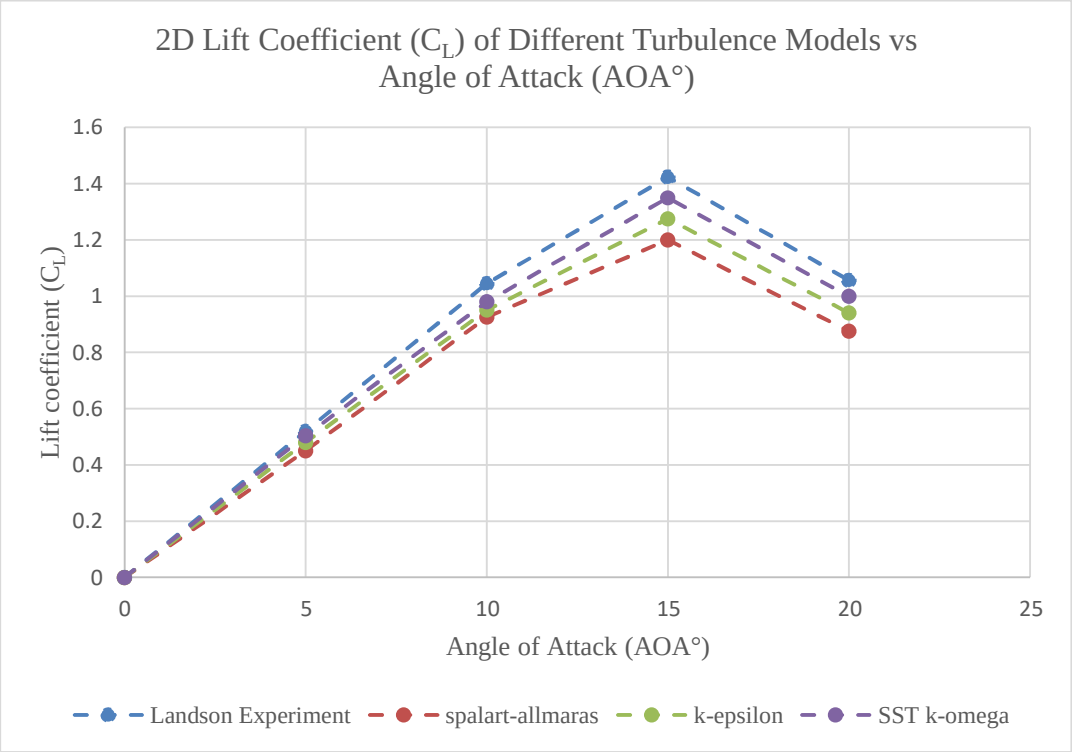

Figure 24: 2D Lift Coefficient (C_L) vs Angle of Attack (AOAº) comparison of different turbulent models using NACA 0012 aerofoil (AR=1) [81]

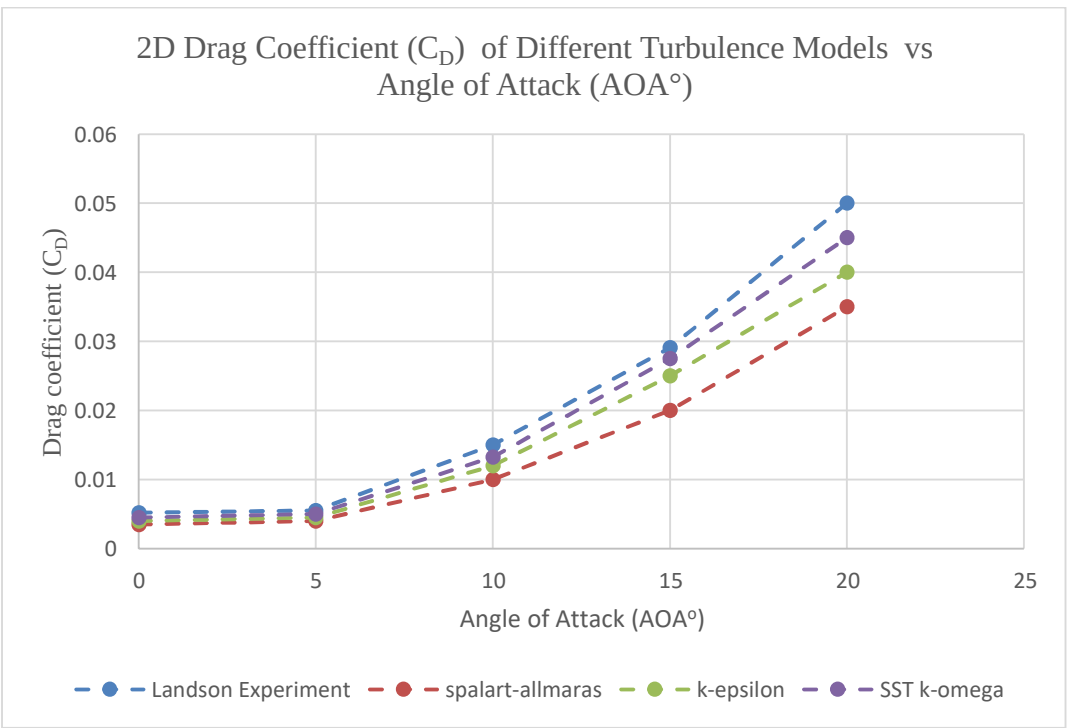

Figure 25: 2D Drag coefficient (C_D) vs Angle of Attack (AOAº) comparison of different turbulent models Using NACA 0012 aerofoil (AR=1) [81]

The lift and drag force produced by the wing vary with the angle of attack, as the local pressure distribution around the wing changes as the wing is rotated in the freestream. Figure 26 shows that the dimensionless lift coefficient increased linearly as the angle of attack increased for the different classes of the aerofoil. The angle of attack significantly impacts the aerofoil's drag, as seen in figure 27. When the angle exceeds 5°, the drag quickly

increases due to the increased frontal area and boundary layer thickness. The NACA 4412 aerofoil shows the highest lift coefficient compared to other aerofoil models.

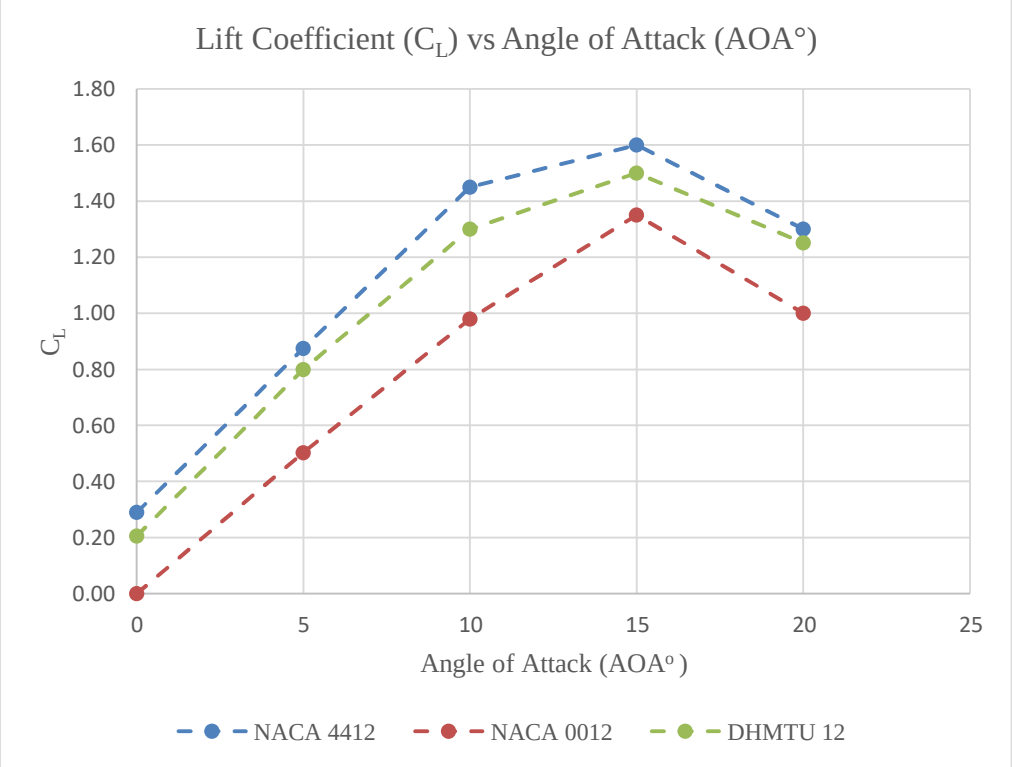

Figure 26: 2D Lift Coefficient (C_L) vs Angle of Attack (AOA°) of different classes of aerofoils using SST k-ω turbulence model (AR=1)

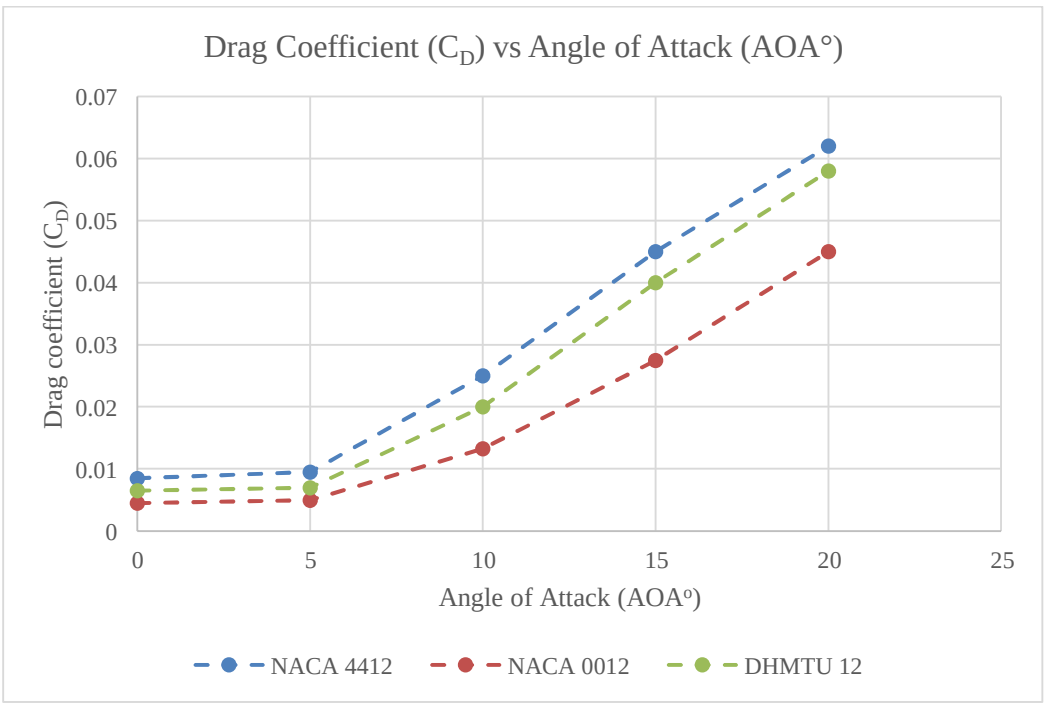

Figure 27: 2D Drag Coefficient (C_D) vs Angle of Attack (AOA°) of different classes of aerofoils using SST k-ω turbulence model (AR=1)

Figures 28 and 29 show the influence of pressure and velocity distribution throughout the aerofoil surface for a 5° angle of attack (AOA) in the NACA 4412 series aerofoil. The

area beneath the aerofoil contains higher pressure air than the incoming flow stream, which causes a push upward, resulting in lift. The differential in pressure between the top and bottom of the aerofoil causes vortex formation along the trailing edge of the aerofoil. The flow accelerates on the upper side of the aerofoil while decreasing on the lower side, and the upper surface will experience lower pressure than the lower surface, according to Bernoulli's theorem. The low-pressure area indicates the area of higher velocity. The leading-edge experiences area of high pressure and is called the stagnation point.

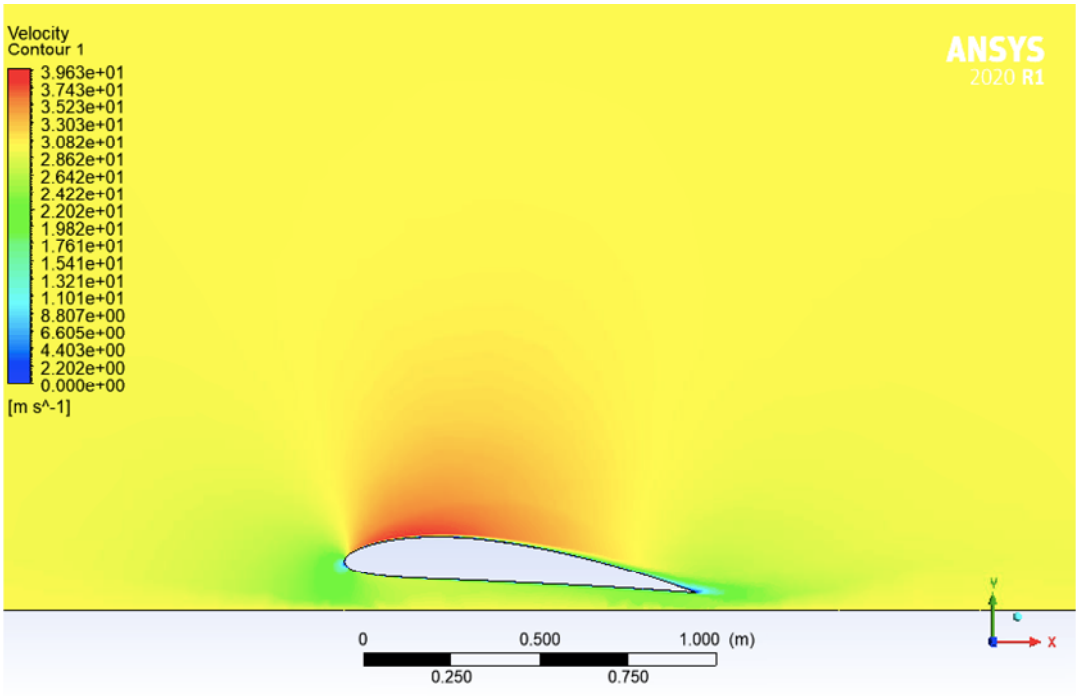

Figure 28: 3D NACA 4412 Velocity Contour of aerofoil at 5° Angle of Attack

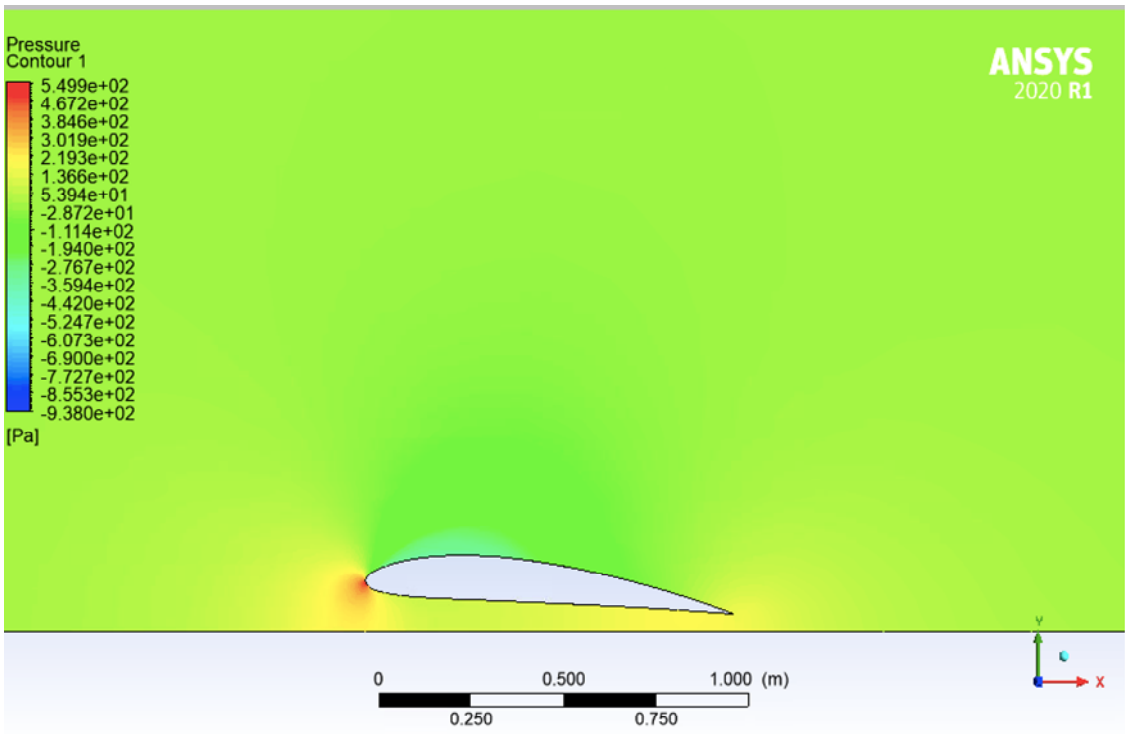

Figure 29: 3D NACA 4412 Pressure contour of Aerofoil 5° Angle of Attack

Since lift and drag are both aerodynamic forces, the ratio of lift to drag indicates the wing's aerodynamic efficiency. The wing has a high C_L/C_D ratio if it produces a large amount of lift or a small amount of drag. Figure 30 shows that the C_L/C_D reduces as the proximity to the ground increases, where h is the distance from the ground and c is the chord length. The constant h/c for this study will be 0.05.

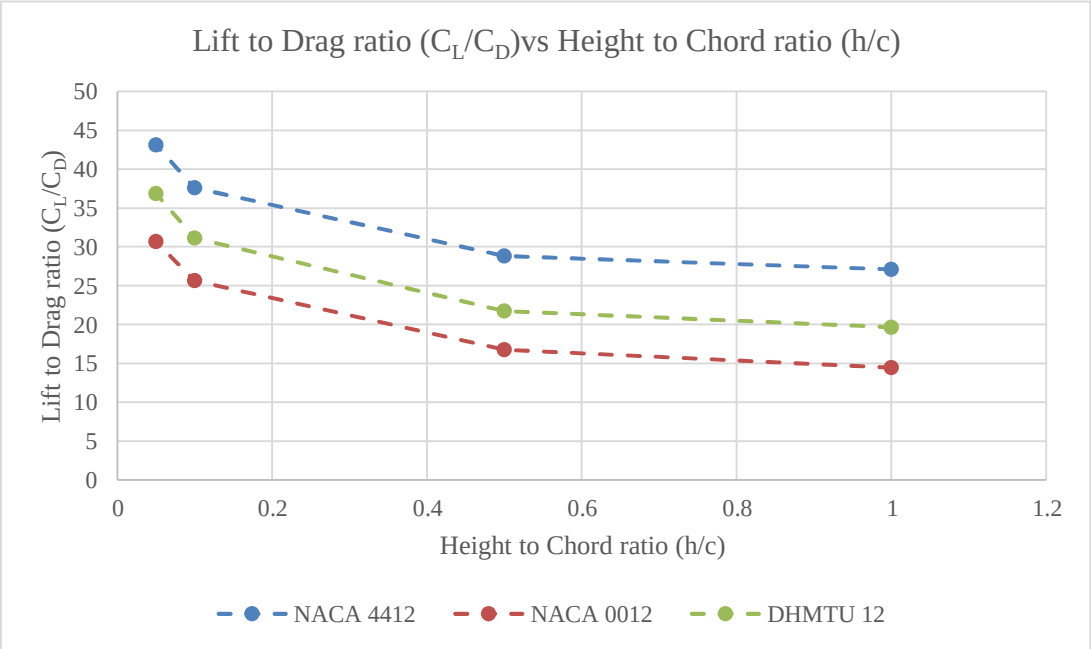

Figure 30: 3D Lift to drag ratio (C_L/C_D) vs height to chord ratio (h/c) at 5° AOA (AR=1)

The comparison of lift and drag coefficients of the different aerofoil models at various angles of attack ranging from -10° to 20° with a constant h/c of 0.05 is shown in Figures 31 and 32. This data shows similar trends to the previous data in Figures 26 and 27. Augmentation of the lift and drag coefficients is attributed to the angle of attack, where the increase in the AOA amplifies the lift and drag coefficients. It was noticed that as the angle of attack increases, so does the lift. At a speed of 30 m/s, the aerofoils have a stall angle of 15°.

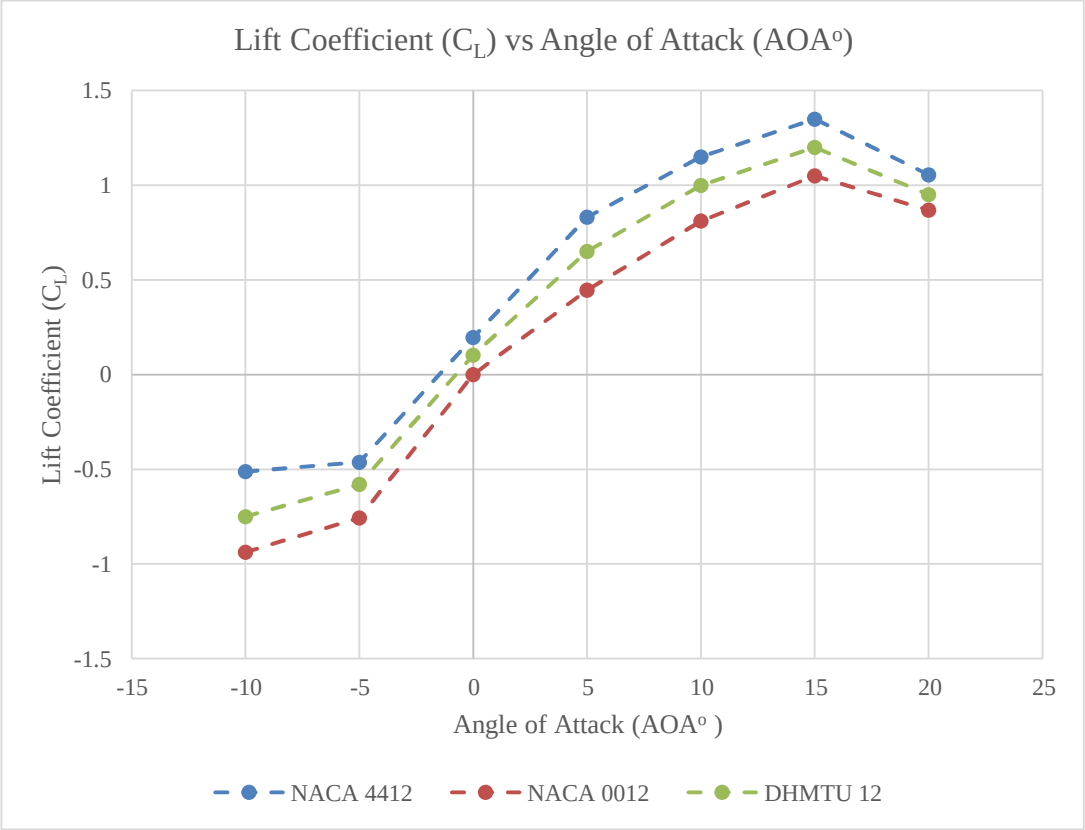

Figure 31: 3D analysis of C_L vs AOA of different classes of aerofoils at height to chord ratio (h/c) = 0.05 (AR =1)

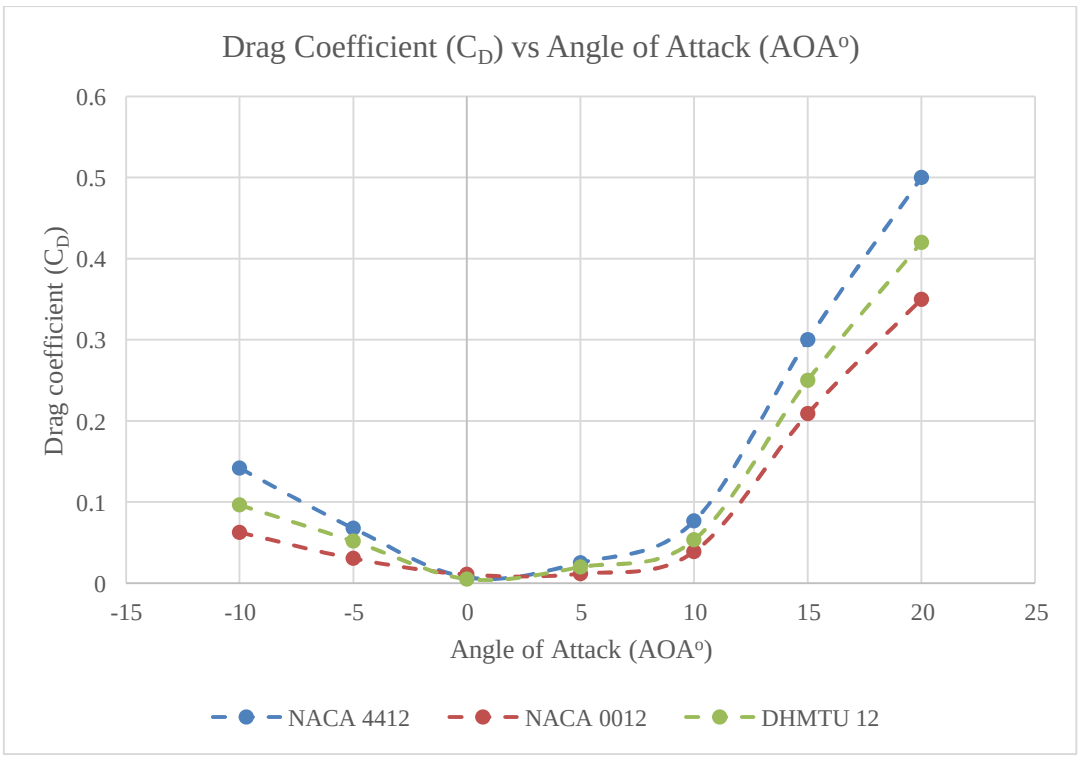

Figure 32: 3D analysis of C_D vs AOA at height to chord ratio (h/c) = 0.05, (AR =1)

The efficiency of the aerofoil works better at a lower height to chord ratio (h/c=0.05), where h= 0.05m and c =1m. The plots in Figures 33 and 34 showed the aerofoils had a peak performance angle of attack of up to 5°. As a result, the integrated wing hovercraft will operate in this area because of the favourable ground effect. The maximum aerodynamic

efficiency of the NACA 4412 aerofoil is roughly 44 in ground effect conditions, making it the preferable aerofoil to employ for the WIG hovercraft. Compared to its value out of ground effect condition (h/c=1), the increase in aerodynamic efficiency is twofold in the ground condition. In the presence of ground effect, the connection between angles of attack and C_L/C_D ratio is the same, except that the magnitude of C_L/C_D is greater than in the absence of ground effect. The maximum value of aerodynamic efficiency is observed in ground clearance 0.05 and 1 for NACA 4412, which is equal to twice its value (about 44) as compared to the ground effect condition (about 22).

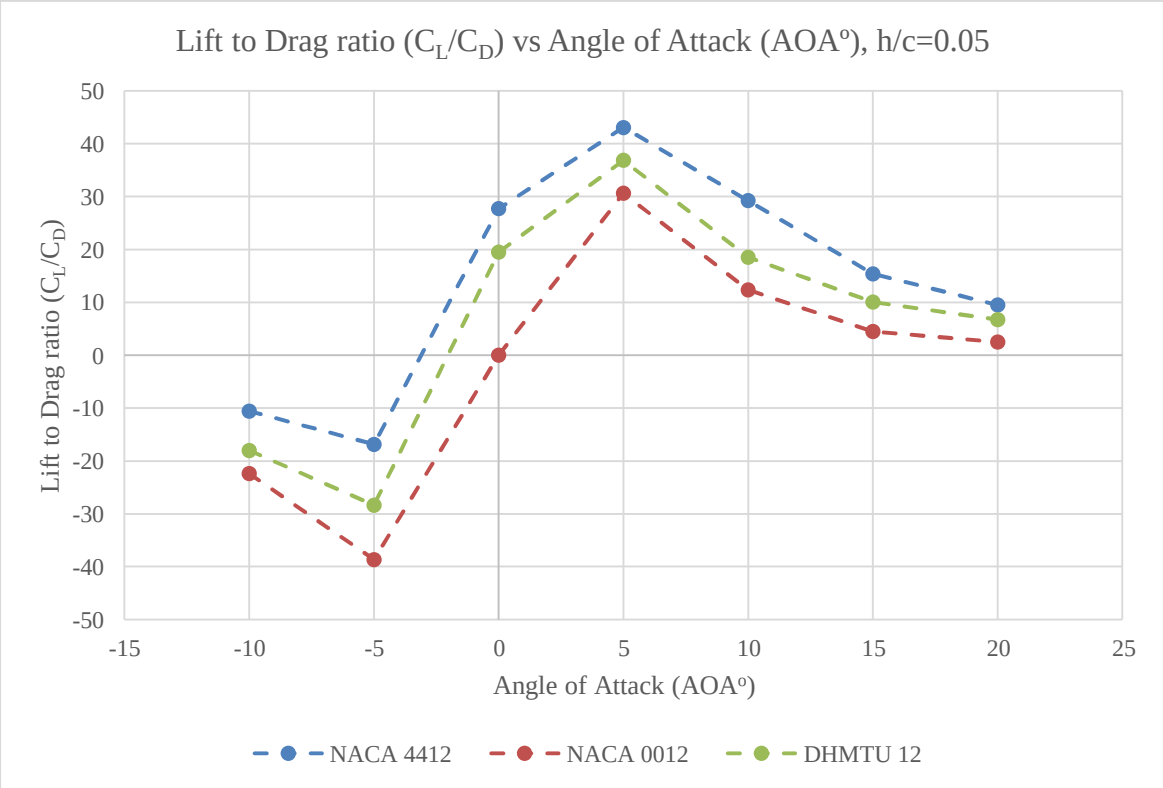

Figure 33: 3D analysis of C_L/C_d vs AOA at height to chord ratio (h/c) =0.05 of different classes of aerofoils (AR =1)

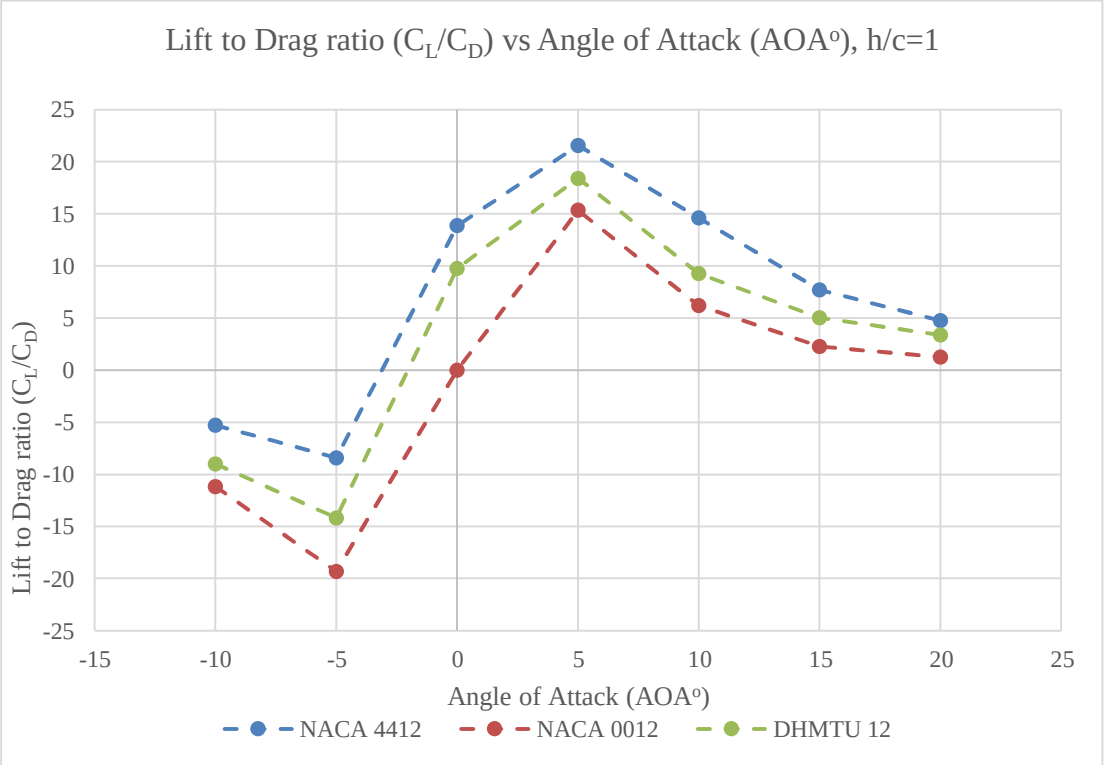

Figure 34: 3D analysis of C_L/C_d vs AOA at height to chord ratio (h/c) =1 of different classes of aerofoils, (AR =1)

The aerodynamic efficiency decreases as the height to chord ratio (h/c) increases, indicating that ground effect functions better with a lower h/c ratio. The goal of this study was to thoroughly investigate the performance of several classes of aerofoils in ground effect, which was quantified in the C_L/C_D ratio and used to evaluate each aerofoil's performance. As the key factors in this research were h/c and angle of attack, understanding how they affect C_L/C_D is critical to obtaining a thorough performance analysis. When examining ground effect, the convergence of C_L and C_D values is significantly more relevant in determining convergence. As a result, a 3D simulation is created for improved analysis and comparison of the on-ground effects situation to obtain much more accurate conclusions.

The aerofoil's lift coefficient improves as the aspect ratio rises from 1 to 3, as seen in figure 35. Experimenting with different aspect ratios (1 and 3) and h/c values was to find any hidden tendencies associated with increasing the wing aspect ratio. The aerofoil aspect ratio is the ratio of the aerofoil's span to the average chord length, which impacts the lift and drag coefficients, which cause resistance to the aerofoil's movement. Hence this parameter is important for investigating an aerofoil's efficiency. Wings with a low aspect ratio have a short span and a large chord, whereas wings with a high aspect ratio have a long span and a short chord. High aspect ratio wings provide slightly greater lift and allow for longer flight times, while low aspect ratio wings are better for swift manoeuvrability.

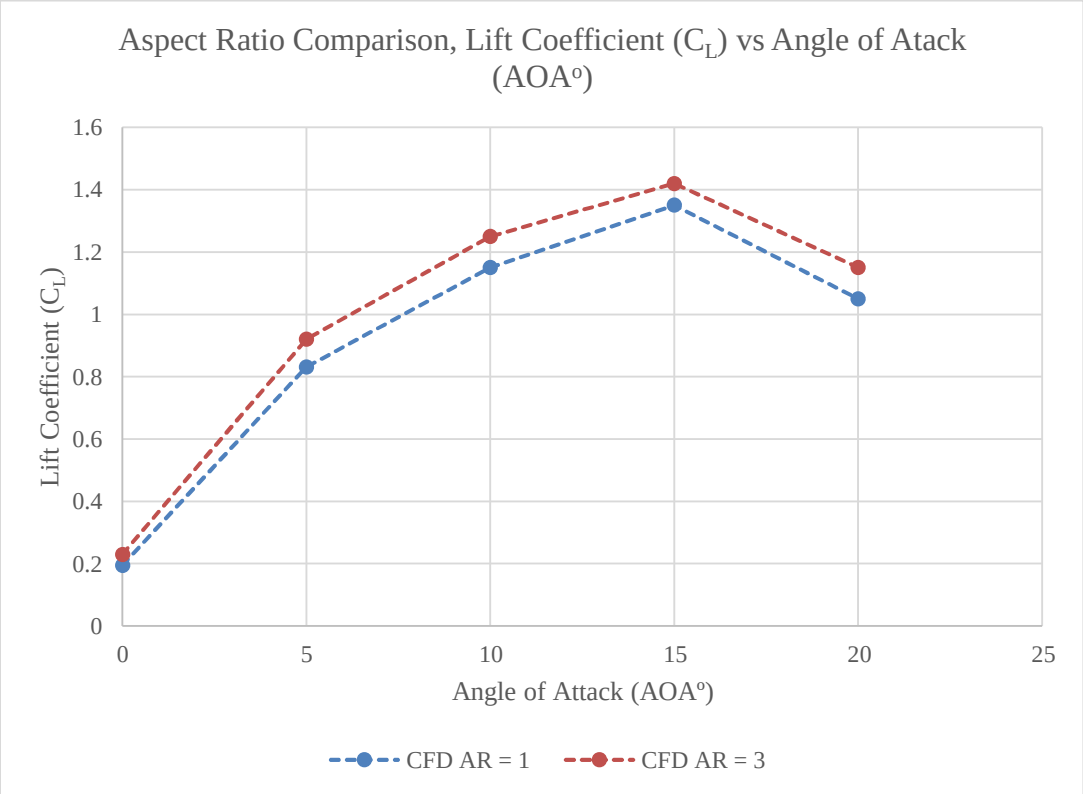

Figure 35: NACA 4412 Lift coefficient (C_L) vs Angle of Attack (AOAº) Aspect Ratio (AR) comparison

The results are validated using experimental data from the University of Southampton, as seen in figure 36 and table 13, where it demonstrates suitable agreement by comparing the lift coefficient against the h/c ratio.

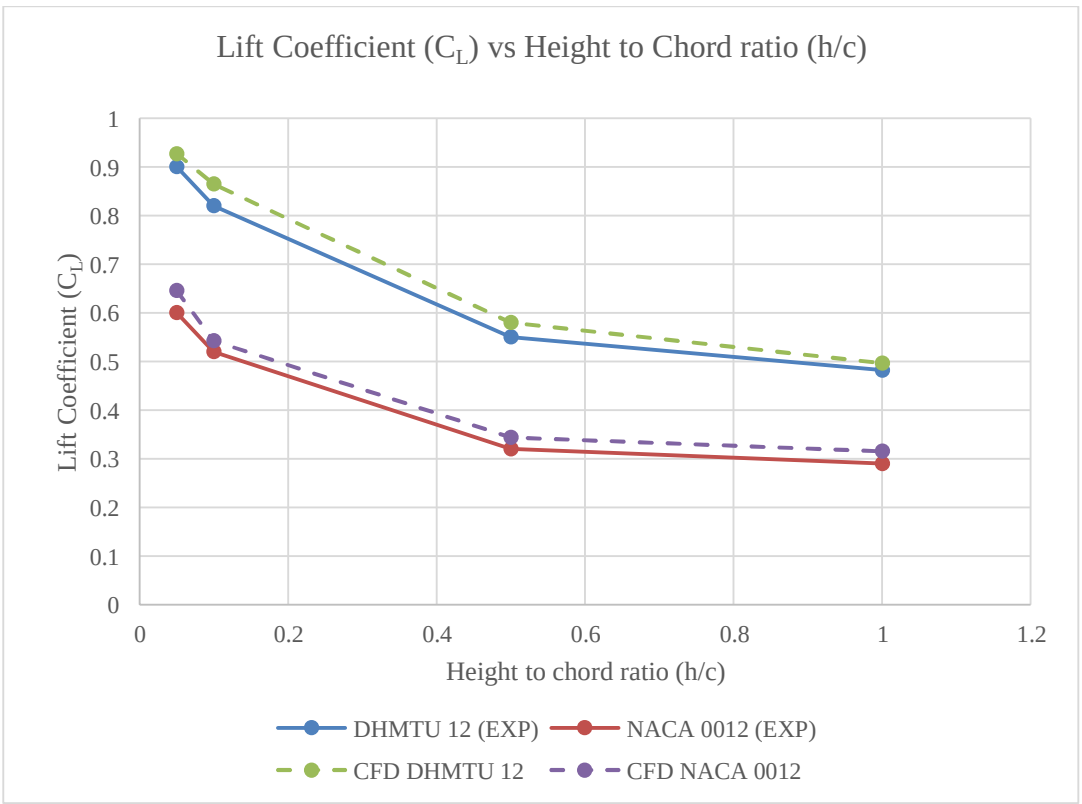

Figure 36: Lift Coefficient (C_L) vs height to chord ratio (h/c) Validation at angle of attack 5° using Aspect ratio=3 [81]

Table 13: C_L vs h/c Comparison (AR=3)

h/c	Experiment of DHMTU 12 [79]	DHMTU 12 (CFD)	Experiment of NACA 0012 [79]	NACA 0012 (CFD)
0.05	0.9	0.93	0.6	0.645
0.1	0.82	0.86	0.52	0.54
0.5	0.55	0.57	0.32	0.36
1	0.48	0.49	0.29	0.32

The geometry of the aerofoil, in addition to the angle of attack and the aerofoil's height to chord ratio (h/c), has a significant impact on the aerodynamic characteristics of the wing configuration when operating in ground effect. Airflow along the trailing edge is critical and significantly impacts aerodynamic efficiency. The data presented here can be used to establish an initial analysis of a combined wing and hovercraft travelling in the ground effect zone. The results presented here can be applied at the preliminary design stage for the initial analysis of an integrated wing and hovercraft moving in the ground effect region.

The effect of the ground is investigated using simulation results obtained by varying the clearance between the vehicle and the ground surface. The computational fluid dynamic analysis results revealed that the NACA 4412 wing had higher aerodynamic efficiency at 5^o angle of attack (AOA). From figure 37, the NACA 4412 wing with an aspect ratio of 3 will be used as the main wing, which will be attached to the hovercraft to produce the required lift. The wing-in-ground effect hovercraft model design will be carried out at an optimized angle of attack of 5° as it had a favourable aerodynamic performance from the analysis that compared various classes of aerofoils. The lift and drag coefficient performance measurements were estimated against the various angles of attack in ground effect using the SST k-ω turbulence model, which produced accurate results from the investigation.

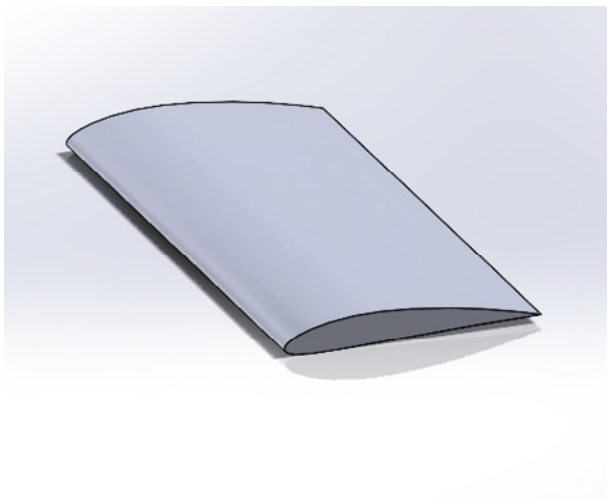

Figure 37: NACA 4412 Aerofoil (Total (b) Span=6, (c) Chord=2).

3.3 INTEGRATION OF A WING AND HOVERCRAFT IN GROUND EFFECT

The hull area of the design is fixed to be 8m in length and 4m in width, as seen in table 14 and figure 38, which shows a round bottom rectangular hull that is comparable to the specification from the current RNLI hovercraft datasheet, which will be used for the CFD simulation [83].

Table 14: Hovercraft hull design parameters (skirt not included)

Design Parameters	Empirical Relation	Value
Weight of Hovercraft (kg)	-	1105kg
Operating speed(m/s)	-	30m/s
Length (*l*)	-	8m
Width (*w*)	*w=l*0.5*	4m

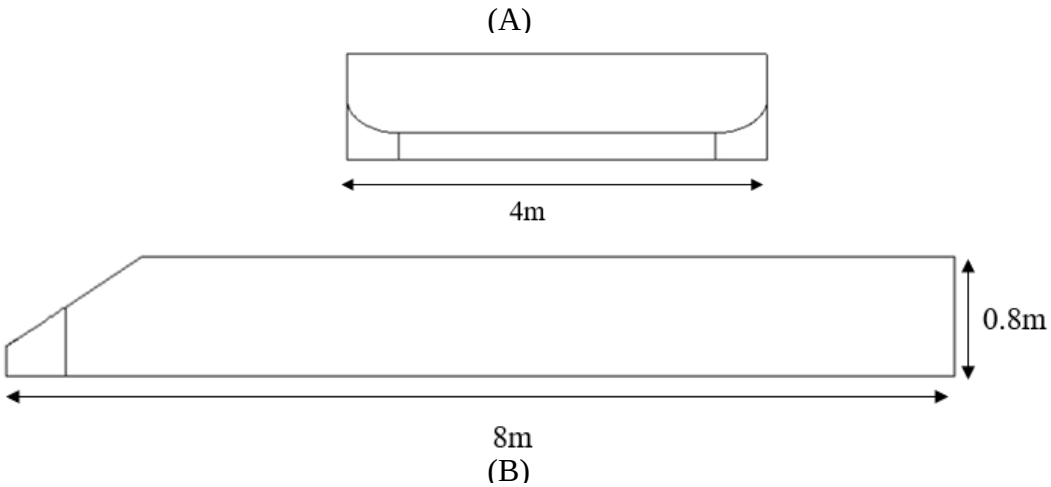

Figure 38: Diagram of hovercraft hull base dimensions (A) Front View, (B) Side View

Table 15 shows the moment data used to determine the position for the centre of gravity of the WIG hovercraft with an accurate view of a simplified hull. Assumptions were made on the location of the weights relative to the centre of gravity (arm distance), the weight of the pilot, crew/passengers, and tail assembly. The other weights were based on the specification of the RNLI rescue hovercraft datasheet [83]. The amphibious vehicle will be used for search and rescue operations suitable for use on shallow water, tidal terrain, and dry ground. It can carry loads of up to 480kg over shallow water, tidal terrain, and dry land.

Table 15: Calculation for the Centre of Gravity Position

Weight	Value (kg)	Arm/distance (m)	Moment(kgm)
Hull weight	480	4	1920
Pilot	80	2.65	212
Crew/Passengers	240	4.25	1020
Additional weight	60	5.50	330
Lift Fan Engine	85	0.82	69.7
Thrust engines	115	6.75	776.25
Rudder/Tail Assembly	45	7.50	337.5
Total	1105		4665.45

Moment (M) = Force x Distance Equation (4)

Centre of Gravity position (COG) = $\frac{Sum\ of\ all\ moments\ (kgm)}{Sum\ of\ all\ weights\ (kg)}$ Equation (5)

From table 14 and equation 5 the centre of gravity position is taken to be 4.2m from the datum line, which is illustrated in figure 39.

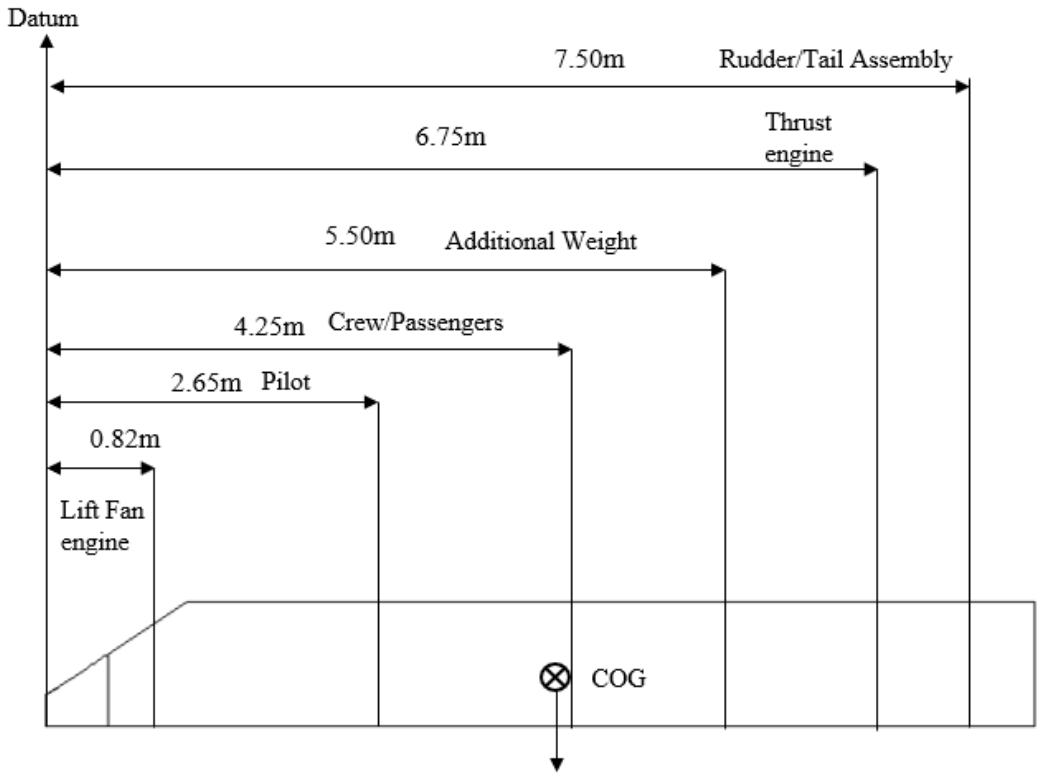

Figure 39: Arm distance and Centre of Gravity position of hovercraft hull

It was assumed that the aerodynamic centre is 25% of the chord length from slender wing theory [84]. This makes the aerodynamic centre (AC) 0.5m from the wing's leading edge. For an initial design investigation to evaluate the stability of the vehicle, the centre of lift (COL) for the wing position was set to coincide with the hovercraft hull's centre of gravity (COG), as illustrated in figure 40.

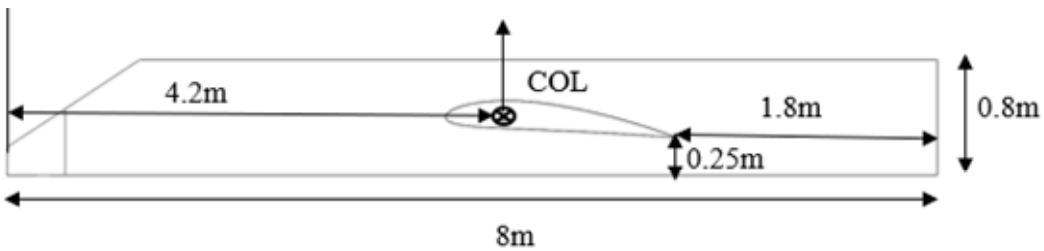

Figure 40: Initial position for centre of lift

The hovercraft operates on the principle of floating above the ground on a cushion of air supplied by the lift fan. The air cushion makes the hovercraft very frictionless. Since the object is not in contact with the ground, the surface tension is reduced, making the object

easier to move. As a result, the WIG hovercraft design includes a flexible skirt to offer enough lift to hover 0.5m over obstacles, as shown in figure 41. This enables the vehicle to pass over rocks and other uneven terrain obstacles with minimal difficulty or damage. The skirt height is assumed to have a depth of 1m for the initial design analysis of the WIG hovercraft.

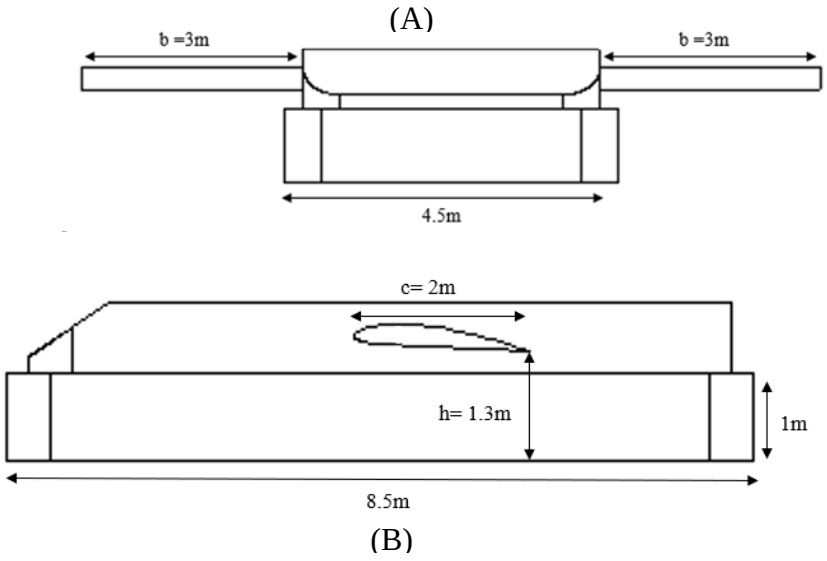

Figure 41: WIG Hovercraft and skirt inclusion (1m high) (A) Front View, (B) Side View

The NACA 4412 wing was used as the main wing to be implemented on the hovercraft as it had the maximum lift coefficient from the previous analysis that compared various classes of wing sections (NACA 4412, NACA 0012, and DHMTU 12). The NACA 4412 wing is a moderately cambered aerofoil with a nearly flat bottom. Cambering an aerofoil helps provide it with a higher maximum lift coefficient [85].

The NACA 0012 wing was used as the tail wing on the WIG hovercraft for stability purposes, as seen in figure 42. The analysis and validation of the NACA 0012 have been investigated from the previous CFD analysis of different classes of wing sections in chapter 3.2. As the tail wing is hidden from the airflow behind the main wings, this ensures smooth airflow and better pitch control of the aircraft. Another advantage of having the pitch control wing at the rearmost part of the craft gives fine pitch control with only minimal additional lift and drag.

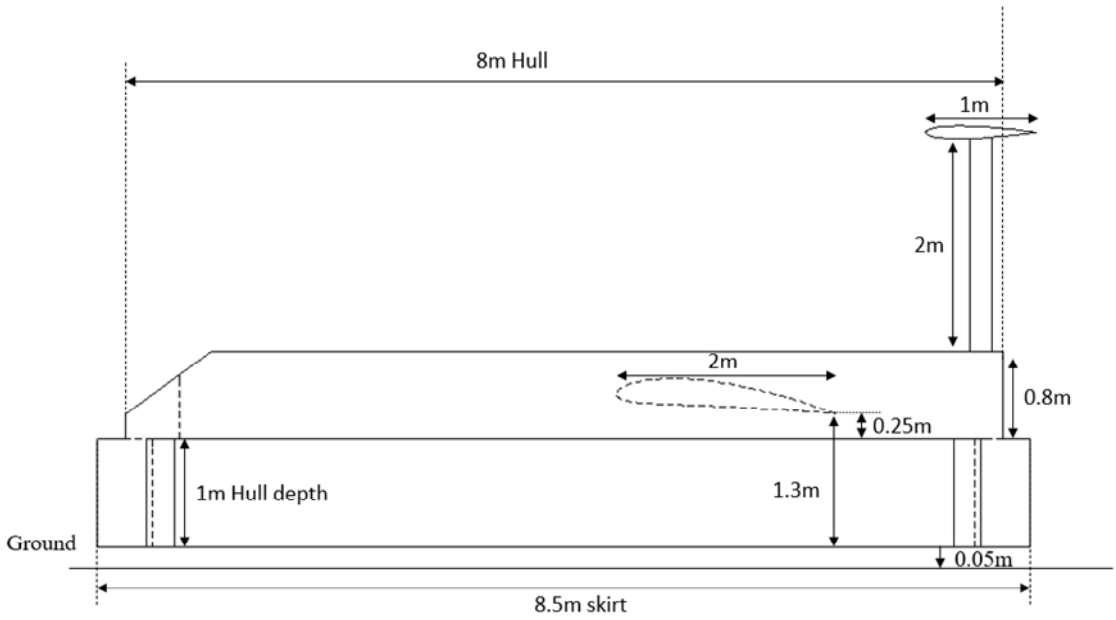

Figure 42: Detail view of a WIG Hovercraft with tail wing

Table 16 shows the lift and drag coefficients of individual components, where the NACA 0012 was selected as the tail wing to provide stability for the WIG hovercraft. From the CFD analysis, the overall lift Coefficient (CL) generated was 0.7048, and the drag coefficient (CD) was 0.347.

Table 16: Lift and Drag coefficients of individual components

Components	Lift Coefficient	Drag Coefficient
Hull	0.159	0.2867
Main Wing (NACA 4412)	0.5348	0.0495
Tail Wing (NACA 0012)	0.0110	0.0108

The speed required to lift the weight of the WIG hovercraft in this study is determined by using aerodynamics from equation 6. Hence the speed required to lift the WIG hovercraft is 28m/s without any lift required from the air cushion. As this gives the craft the ability to fly higher and faster while the air cushion keeps it high above waves and ground obstructions, allowing the vehicle to be amphibious.

$$V = \sqrt{\frac{2L}{C_L \rho A}}$$ Equation (6)

$$V = \sqrt{\frac{2 * 1105 * 9.81}{0.704 * 1.225 * 32}} = 28m/s$$

When it comes to stability, the feature that makes WIG craft vehicles stable about their lateral axis is longitudinal static stability. It is the stability of the pitch; this relates to the

stability of the aircraft in its plane of symmetry about the lateral axis (the axis along the wingspan). The rotation of an axis running from nose to tail is the stability of a vehicle's roll, known as its lateral stability. The stability of the aircraft's yaw is referred to as directional stability. Yaw is an aircraft's left and right motion.

The longitudinal static stability of WIG craft vehicles is important for pilots to determine if they can easily control the pitch of an aircraft in flight. As a result, pilots prioritise longitudinal static stability over lateral and directional stability. A longitudinally unstable WIG craft tends to gradually dive or stall as this could be disastrous while flying at high speeds so close to the ground.

Table 17 displays the lift and drag coefficient results from CFD for the individual components of the WIG hovercraft. As it was adopted to calculate the moment of the WIG hovercraft.

Table 17: Lift and drag forces acting on the individual components of the WIG Craft

	$X_{Distance}$ (m)	**$Y_{Distance}$ (m)**	**F_L (N)**	**F_D (N)**
Hull	2.6	0.45	968.5	2139.8
Main Wing	3.69	0.3	3938.5	381.8
Tail Wing	7.6	2.4	78.1	84.1

From table 14, the Lift force of the WIG hovercraft is $L_{full\ WIG\ hovercraft}$ = 10,840N (1105kg*9.81), the centre of gravity is located 4.2m from the front of the craft, and the empty weight of the hull is 480kg.

From moment sign convention, the moment is taken to be at the datum (front edge of the hovercraft), as seen in figure 42. Convention dictates that a moment acting in the clockwise direction is a positive moment while a moment acting in the anticlockwise direction is a negative moment.

Moment about X_{axis}=0, Y_{axis}=0. COL= 4.7m from datum

$M = mg * X_{cog} + L_{hull}*X_{hull} + L_{wing}*X_{wing} + L_{rear\ wing}*X_{rear\ wing} + D_{hull} + Y_{hull}\ D_{wing}*Y_{wing} + D_{rear\ wing}*Y_{rear\ wing} + Thrust*Y_{thrust}$ Equation (7)

(480*9.81)*4.2 - 968.5*2.6 - 3938.5*3.69 - 78.1*7.6 + 2139.8*0.45 + 381.8*0.3 + 84*2.4 -2606*1.8 = +**852 Nm.**

Figure 43 shows the plot of the moment coefficient vs. AOA of the WIG hovercraft. Aerodynamic stability was not reached based on the moment calculation on equation 7 since aligning the COL with the COG results in an unstable craft, resulting in a moment of +852Nm.

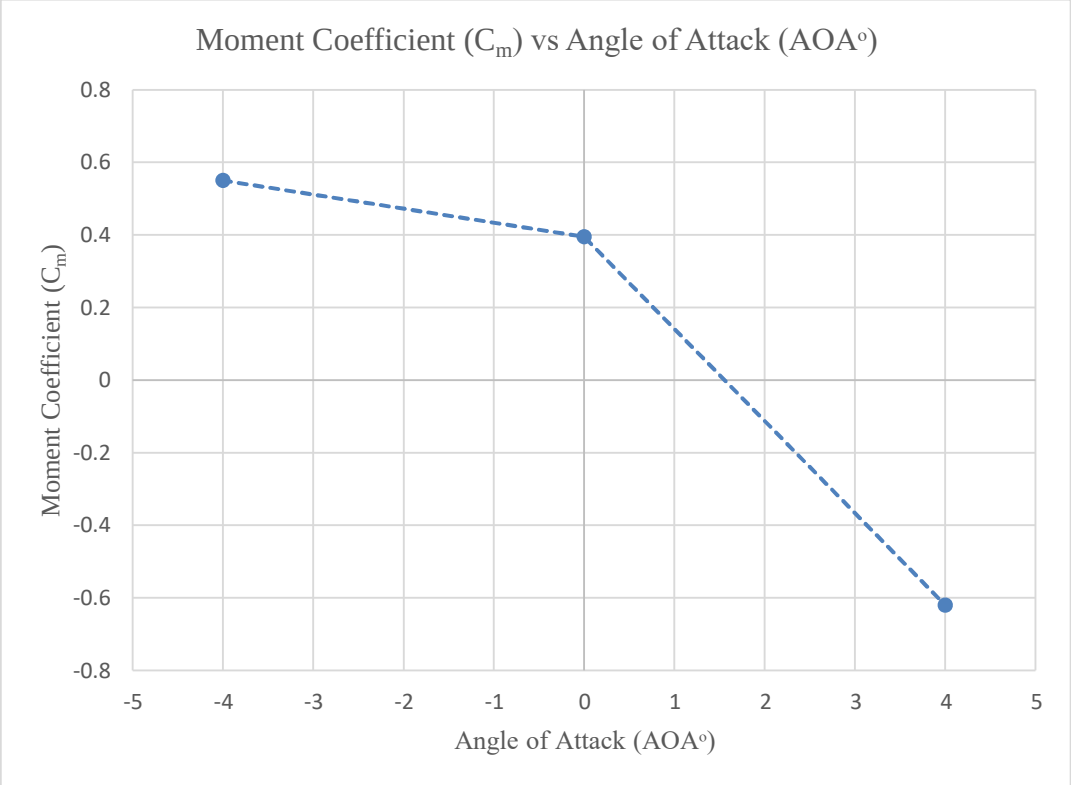

Figure 43: Pitching Moment coefficient (C_m) vs Angle of Attack (AOA°) of the WIG hovercraft with COL= 4.7m

As the COL is moved backward by putting the COG in front of the COL, aerodynamic stability is achieved, resulting in a moment of 0Nm based on the moment calculation in equation 8. This made the new COL position 4.9m from the datum, as seen in figure 44. Tables 18 and 19 show the new lift and drag coefficient results for individual components generated using CFD, that is used to determine the moment of the WIG craft as the COL was placed behind the COG. From the calculation of the moment, aerodynamic stability was achieved.

Table 18: CFD Calculation for COL=4.9m

	C_L	**C_D**
Hull	0.12	0.27
Main Wing	0.52	0.051
Tail Wing	0.011	0.0109

Table 19: Lift and drag forces acting on the individual components of the WIG Craft.

	$X_{Distance}$ (m)	**$Y_{Distance}$ (m)**	**F_L (N)**	**F_D (N)**
Hull	2.6	0.45	946	2070
Main Wing	3.9	0.3	3951	391
Tail Wing	7.6	1.8	86	84

Moment about x=0, y=0. COL= 4.9m from datum

$M = mg * X_{cog} + L_{hull}*X_{hull} + L_{wing}*X_{wing} + L_{rear\ wing}*X_{rear\ wing} + D_{hull} + Y_{hull}\ D_{wing}*Y_{wing} + D_{rear\ wing}*Y_{rear\ wing} + Thrust*Y_{thrust}$ Equation (8)

(480*9.81) *4.2 - 946*2.6 - 3951*3.9 - 86*7.6 + 2070*0.45 + 391*0.3 + 84*2.4 -2545*1.8= **0 Nm**

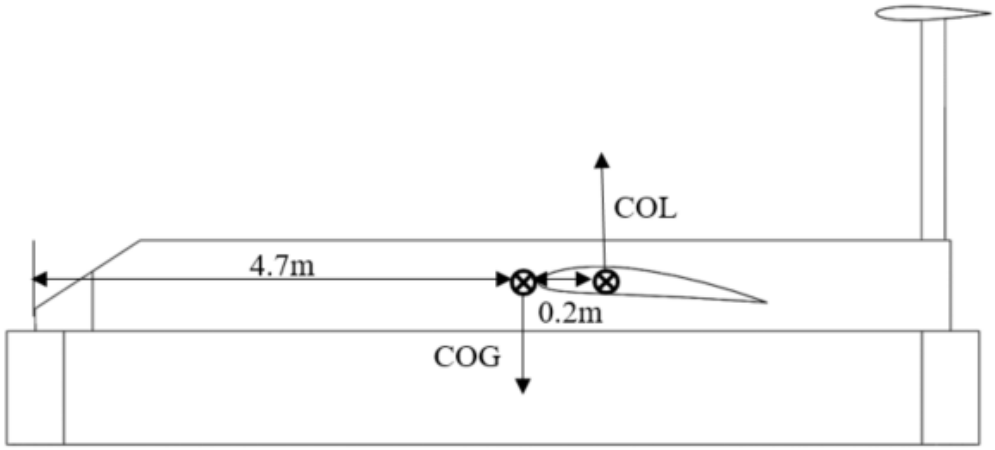

Figure 44: New position of COL (4.9m from the datum)

Figure 45 shows the graph of pitching moment versus angle of attack. The curves show the same trend as the angle of attack increases. The moment will decrease. The moment coefficient shows a positive value between the angle of attack -4° to 0°. At this point, the WIG Hovercraft will tend to pitch the nose upward. After this point, the moment coefficient decreases steadily and becomes negative values.

A negative pitching moment is stabilising. It is a nose-down pitching moment, which is required for static stability. As a result, a negative pitching moment is either nose down or tail up, whereas a positive pitching moment is either nose-up or tail down. The craft pitch is kept at the height of the lowest point of the hull constant (h/c= 0.65, h=1.3m), and the pivot point is towards the bottom edge of the WIG hovercraft.

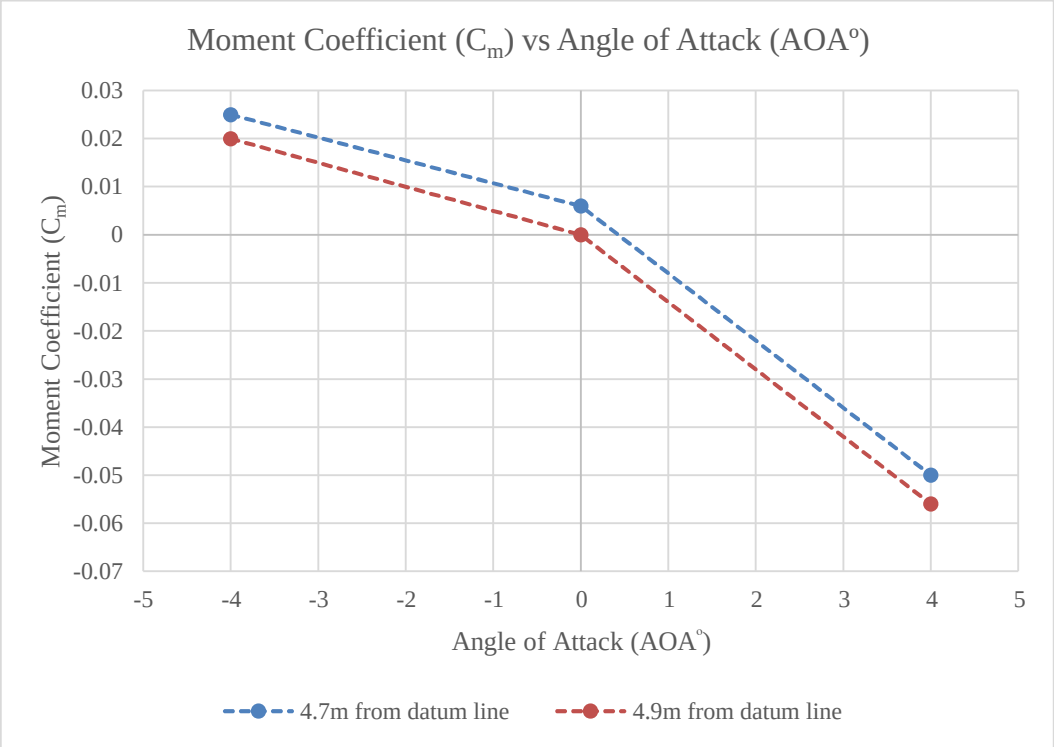

Figure 45: Variation of Moment coefficient (C_m) vs Angle of Attack (AOA°) for WIG hovercraft with change to main wing.

Figure 46 gives a general illustration of the WIG hovercraft model pitching position at an AOA of 2°. Generally, the moment become more negative with increased AOA.

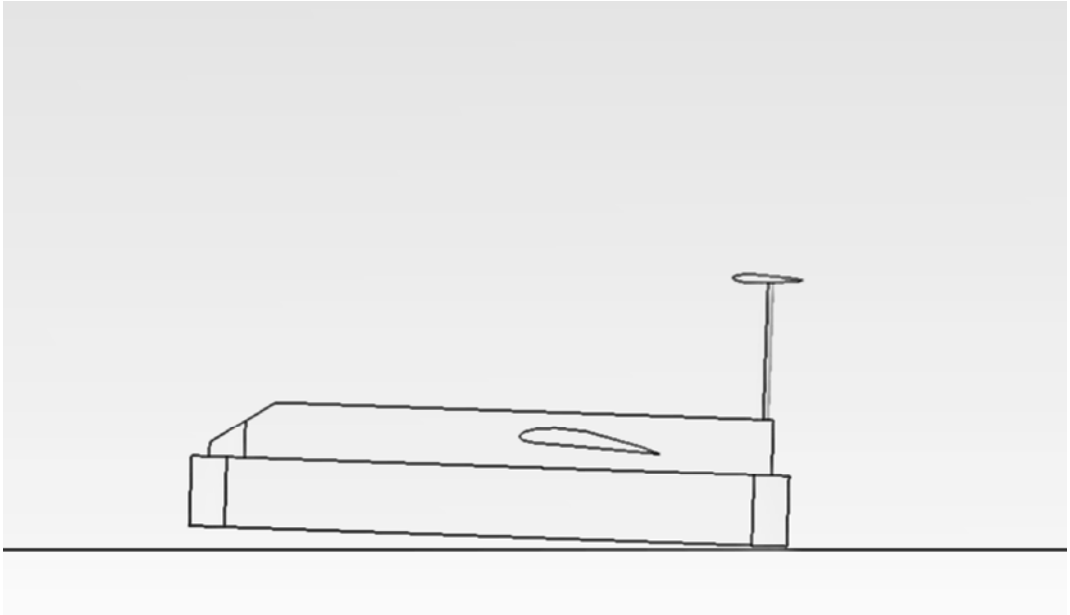

Figure 46: WIG hovercraft Pitched at 2-degree angle of attack

Figure 47 shows that increasing the height to chord ratio increased the pitch moment for the varied angle of attack (AOA). Decreasing the ground clearance increases the lift coefficient and decreases the drag coefficient for varied AOA. Because the bottom surface of the wing has a bigger radius of curvature than the top surface, the pressure gradient increases with the angle of attack. This means the bottom surface will have more pressure

than the top surface, causing the wing to lift. The increase in ground proximity-induced lift was found to be accompanied by an increase in the nose-down pitching moment for AOA > 2º.

On the other hand, the proximity to the ground for AOA< 2º the nose-up pitching moment is higher. Lowering the ground clearance increases the nose-up pitching moment. As AOA increases, lift on the main wing grows more slowly relative to tail lift because the coefficient of lift on the main wing is larger than that on the tail.

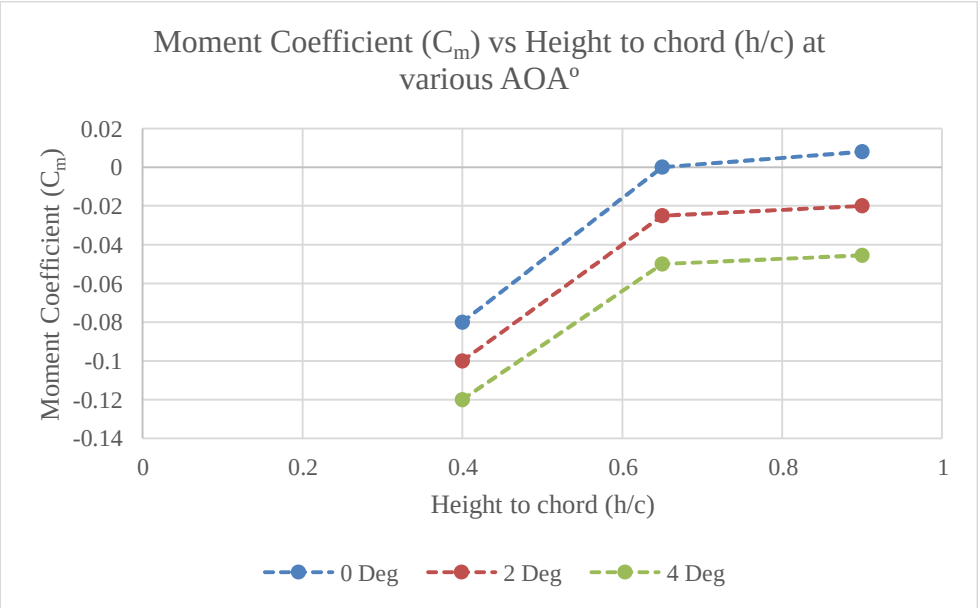

Figure 47: WIG Hovercraft Moment coefficient (C_m) vs height to chord ratio (h/c) at various angle of attack (AOAº).

In addition, C_L increases as the height to chord ratio reduces. Figures 48 and 49 show that, As the WIG hovercraft AOA changes, it produces a large amount of lift and a low amount of drag as it approaches the ground. The pressure on the top of the wing is less than that on the bottom of the main wing. This phenomenon occurs because of the alteration of flow that occurs due to proximity to the ground leading to an increase in lift coefficient and a corresponding decrease in drag coefficient as the angle of attack increases.

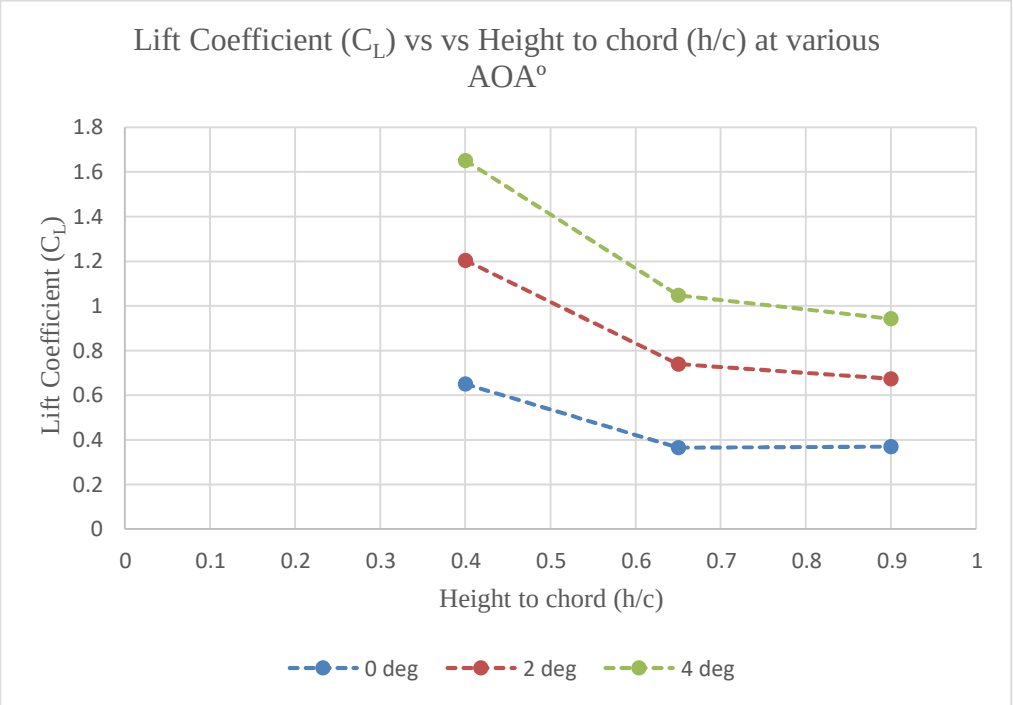

Figure 48: WIG Hovercraft C_L vs h/c at various AOA

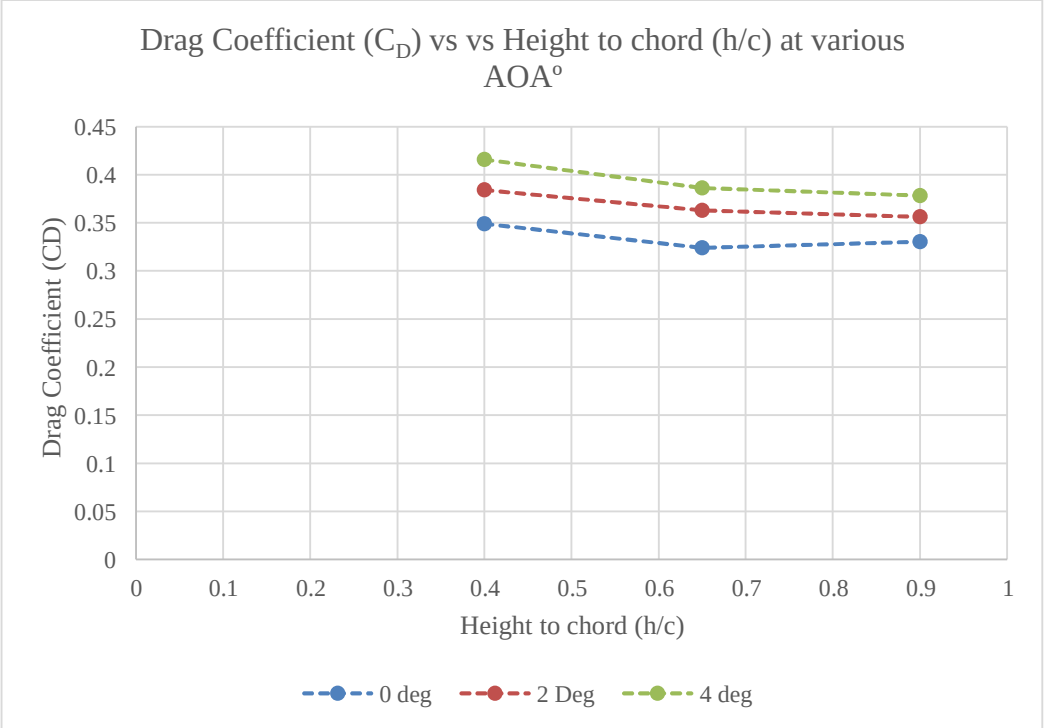

Figure 49: WIG Hovercraft C_D vs h/c at various AOA

From the calculation, the effect of the wing area and distance from the ground is investigated to determine the amount of lift generated by the craft. “h” is the distance from the ground to the trailing edge of the aerofoil as it is attached to the hovercraft and “c” is the chord length of the wing. “V” is the velocity required to lift the craft. Table 20 shows a Comparison of different height to chord ratios (h/c) based on skirt size. Figure 50 shows the

sizes of the skirts. As the height to the ground reduces, the lift coefficient increases and drag decreases as a result of the ground effect.

Table 20: Effect of ground clearance on the craft, with a constant chord length of 2m and span length of 6m

Skirt size	Height (h)	h/c	C_L	C_D	C_L/C_D	V (m/s)
Big	1.8m (A)	0.9	0.464	0.4048	1.14	34
Medium	1.3m (B)	0.65	0.7048	0.347	2.03	28
Small	0.8m (C)	0.4	0.9684	0.33446	2.895	25.16

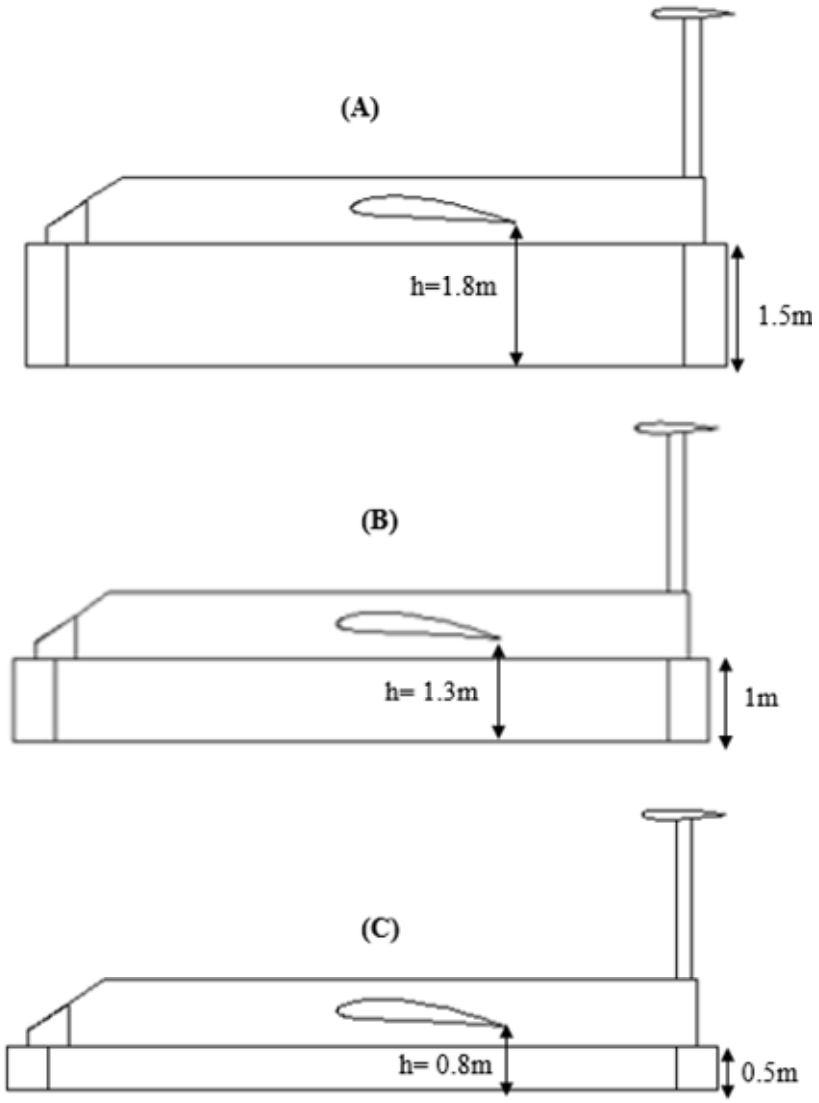

Figure 50: Various Skirt sizes with a constant chord length of 2m and span length of 6m

From equation 6, the velocity required to lift the WIG hovercraft was analysed against the h/c. The relationship between the height of the wing and the required velocity to lift the craft is shown in table 20. This shows that the lower the wing of the WIG hovercraft gets to the ground, the lower the velocity required to lift the craft reduces and vice versa. This graph shows that the required speed to lift the hovercraft depends on the ground's distance.

In table 20, the effect of velocity required to lift the craft is evaluated and plotted in figures 51 and 52, which show the lift and drag coefficient vs. required velocity to lift the individual components of the WIG hovercraft. The overall lift and drag coefficient are plotted by combining the individual components (the hull and wing), giving a higher overall lift and drag coefficient. According to the plots, the relationship between the effect of the ground and the velocity required is evaluated against the lift and drag coefficients, and it reveals that as the WIG hovercraft gets closer to the ground, less speed is required to lift the craft as a result of the ground's vicinity. At h/c of 0.4, the speed required to lift the vehicle is 25.16m/s, resulting in a higher lift coefficient of 0.96 due to the ground effect, and hence less fuel is consumed. When the h/c is 0.9, the speed required to lift the vehicle is 34m/s, with a lower lift coefficient of 0.464 and higher fuel consumption. Therefore, this indicates that the closer the craft gets to the ground level, the less the velocity required to produce the lift and vice versa. As the air flows over the wing, it also flows over the entire assembly structure, increasing pressure and causing the lift. This is observed in the overall lift coefficient of assembled components. The pressure difference increases as the wing get closer to the ground, resulting in less speed required to lift the vehicle.

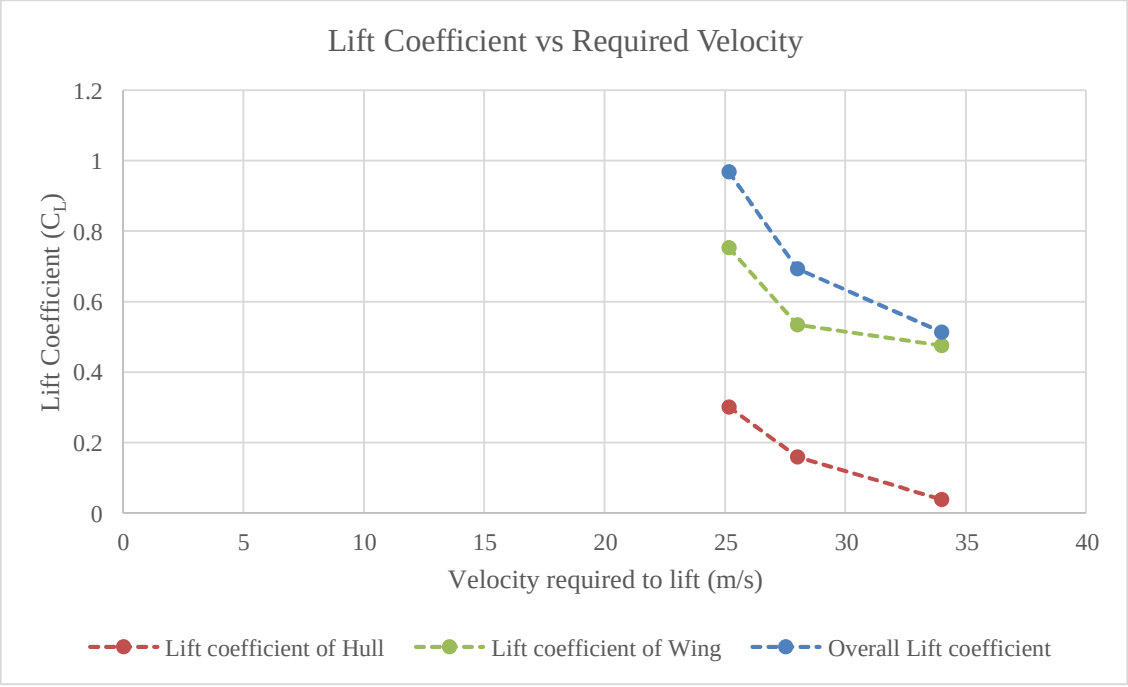

Figure 51: Lift coefficient vs velocity to required lift individual components

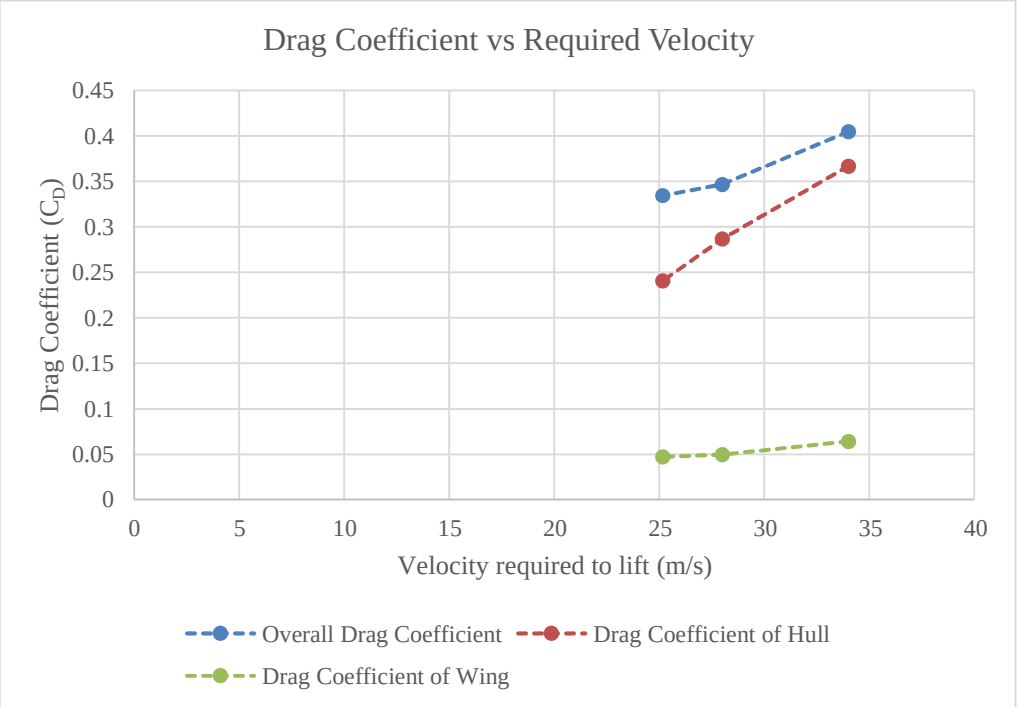

Figure 52: Drag coefficient vs velocity required to lift individual components

Table 21 compares the NACA 4412 wing with a constant "h" of 1.3m and its effect on the lift and drag coefficient. Figure 53 to 56 shows the diagram for the cases. The effect of the lift and drag coefficients is analysed from the table. Wings 1 and 2 had the same chord length and different span lengths. As the span length increases, the aspect ratio increases, causing an increased lift coefficient and a further reduction in the drag coefficient. While wings 3 and 4 had the same chord length and variation in span length. As the span length increases, the aspect ratio also increases, causing an increased lift coefficient and a further reduction in the drag coefficient. Furthermore, the height to chord ratio is affected by the increase in chord length for different wing cases, as wings 1 and 2 had a h/c of 0.65 while wings 3 and 4 had a h/c of 0.43 which causes an increase in lift coefficient for the lower h/c wing.

Table 21: Comparison of increased chord and span with h=1.3m

	Chord (c)	**Span (b)**	**h/c**	**Aspect Ratio**	**C_L**	**C_D**	**C_L/C_D**
Wing 1	2m	6m	0.65	3	0.7048	0.347	2.03
Wing 2	2m	9m	0.65	4.5	0.9757	0.3309	2.95
Wing 3	3m	6m	0.43	2	0.7441	0.3358	2.215
Wing 4	3m	9m	0.43	3	1.149	0.3225	3.6

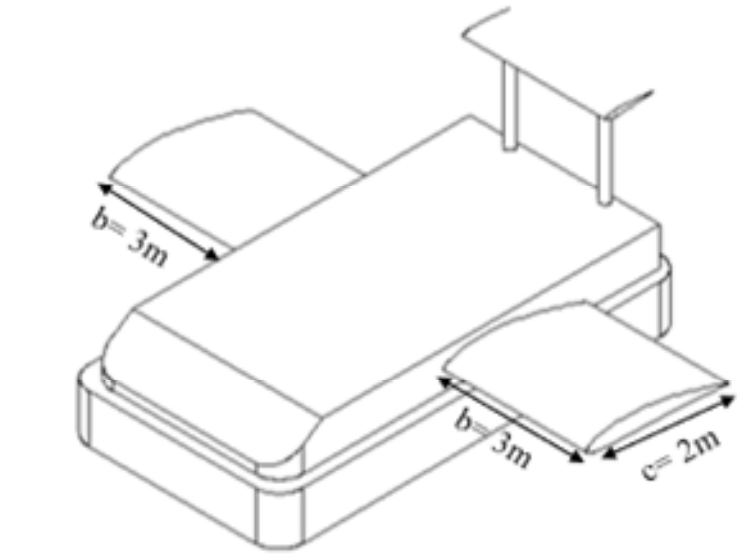

Figure 53: Wing 1- Chord (2m) and Span (6m)

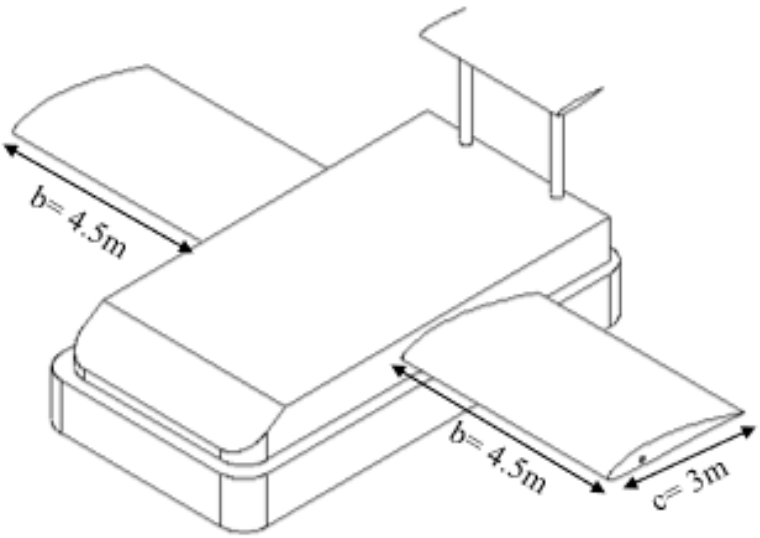

Figure 54: Wing 2- Chord (3m) and Span (9m)

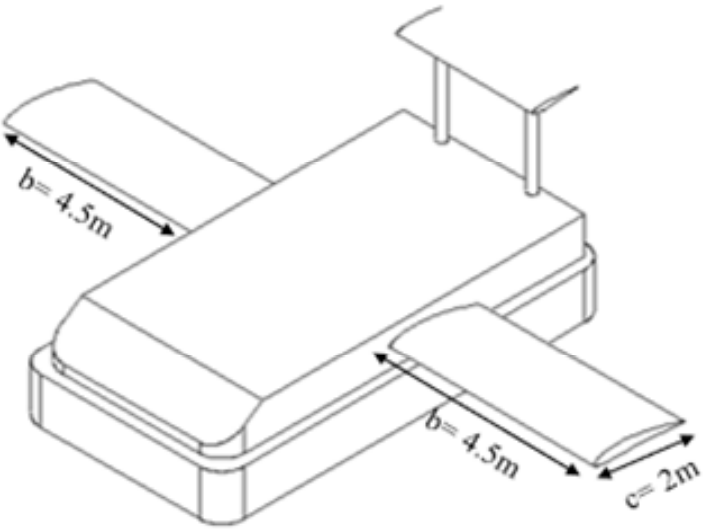

Figure 55: Wing 3- Chord (2m) and Span (9m)

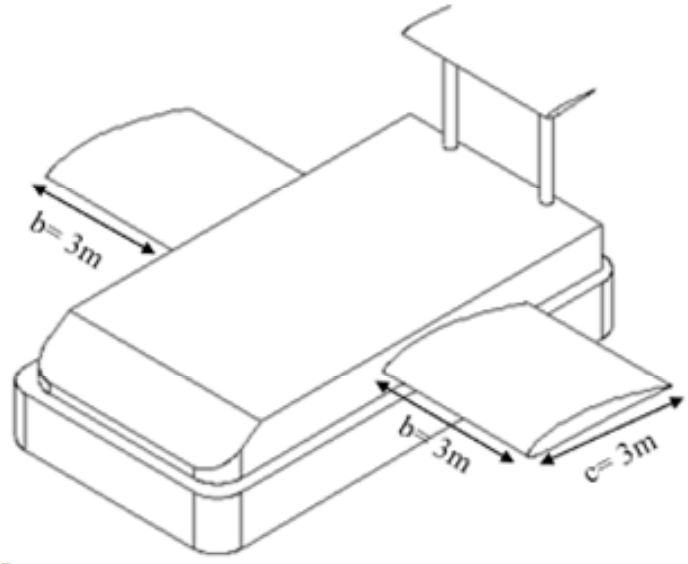

Figure 56: Wing 4- Chord (3m) and Span (6m)

From the analysis of Tables 19 and 20, it can be said that the h/c and aspect ratio influences the WIG hovercraft's aerodynamic performance. Table 19 showed that reduction of the h/c causes an increase in lift coefficient due to ground effect. In table 20, as the chord length was the same for wings 1 and 2, the aspect ratio differed due to the change in span length. This led to an increase in lift coefficient for the wing with a higher aspect ratio of 4.5 compared to the wing with an aspect ratio of 3. While wings 3 and 4 showed similar attributes to wings 1 and 2. As the aspect ratio increased, the lift coefficient and the drag coefficient decreased. Hence, the higher the aspect ratio, the more efficient the wing is, which means more wingspan and less lift-dependent drag. A higher aspect ratio at the same angle of attack also means more lift coefficient (within limits). Thus, this analysis agrees with the literature studies showing an increase in the aspect ratio. The lift coefficient and ground effect depend on the height above the ground [86].

3.4 DETAIL DESIGN AND ANALYSIS OF WING-IN-GROUND EFFECT HOVERCRAFT.

From previous research on hovercraft analysis, the WIG hovercraft investigated in this study adopted the design method to meet the search and rescue hovercraft criteria. The designed Wing-In-Ground (WIG) effect hovercraft should be able to support the primary structural and subsystem loads, as well as offer space for on-board components. It was assumed that the WIG hovercraft would be used for search and rescue operations in aquatic bodies and could transport loads of up to 625 kg over shallow water, tidal terrain, and dry ground. The WIG hovercraft shape was adopted using Royal National Lifeboat Institution (RNLI) data. It was assumed to have a total weight of 1105 kg, the hull weighed 480kg, and the tail assembly was assumed to weigh 45 kg. Based on the average weight of a male human

being, the passengers/crew weigh 320 kg (4x80 kg pp), and the weight of on-board items, including first aid kits, cabin tools and equipment, luggage, engine frame, and fuel tank is assumed to weigh 60 kg. The thrust engine weighs 115 kg, while the lift engine weighs 85 kg. The vehicle will be able to carry the pilot, crew members, and people in distress for a search and rescue service. It will also require storage for first-aid kits, fluids, and glides on the water surface for 4 hours over an 80-kilometer range at a speed of 30m/s, as well as ground effect heights varying from 0.5 to 5 metres. The following design method is examined to meet these criteria [87 - 89].

Based on the design considerations, the summary of the WIG hovercraft design parameters is shown in table 22. The estimate of crucial parameters and sizing of major hovercraft components are part of the design for an integrated wing-in-ground effect hovercraft. The higher surface area for effective cushion pressure determines the vehicle's length (l). The longitudinal and transverse stabilities of hovercraft will be affected when the length to width ratio is greater than half and lesser than half, respectively. For better stability, the vehicle's width (w) is set as half of its length. The plenum chamber lies between the top and bottom surfaces of the hull, whose height is called hull depth (h_D). The condition of water in the operating environment and the obstacles present in water, such as rocks, waves, and tides, must be considered while determining cushion clearance (h_C). The gap which allows the excess air to escape from the cushion region to produce lift is the hover gap (h_G), and it helps the vehicle to be in hover condition. The hover gap is controlled by the pressure built inside the cushion region. The height of the hovercraft (h) is measured from the bottom of the skirt to the top surface of the hull. The effective region at the bottom of the hull is considered a cushioned area (A_C) which differs from the top surface area of the vehicle. The amount of weight lifted by a hovercraft determines the cushion pressure (P_C) to be produced, which is directly proportional to the vehicle's total weight. The stagnation of flow inside the plenum chamber and skirt will produce the bag pressure (P_B), which is higher in value than cushion pressure. These assumed calculations were adopted from previous research on hovercraft design parameters [90].

Table 22: Calculation of WIG hovercraft design parameters [90, 91]

Design Parameters	Empirical Relation	Value
Weight of Hovercraft (W)	m*g= 1105*9.81	10840N
Operating speed(m/s)	-	30m/s
Length (l)	-	8m
Width (w)	$w=l$*0.5	4m
Hull depth (h_D)	$h_D= l$*0.1	0.8m
Cushion clearance (h_C)	$h_C= l$*0.07	0.56m
Assumed Hover gap (h_G)	-	0.013m
Hovercraft height (h)	$h= h_D+ h_C$ - h_G	1.347m
Cushion Area (A_C)	$A_C = l_b*w_b$	32m^2
Cushion Pressure (P_C)	P_C= W/ A_C	338.75N/m^2
Air escaping velocity (V_e)	$V_e=\sqrt{2P_c/\rho}$	23.5m/s
Air escaping area (A_e)	$A_e= (2l+2w)\ h_G$	0.312m^2
Escaping air flow rate (Q_e)	$Q_e= A_e*V_e$	7.3m^3/s
Power required (P_r)	$P_r= \frac{Q_e*\rho*V_e^2}{2}$	2.5Kw
Bag pressure (P_B)	$P_B= P_C$*1.2	406.5N/m^2
NACA 4412 chord length (c)	-	2m
NACA 4412 span length (b)	-	6m
Wing model aspect ratio	AR= $\frac{Chord\ length\ (c)}{Span\ length\ (b)}$	3

M-mass of the hovercraft; w-width of the hovercraft; l-length of the hovercraft; ρ- air density; h-hovering height.

Conditions such as hull length, width, air gap, and gross mass weight of the craft were entered into the hovercraft calculating software to assist with fan selection, as shown in figure 57. This software was also used to validate the calculations from table 21.

Approximate lift perimeter	(m)	23.99934	(ft)	78.738
Total hover gap area	(m^2)	0.311984	(sq. ft.)	3.358175
Total cushion area	(m^2)	31.99823	(sq. ft.)	344.4262
Cushion pressure	(N/m^2 = Pa)	338.6536	(lbs/sq. ft, PSF)	7.072923
Cushion pressure	(mm of water @ 4degC)	34.53398	(inches of water @ 60degF)	1.360928
Expected actual air velocity	(m/sec)	14.26464	(ft/sec)	46.8
Lift air volume	(m^3/sec)	4.450349	(CFS)	157.1625
Estimated lift engine power	(kW)	2.511807	(HP)	3.368479
Estimated fan diameter	(m)	0.861037	(inches)	33 29/32

Figure 57: Hovercraft calculator [91]

3.4.1 Fan Selection

Figure 58 shows the breakdown of the impeller part number code that would be used in this study integrated hovercraft to provide both lift and thrust. The size of the impeller, the number of blades, the pitch angle of the blade, and the power required are some of the most important factors to consider when choosing an impeller. The power source (in this

case - the engine) should provide enough power to run the impeller under the required operating conditions. Industrial fans are commonly employed for this purpose.

This study requires a pressure of 339 N/m2 (Pa) and airflow of 7.3m3/s. The Multi-Wing Optimizer database was used to provide the specification of the impeller chosen for the WIG hovercraft [92].

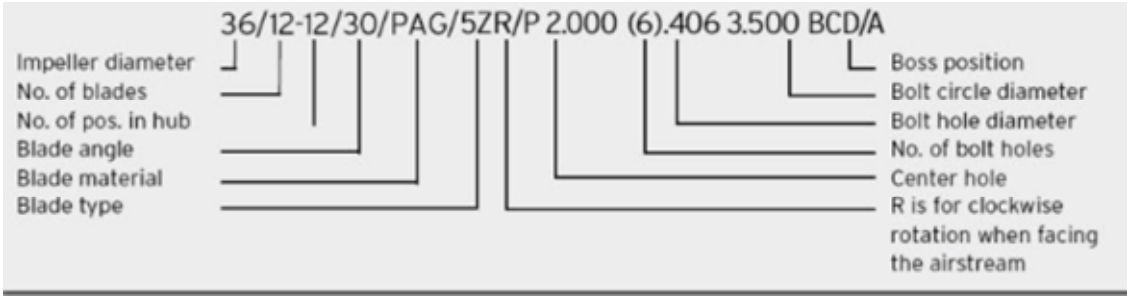

Figure 58: Z- series impeller part number code breakdown [92]

The following design and modelling parameters were chosen for the final design based on the results and analysis described in earlier chapters.

3.4.2 Solution

Ansys Fluent was used to simulate the WIG Hovercraft in flying conditions with ground to the surface of the WIG craft is 0.05m for ground effect height. The coupled pressure velocity scheme was adopted since it converges faster than the simple system. For a more accurate result, a second order upwind approach was used on momentum, turbulence kinetic energy, and turbulence dissipation rate special discretization for five hundred iterations.

3.4.3 Geometry

Solidworks was used to create the WIG hovercraft, which was then loaded into the Ansys design modeller. The model's overall length is LOA= 8.5m, the overall width is WOA= 4.5m, and the overall height is HOA= 4.2m. To keep the simulation process simple, a propulsion fan to propel the WIG hovercraft forward is not included in the simulation as only the main WIG body was considered. The primary wing was a NACA 4412 with chord and span lengths of 2m and 6m with an initial angle of attack of 5°. The horizontal tail wing (NACA 0012) was designed to be 1m long and 3m wide. The design considered adding the windshield to protect the drivers from facing the high wind speed. The geometry of the WIG Hovercraft model is shown in figure 59.

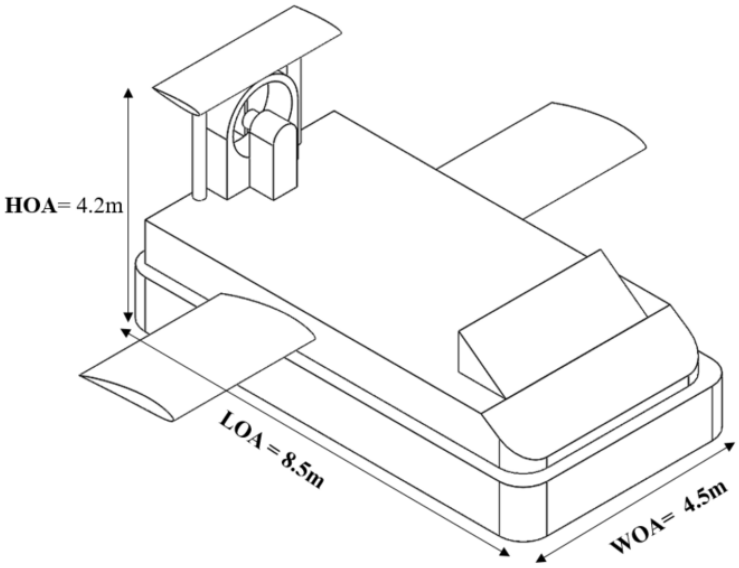

Figure 59: WIG Hovercraft Model

3.4.4 Domain and Boundary Condition

A previous study on CFD domain size has suggested a minimum length of 5 times the body's dimension along the flow direction to enable enough space for the boundary condition imposed at the domain outlet. Similarly, it is recommended to leave nearly double the body's width on each side to allow for local flow deviation [93].

The solution domain was configured to be as long as 10 model lengths, as wide as 6 model widths, and as high as 5 model heights. The model was placed 5m from the velocity inlet with the height from the bottom domain to the wing as 1.3m. The velocity inlet was set to 5m from the front point of the WIG model, with an air velocity inlet of 30m/s and a turbulence intensity of 1%. The pressure outlet is positioned 70m behind the aft point of the WIG hovercraft model, with an outlet pressure of 0 Pascal and a backflow turbulent intensity of 5%. No-slip wall condition was assigned to the WIG hovercraft model and the bottom plane of the domain. The domain's side and top boundaries were designated symmetry and wall, respectively. Figure 60 displays the simulation domain and boundary conditions.

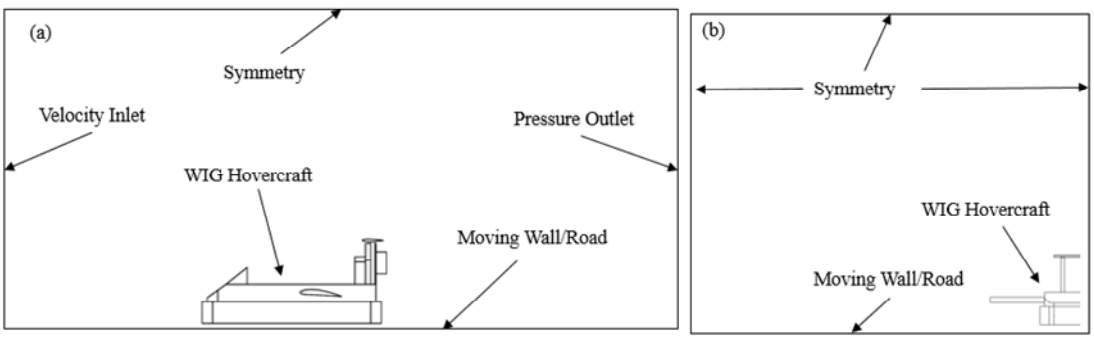

Figure 60: WIG Hovercraft domain and boundary conditions (a) Side View (b) Front View

3.4.5 Mesh, Turbulence Model and Validation

In this simulation, three mesh configurations were evaluated. From a previous literature survey, decreasing the size of the mesh attached to the surface may increase accuracy but require more memory and time [93]. As a result, an optimal mesh number for the simulation process is necessary to provide an accurate result while consuming less time and memory. To determine the result dependency on mesh amount, coarse mesh with less than 0.7 million meshes, fine mesh with more than 0.7 million but less than 4 million meshes, and finest mesh with more than 4 million meshes were simulated and tested. Thus, fine mesh with a mesh number of more than 0.7 million was chosen for the simulation process as it gives almost accurate data as those with more than 4 million meshes. As seen in table 23 and figure 61. Mesh independence tests were run using the SST k-ω turbulence model, which consists of tetrahedral mesh.

Table 23: Variation of lift coefficient with different mesh number

Mesh Number	**(A) Coarse Mesh**	**(B) Fine Mesh**	**(C) Finest Mesh**
Number of Elements	664655	3393856	4647125
No of Nodes	119896	1081034	1419012
Lift Coefficient (C_L)	0.6492	0.6510	0.6512
Drag Coefficient (C_D)	0.328	0.332	0.334

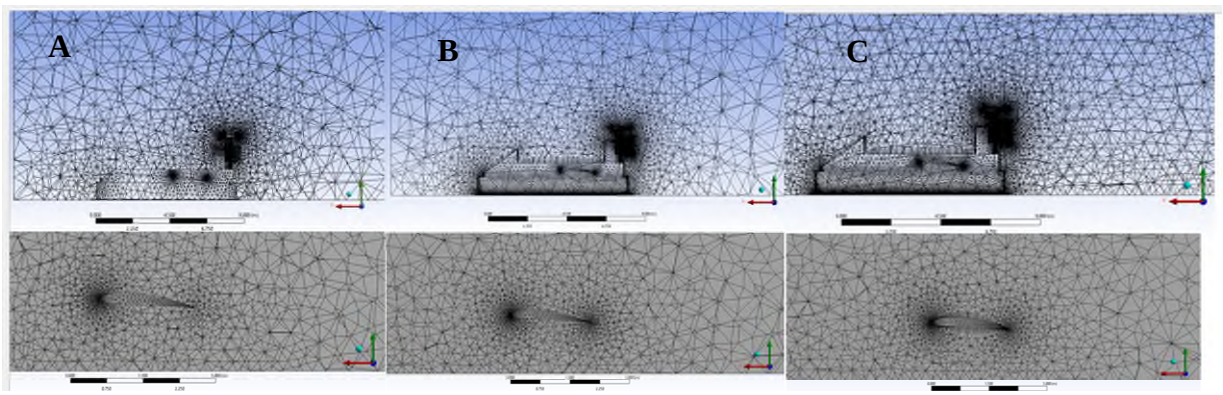

Figure 61: Mesh quality (a) Coarse, (b) Fine Mesh, (c) Finest Mesh

Figure 62 depicts the fluid (air) pressure contour around the WIG hovercraft model body at 0^o pitch. Pressure is higher at the bottom of the WIG hovercraft model body and wing than at the top. This indicates that the fluid velocity below the WIG model travelled slower and almost stagnated while creating lift force upward. The pressure contours indicate a high-pressure region formed along the thickness of the platform's front face. As a result, the sloped front is projected to allow the installation of the lifting fan with a maximum flow

rate. Lifting power is generally determined by the mass rate and momentum change of the airflow beneath the WIG hovercraft body. As a result, the fan inlet should be positioned in the high-pressure areas near the front stagnation point to maximize lifting power. This is required to provide a high-pressure air cushion beneath the body in comparison to the pressure on the body's upper surface.

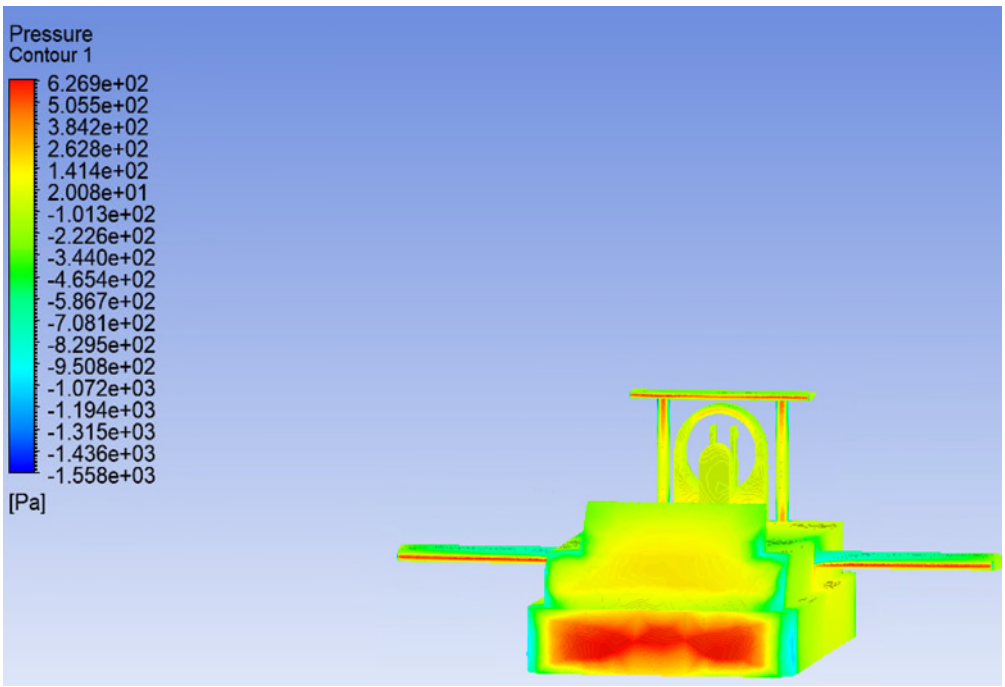

Figure 62: Pressure contour around the WIG Hovercraft

The important parameters in aerodynamics are based on the pressure and, therefore, forces generated on the body. The velocity domain around the WIG hovercraft is directly linked with the pressure domain. In the present incompressible flow, the high-velocity regions generate low pressure and vice versa. Therefore, the pressure contours are generated in the post-processing of the present study to show the pressure acting on the WIG hovercraft.

3.4.6 Modelling

The CAD model depicted in Figure 63 is used to perform CFD analysis to examine the vehicle's flow characteristics. The WIG hovercraft body is imported into the Ansys workbench. The body is taken as a computational domain to simulate the flow beneath the skirt, and the edges of the domain are set as boundary limits for the CFD analysis. The domain's side and top boundaries were designated symmetry and wall, respectively. The gap between the bottom of the skirt and the ground is specified as a flow rate boundary condition to simulate the external flow of the skirt. Table 24 shows boundary condition for how the design and modelling parameters for analysing the flow around the WIG hovercraft body was determined based on the results and analyses given in previous chapters.

Table 24: Boundary Conditions

Boundary Condition	Description
Moving Wall	No-slip wall moving at the free stream velocity of 30m/s in +ve x-direction
Aerofoil surface	Stationary wall with no slip condition
Top and Side walls	Symmetry
Velocity inlet	Inflow velocity of 30 m/s
Pressure Outlet	Absolute static pressure
Mass flux rate	Pressure boundary to generate the flowrate underneath the skirt.

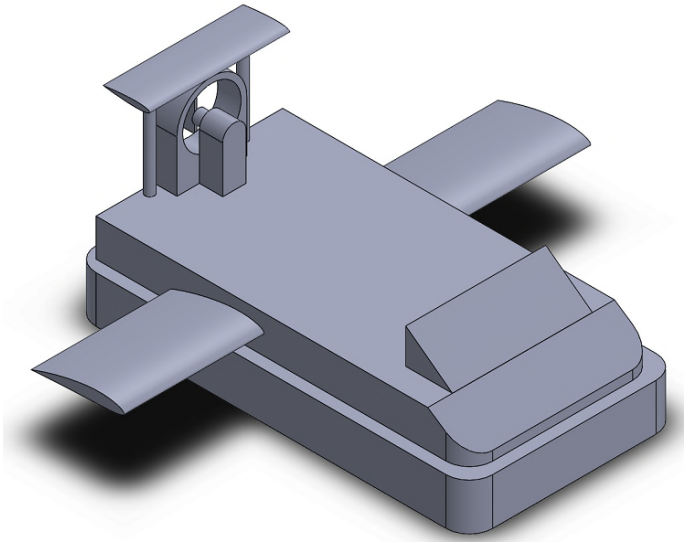

Figure 63: Isometric views of WIG hovercraft

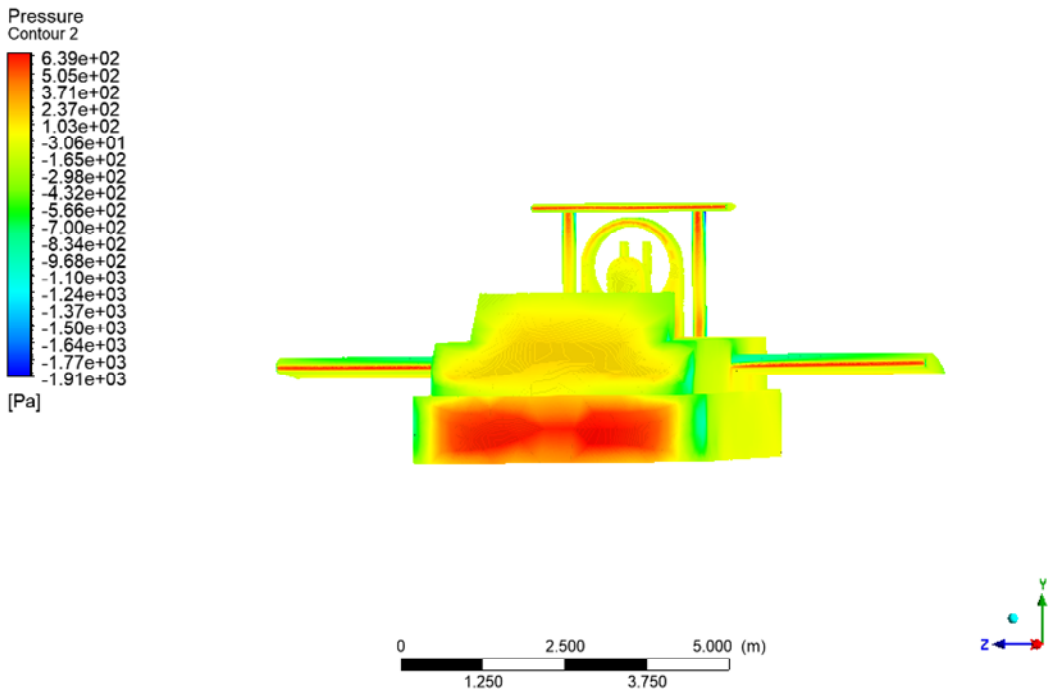

Figure 64: Pressure distribution around the WIG hovercraft with flowrate boundary condition

Figure 64 shows the pressure distribution around the WIG hovercraft with a pressure boundary applied underneath the skirt to generate the flowrate. The CFD analysis is performed in ANSYS Fluent post processor, and the results predicted a pressure rise inside the skirt region and generated a mass flux rate of 6.4kg/m^2/s, as seen in figure 65.

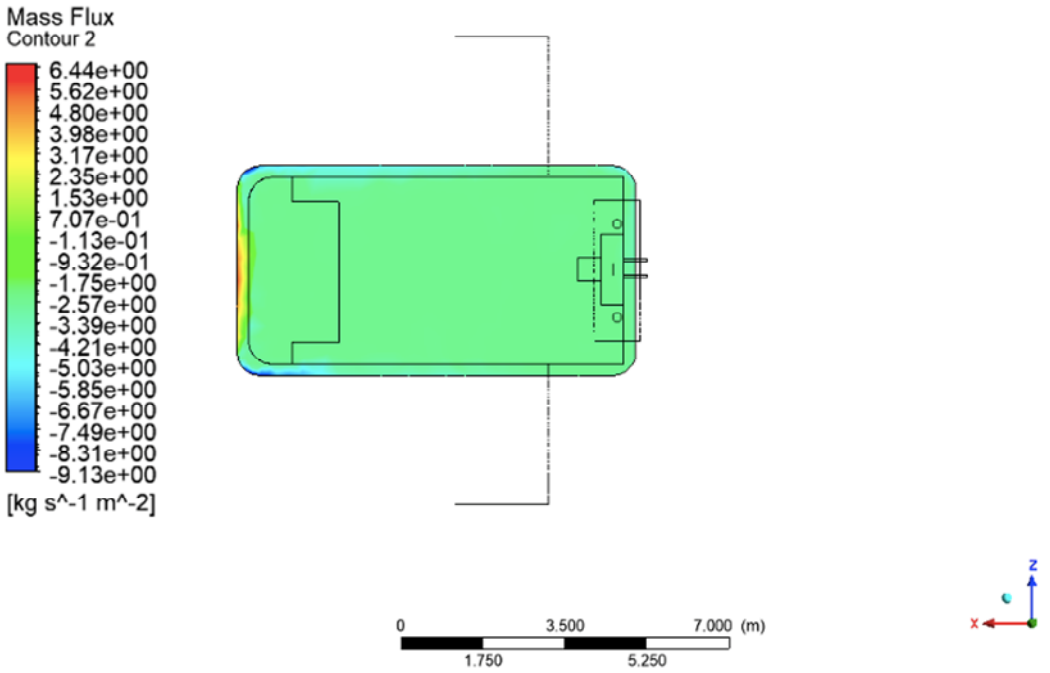

Figure 65: Mass Flux Rate

As the flux rate is positive, the fluid (air) flows outward of this region as a result of forward motion. The velocity of escaping air is obtained in this location, as seen in Figure 66, and the fluid (air) flows out from the front of the skirt, with an outflow of 365Pa. As a result, the pressure difference is created by the pressure differential between the model's front and rear faces, which results in an increase in pressure and flowrate. There is pressure loss underneath of the craft. In other words, air flows out from that region.

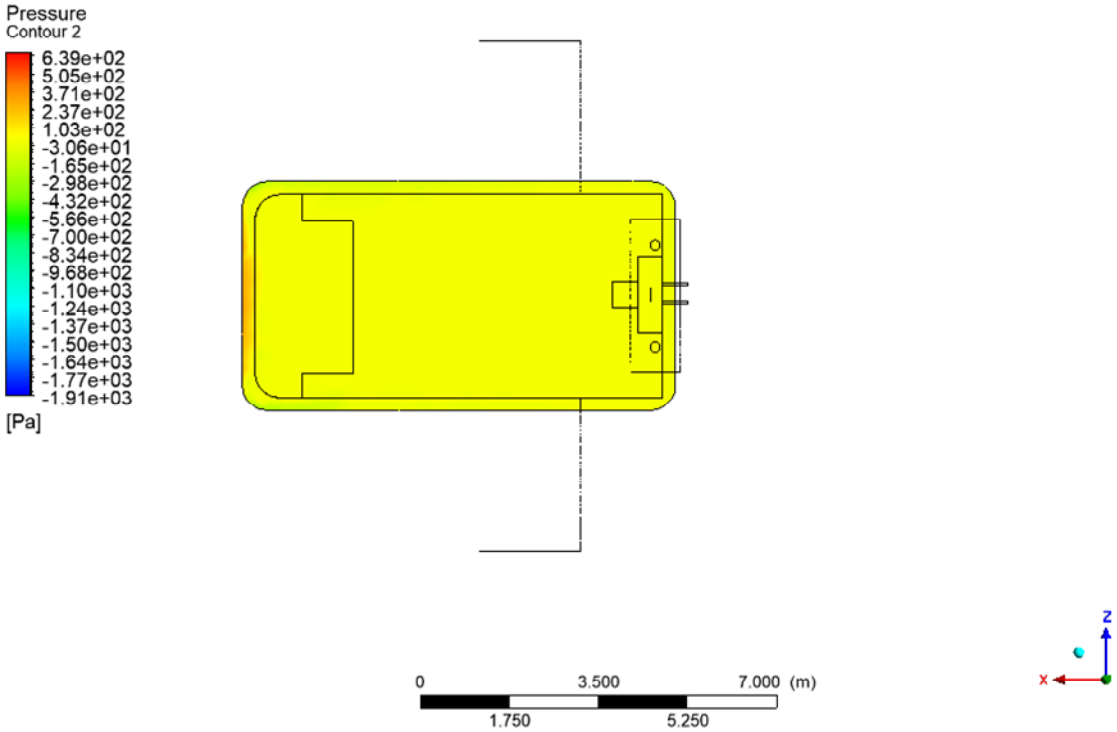

Figure 66: Pressure contours underneath the skirt flowrate boundary

3.5 ETHICS AND LIMITATIONS

Both COVID-19 and the cyber-attack caused disruptions to the original work plan. The lack of access to both computational and experimental resources for an extended period warranted significant amendments to the original plan. It was not deemed feasible to complete practical work within the available time frame and therefore removed from the work plan. Ansys workbench software was used to validate computational results against data from the literature. It has been widely used in the literature studies from previoue researchers for the simulation of wing-in-ground effect crafts.

Chapter 4: Results and Discussion

From the simulations, the pressure loss over a wing's top surface is greater than the pressure loss over the wing's bottom surface. As a result, there is an upward (positive) net pressure force. This pressure force is the lift force. In this research, several wing designs have been analysed to compare their performance efficiency based on the lift coefficient ratio to drag against an increase in the angle of attack. The NACA 4412 has a greater efficiency as compared to the NACA 0012 and DHMTU 12 wing design with the same chordal length of 2m and span length of 6m, as seen in figure 67.

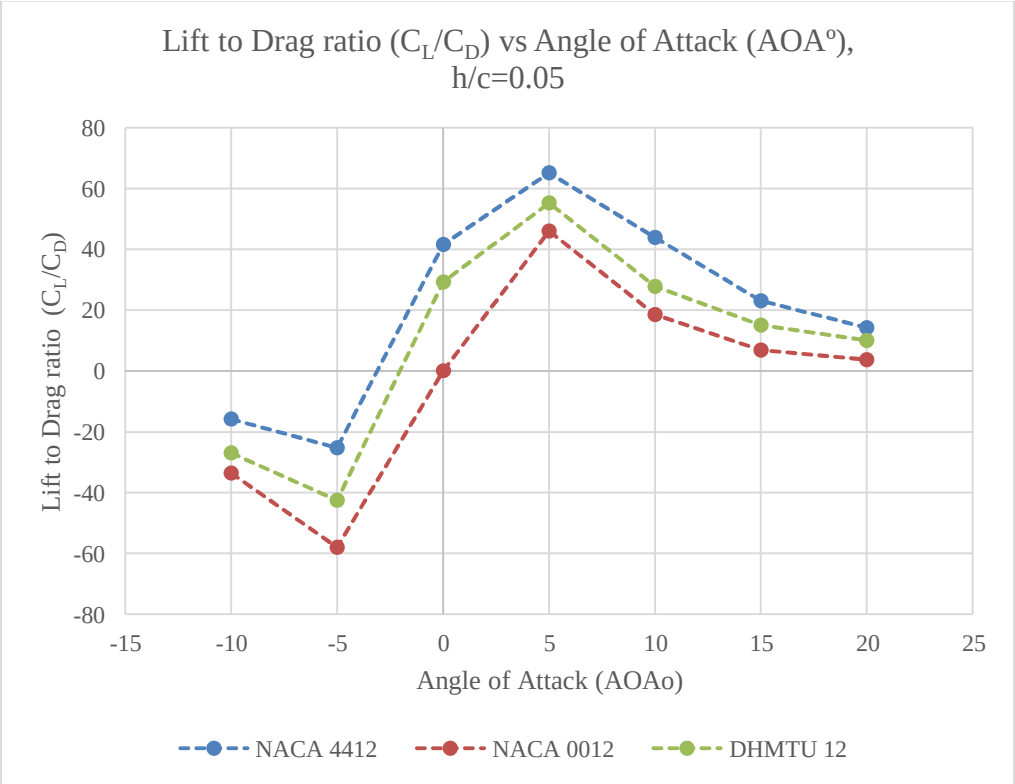

Figure 67: Lift to drag ratio (C_L/C_D) vs Angle of Attack (AOA°) of different classes of aerofoil. (AR = 3)

Figure 68 shows the lift coefficient versus angle of attack for the isolated NACA0012 in ground effect and the tail wing, which is 3.8m above the ground ranging from -5 o to 5° AOA. The diagram shows that as the angle of attack increases, the lift coefficient increases and vice versa for both cases. The Isolated wing produces a higher lift than it is in ground effect, which was expected.

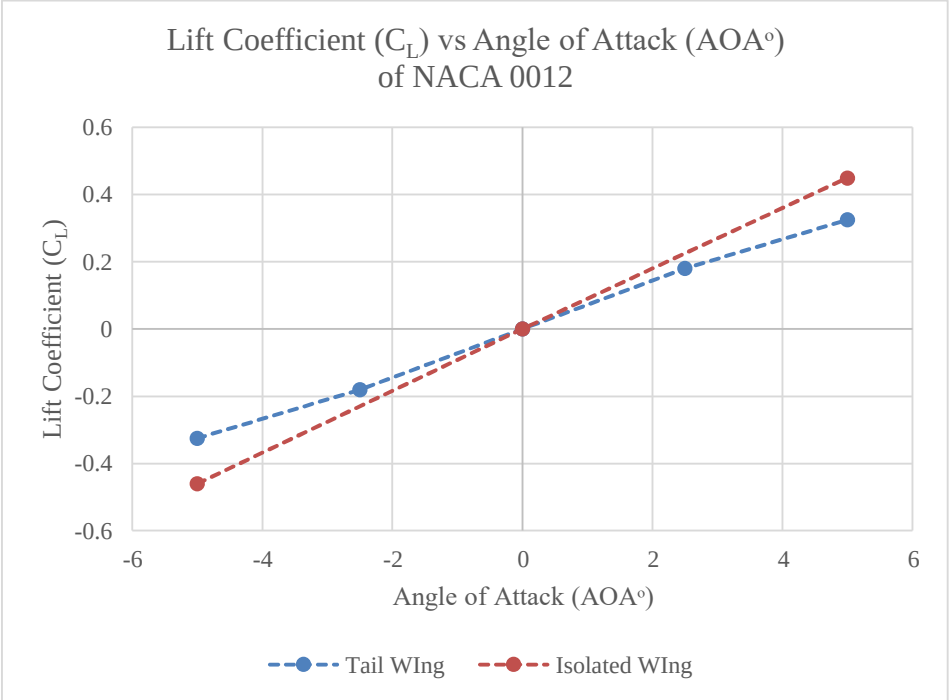

Figure 68: Lift Coefficient vs Angle of Attack Tail Wing and Isolated wing (AR =3).

4.1 SOLID SKIRT VS HOLLOW SKIRT

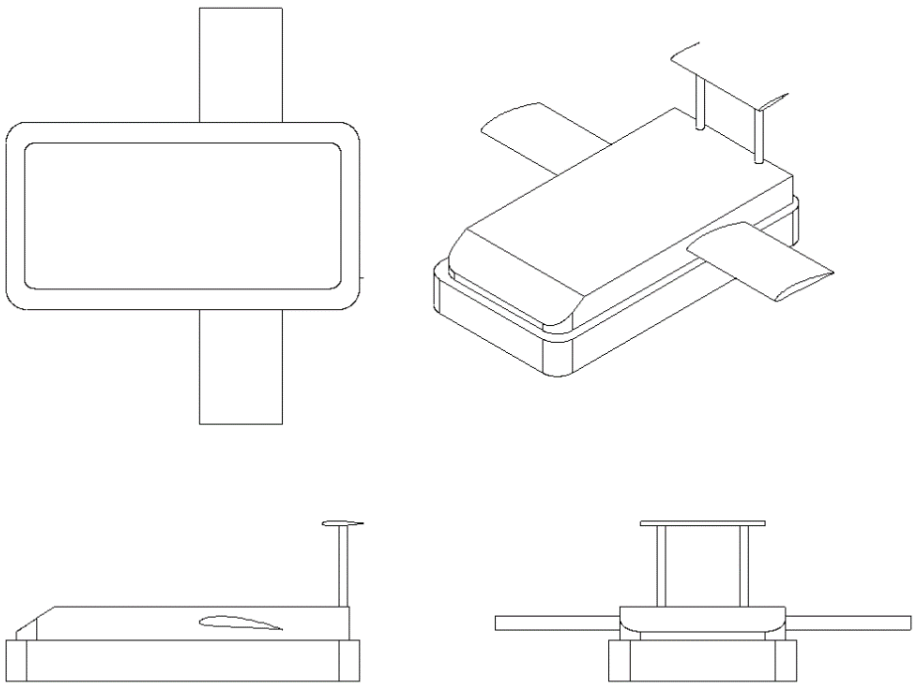

Figure 69: Orienting views WIG hovercraft with Hollow Skirt with h/c = 0.65

Figure 69 shows the orienting views of the WIG Hovercraft with a hollow skirt with a hollow depth of 0.5m. Figure 70 & 71 shows the comparison of coefficients of moments and lift for a hollow skirt and solid skirt. The figures show similar trends to the previous figures mentioned above, but the solid skirt tends to generate more lift than the hollow skirt because there is no hollow shape beneath the skirt. As the fluid (air) that flows across the hollow skirt is slower compared to the solid skirt, which results in the difference in lift coefficient.

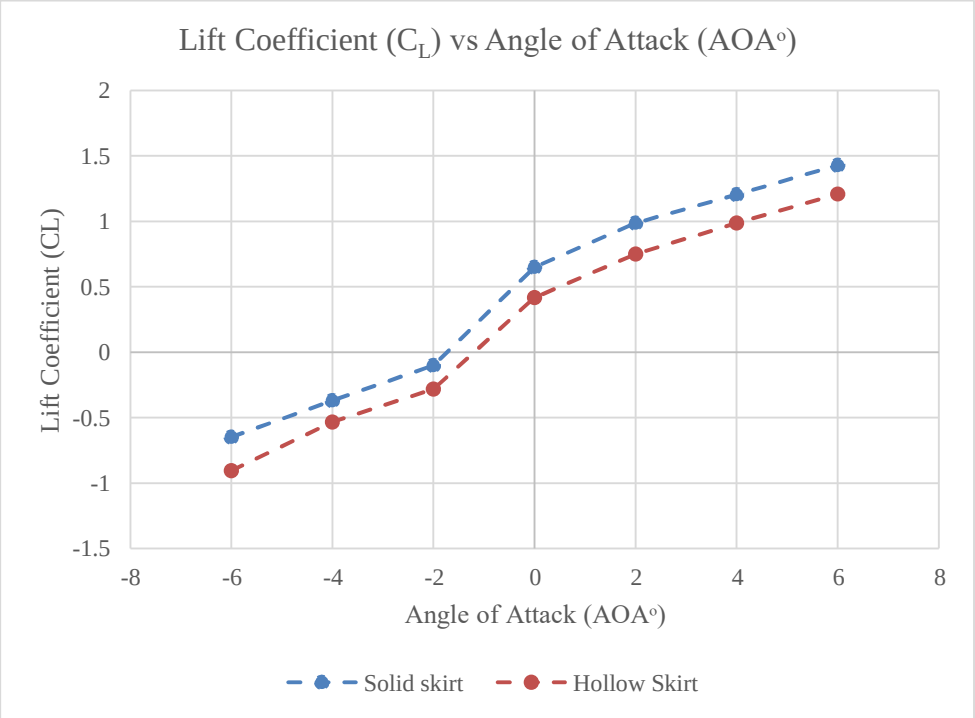

Figure 70: Lift coefficient (C_L) vs Angle of Attack (AOA°) of solid and hollow skirt

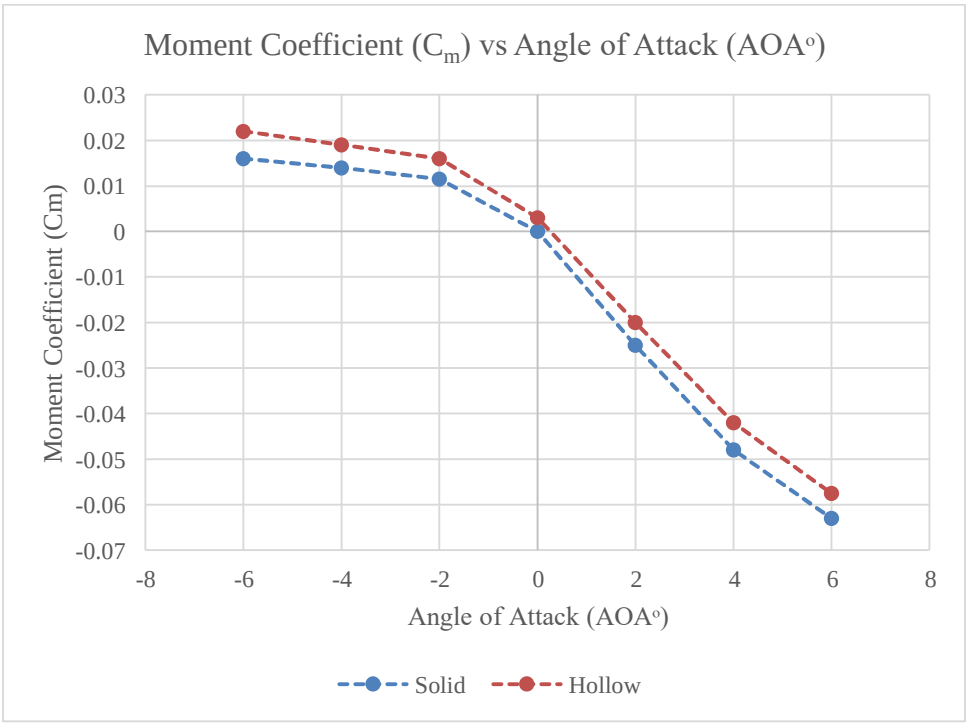

Figure 71: Moment coefficient (C_m) vs Angle of Attack (AOA°) for Hollow and Solid Skirt

The essential parameters in aerodynamics are based on the pressure changes across the surface. The velocity domain around both skirts is directly linked with the pressure domain. In the present incompressible flow, the high-velocity regions generate low pressure and vice versa. Therefore, the pressure contours are generated in the post-processing of the present study to show the pressure acting on the solid and hollow skirt.

The simulated results, as shown in figure 72 to figure 76, it shows pressure and velocity distribution around the solid and hollow skirt of the WIG hovercraft. The pressure analysis

shows that the solid skirt experiences more pressure around its body region. The solid skirt has greater pressure than a hollow, and the velocity around the body is high in solid compared to a hollow. Hence more pressure is generated around the solid skirt region to achieve its lift, where a higher-pressure stagnation region is formed at the front of the solid skirt, and a wake is formed behind the body, which is the low-pressure region. While less pressure is generated around the hollow skirt body as a result of the hollow shape due to the increased surface area as the air that flows beneath the hollow is slower than that of the solid skirt.

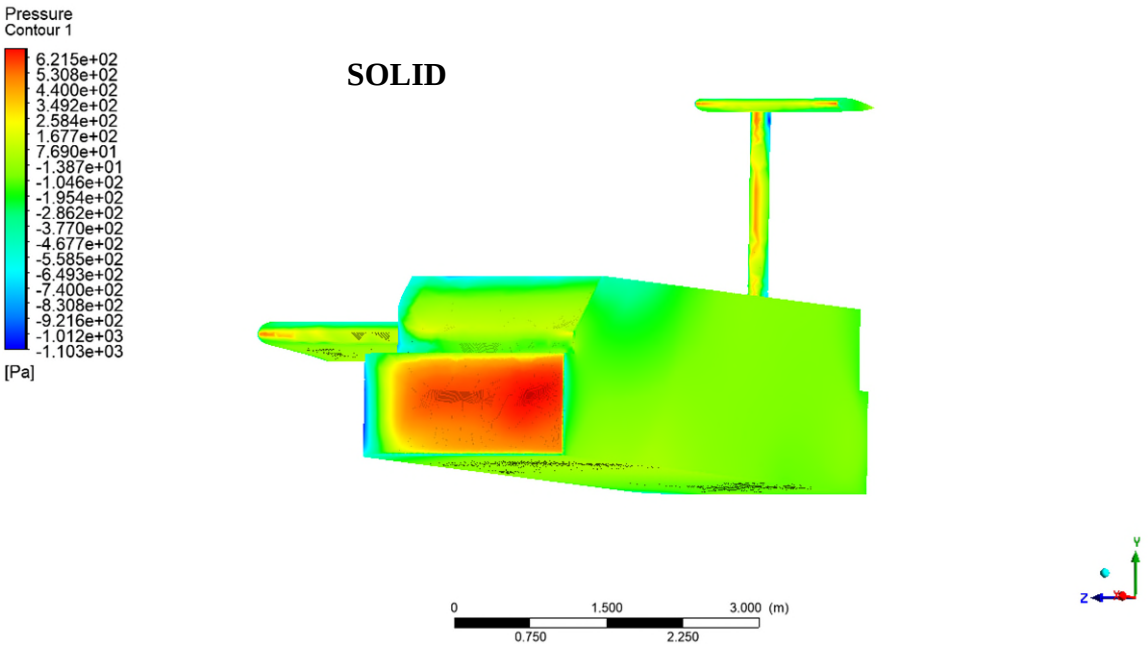

(a)

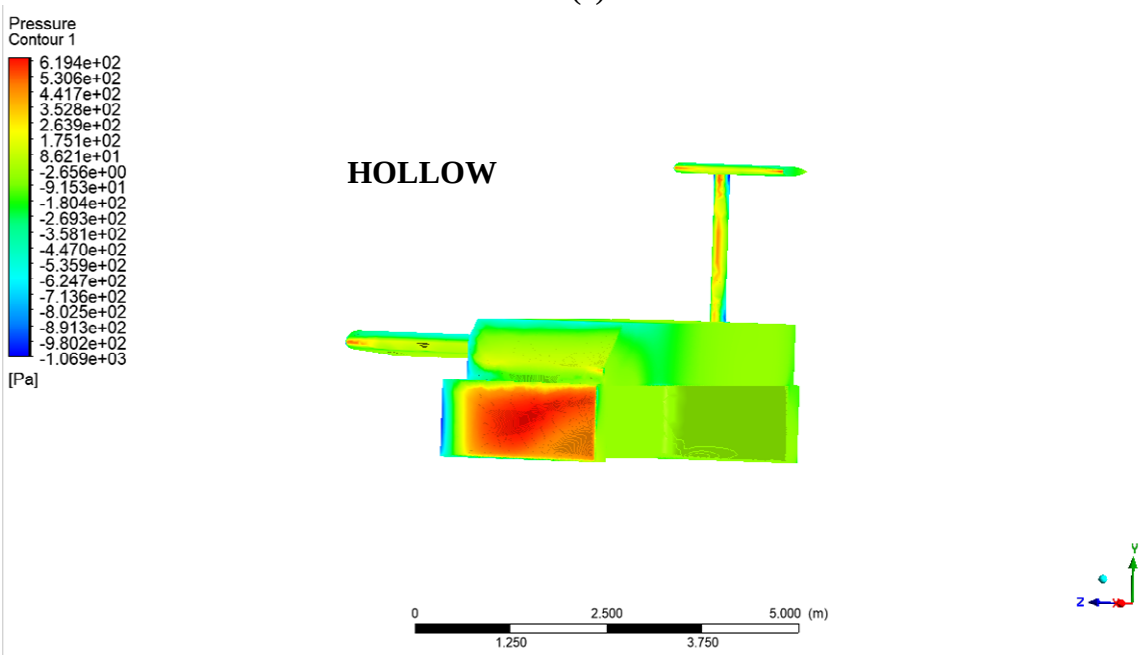

(b)

Figure 72: Pressure contour showing the flow around the solid skirt (a) and hollow skirt (b)

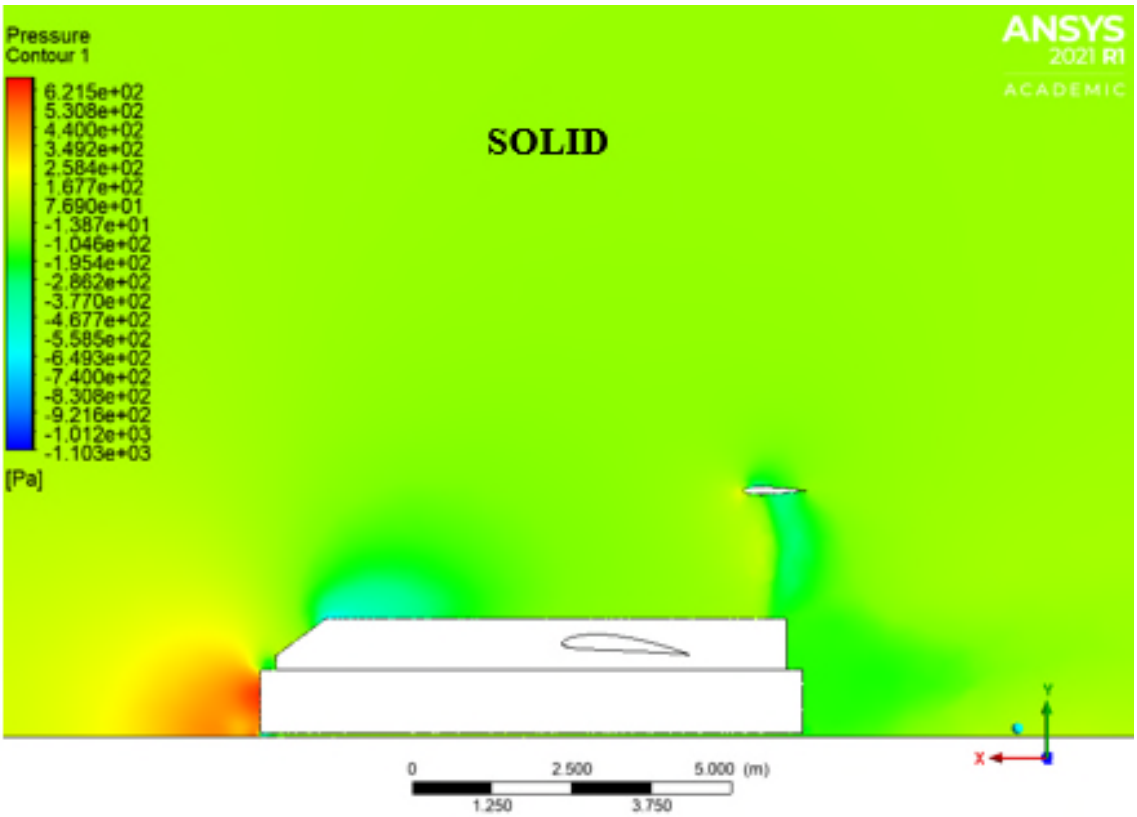

(a)

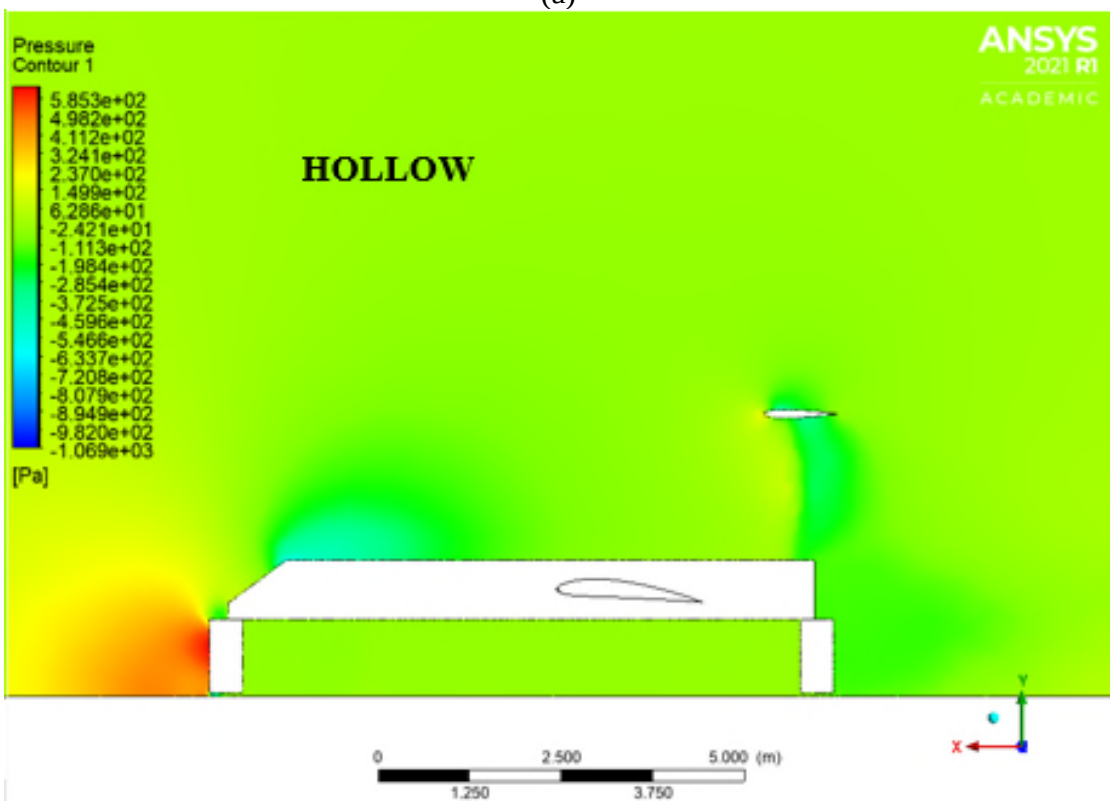

(b)

Figure 73: (Mid-section) Pressure contour side view of the solid skirt (a) and hollow skirt (b)

(a)

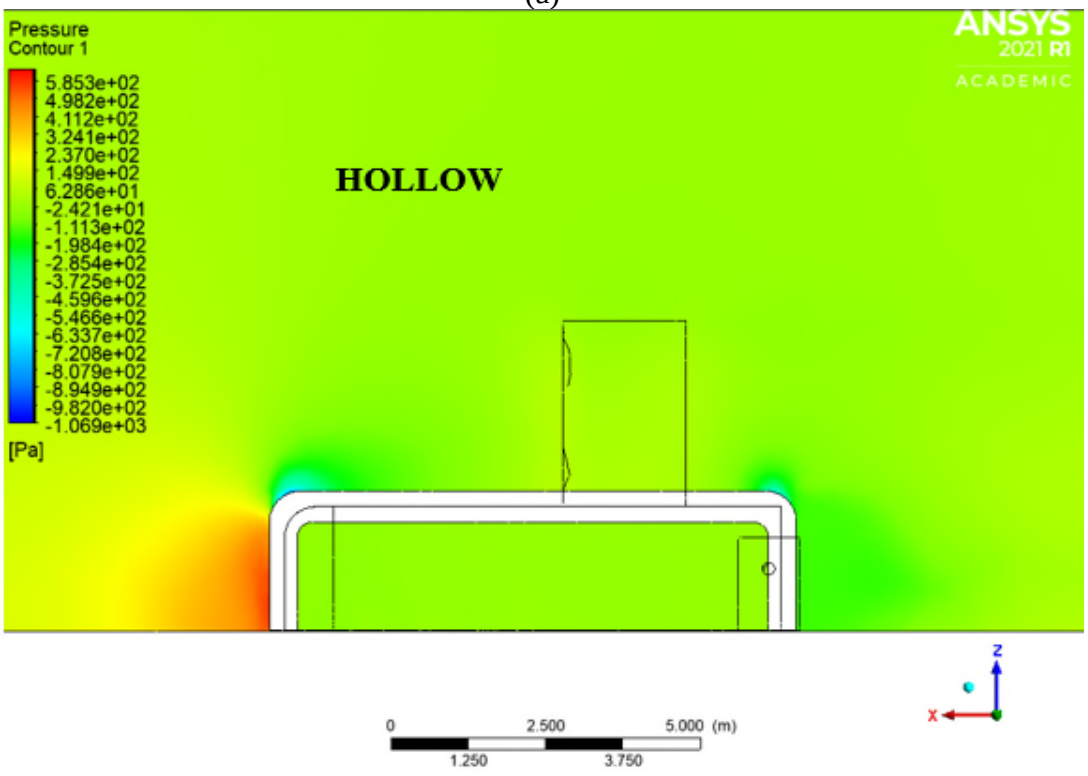

(b)

Figure 74: Pressure Contour Beneath the solid skirt (a) and hollow skirt (b) with the view from the top of the craft

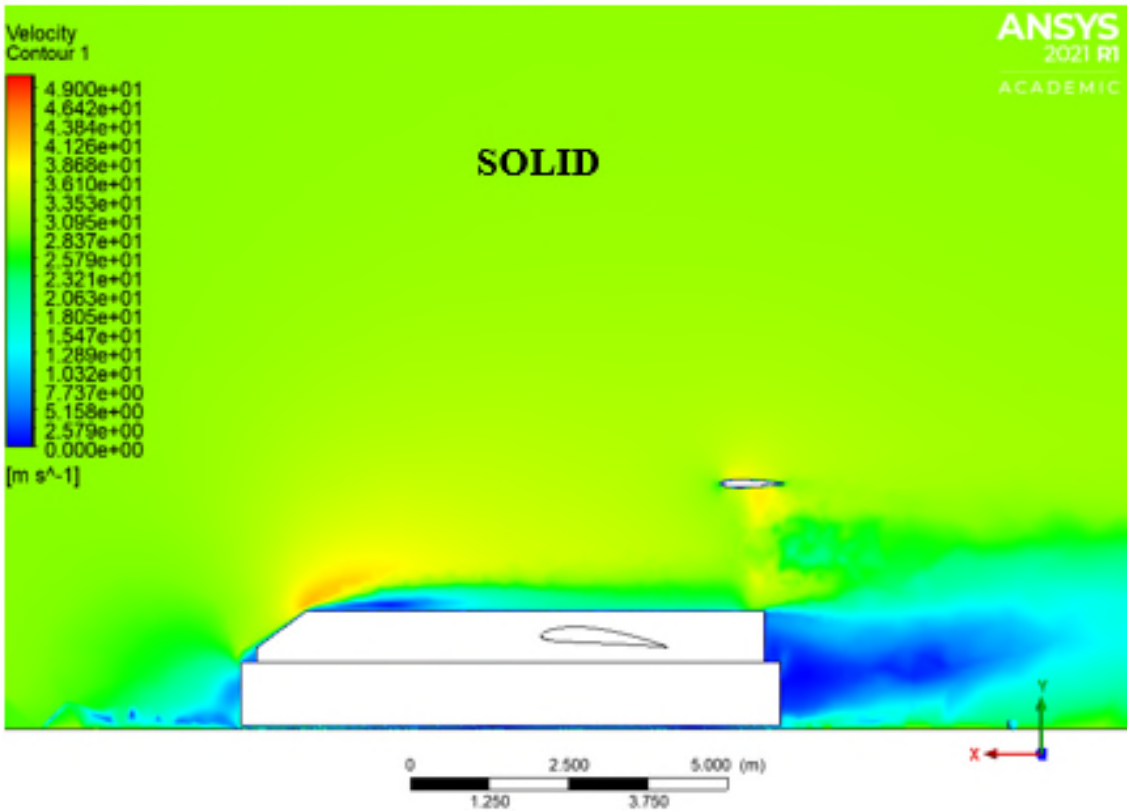

(a)

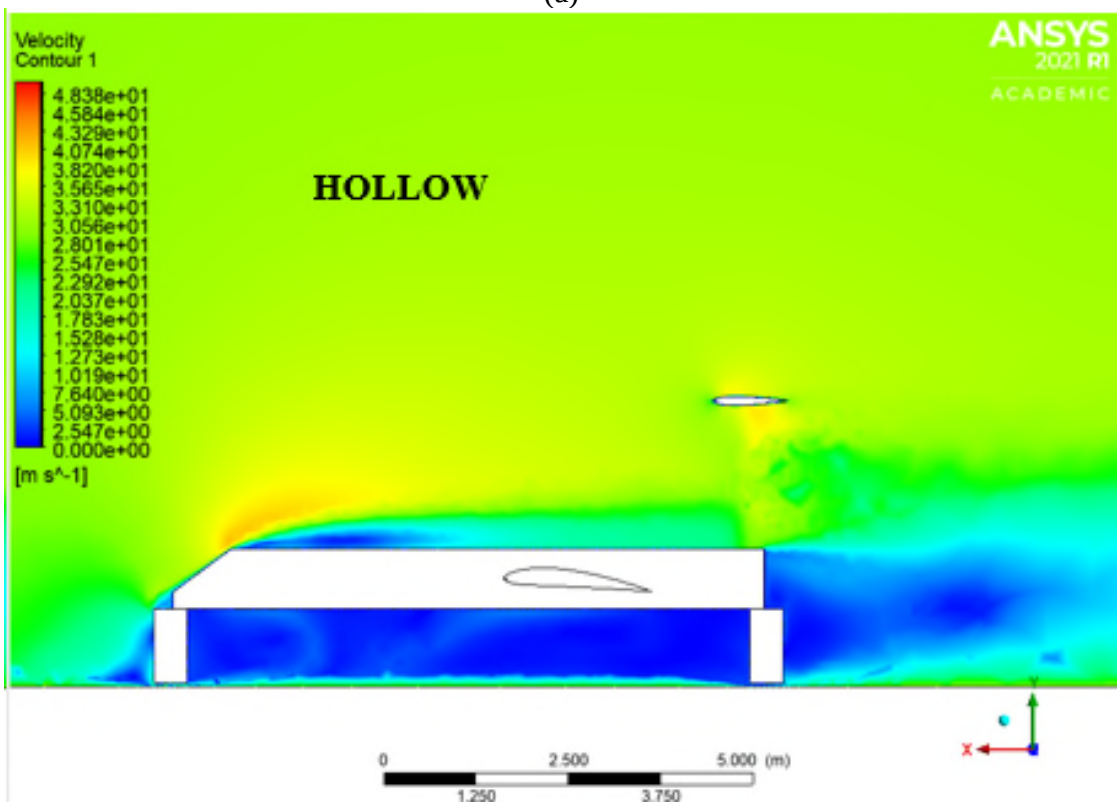

(b)

Figure 75: (Mid-section) Velocity Contour side view of the solid skirt (a) and hollow skirt (b)

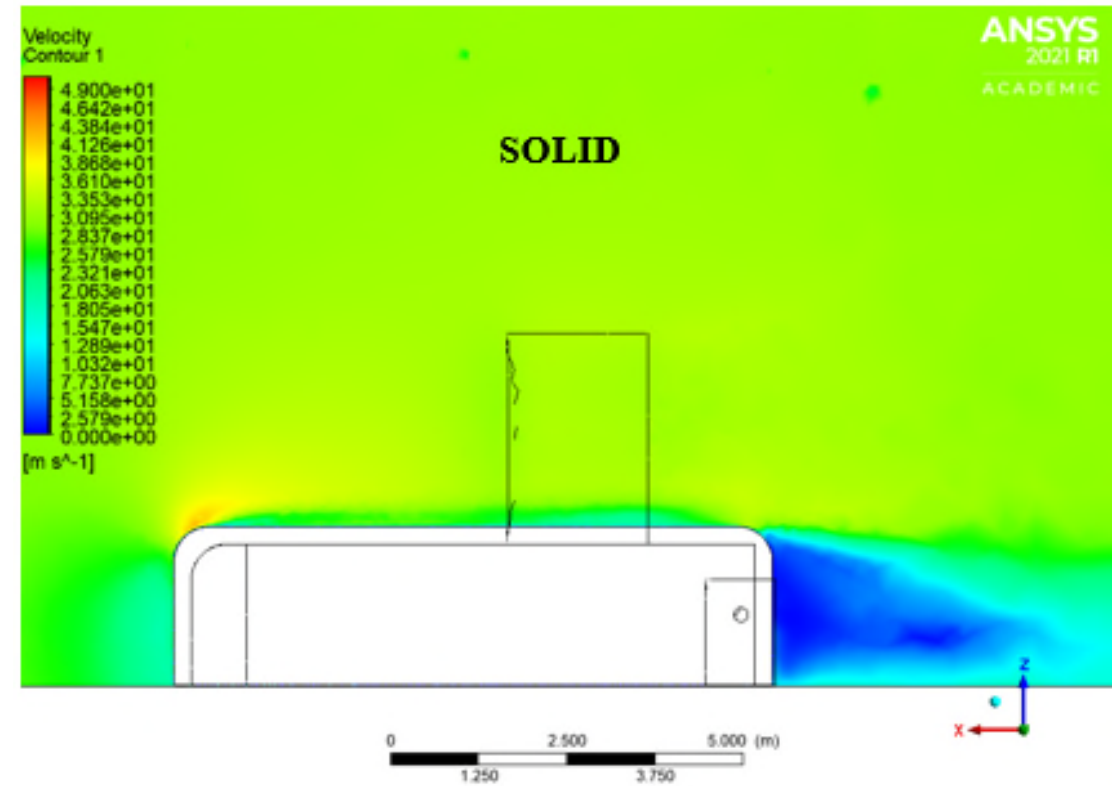

(a)

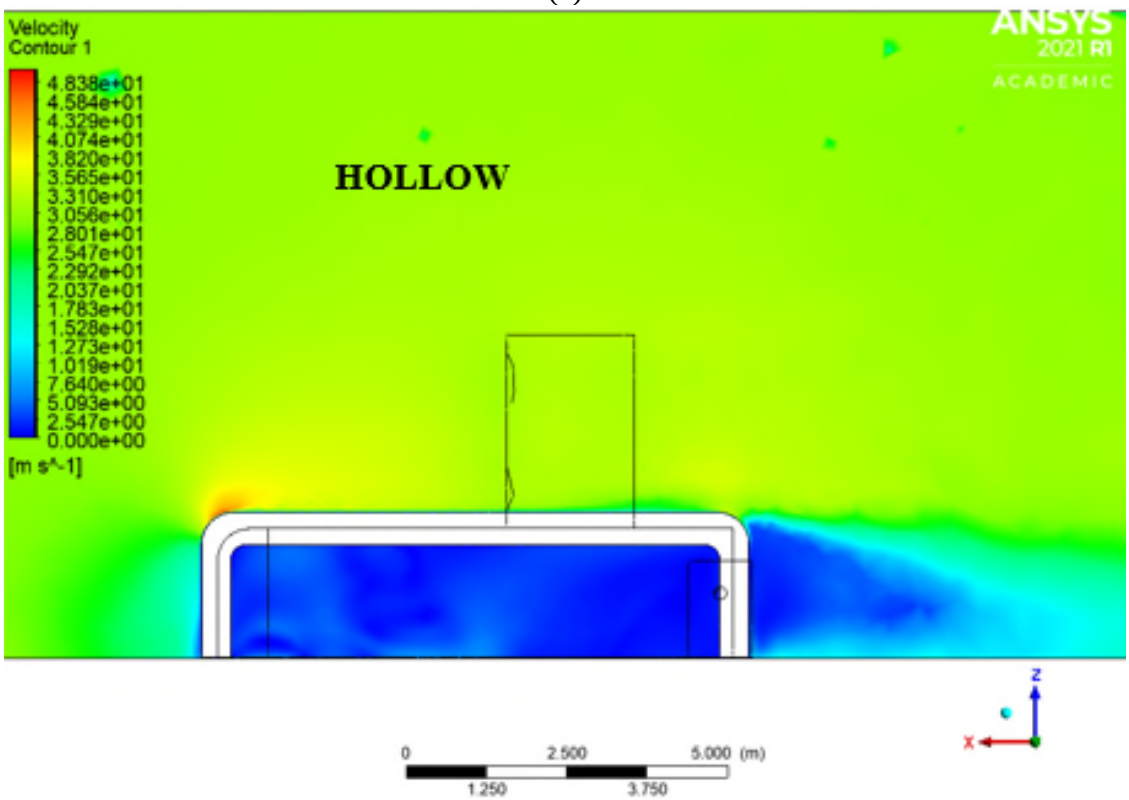

(b)

Figure 76: Velocity Contour Beneath the solid skirt (a) and hollow skirt (b) with the view from the top of the craft

The hollowed-out model creates a larger wake behind the skirt. The low-velocity area behind the skirt causes the form to drag on the hollow skirt, resulting in a higher drag coefficient and a more realistic analysis of a hovercraft hull. The velocity contour plots of the solid and hollow skirts are shown in Fsigures 75 and 76, where the absolute values of velocity differ slightly due to the different

incoming fluid velocities. The hollow skirt generated a lift and drag coefficient of 0.42 and 0.38, respectively, while the solid skirt generated a lift and drag coefficient of 0.651 and 0.33, respectively.

Based on the simulation results, the wing is placed 4.9m from the COG, and the wing should be located slightly near the ground to provide sufficient lift with a reduction in drag coefficient, from this study simulations. Hence from the analysis, the speed required to lift the WIG hovercraft is 29m/s. The NACA 4412, with a chord length of 2m and span length of 6m, was used as the main wing, while the NACA 0012, with a chord length of 1m and span length of 3m, was used as the tail wing for the initial design analysis of the WIG hovercraft, as validation was carried out on this wing. From the analysis, implementing WIG technology has been seen to increase the lift coefficient of a WIG hovercraft based on it flying in ground effect.

4.2 FLOW INTERACTION

There is a strong flow field at the rear of the craft, where the vortex formation is at its strongest, as seen in figure 77. The direction of the flow as it interacts with the wing and skirt moves in the opposite direction at the bottom of the skirt in figure 78. As air (fluid) flows across the WIG hovercraft, there is an outward flow underneath the skirt, as seen in figure 79.

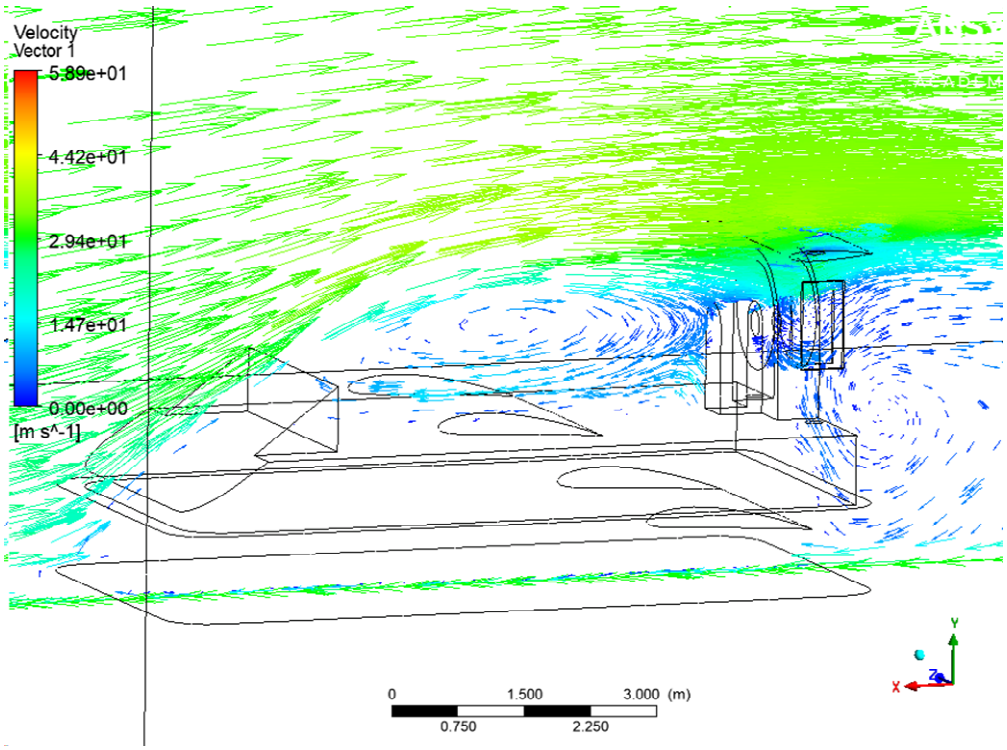

Figure 77: Vector plot of flow around the mid-section of the WIG hovercraft

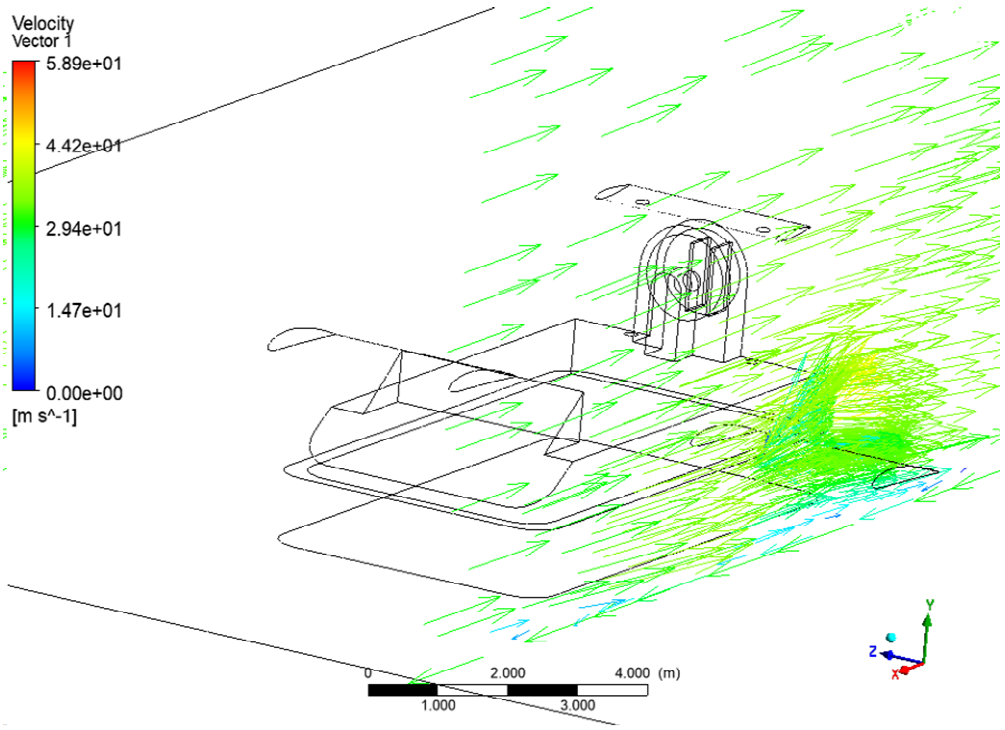

Figure 78: Vector plot of flow between the wing and bottom of the skirt.

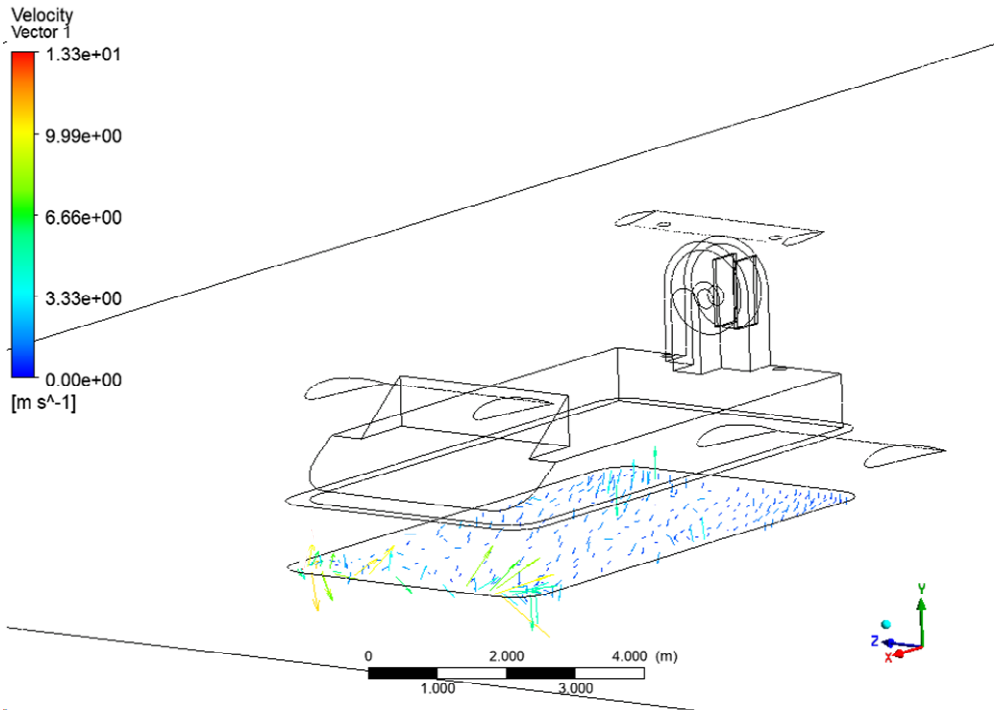

Figure 79: Direction of flow underneath the skirt.

A further assumption on the interaction of flows between the wings and the hull body is established. Through the interaction of flow over the hull body, increasing the lift of the wing can reduce the total drag experienced by the hull. Changing the flow from the main wing will also change the flow experienced by the rear wing. Due to these interaction effects, the aerodynamic features of the entire vehicle would need further investigation on each wing position. This is a complex process that is beyond the scope of this study. The proximity of the main wing to the hull can lead to interactions of the flows from the wing and skirt, as the

wings tend to generate lift and vortices. Interaction between the wing and skirt can reduce this lift and increase the downforce generated by the wing, or the reverse, depending on wing location.

From the comparison between the WIG Hovercraft and other search and rescue vehicles in section 2.4, Studies indicate that the ground effect increases static pressure by 45 percent, resulting in lifting force increases [94]. The development and operational costs of a WIG hovercraft are low, as it can operate without the need for airports or other facilities. The speed of a WIG hovercraft would be faster than other rescue vehicles as it would be able to save more lives at a quicker rate for maritime accidents. Based on these benefits, the vehicle has the potential to be used in search and rescue operations to save lives at a quicker rate. However, the safety of the WIG hovercraft has not been fully developed to a certain grade, particularly in terms of vehicle maintenance and production costs. Table 25 shows the comparison of the lift and drag values of the hovercraft model. The drag force for the WIG hovercraft was expected to have a slight increase in its drag value as a result of the additional components, such as the wing and tail wing.

Table 25: Comparison of Lift and Drag values of the hovercraft model.

Force (CFD Result)	Without Wing	With Wing
Lift	2117N	11466N
Drag	4763N	5821N

Using the current position rescue and distribution facilities accidents, the distance and time required to reach the crash site of each type of vehicle are determined. In this case, the current rescue facilities and various rescue vehicles have been selected. The distance from the accident is 193 km (120 miles) from the Aberdeen RNLI rescue facility based on the pipe alpha accident as seen on figure 80 [95]. Table 26 shows the various rescue times of different rescue vehicles.

Figure 80: Piper Alpha's location in the North Sea, 193 kilometres (120 miles) north-east of Aberdeen, Scotland [95]

Equation 9 solves for the rescue time of the Piper Alpha accident for table 26 by using the speed formula to calculate how long it will take each rescue vehicle to arrive at the scene and save the victims. The distance between the rescue facility and the accident is 193 kilometres (120 miles).

$$Speed = \frac{Distance}{Time}, \text{ hence } Time = \frac{Distance}{Speed} \qquad \text{Equation (9)}$$

Table 26: Current Prototype rescue vehicles (RNLI) and WIG hovercraft [96 - 98]

Rescues Vehicles	**Speed (m/s)**	**Weight (kg)**	**Seat**	**Rescue time (mins)**
RNLI Shannon lifeboat	13 m/s	18288 kg	6-18 passengers	247.6 mins
RNLI Inshore Rescue Boats	13.4 m/s	165 kg	2-6 passengers	240.2 mins
RNLI Rescue Hovercraft	15m/s	3922 kg	2-6 passengers	214.6 mins
Recreational WIG Hovercraft (UH-18SP	33 m/s	383 kg	2-6 passengers	97.5 mins
WIG Hovercraft	30m/s	1105 kg	2-6 passengers	107.3 mins

According to table 26, current rescue vehicles required up to 3.5 hours to reach the accident site, whereas the recreational WIG hovercraft and WIG hovercraft required up to 1.7 hours. As a result, this creates the possibility for a faster vehicle to be adopted in search and rescue operations to save victims of maritime accidents more quickly. Furthermore, the rescue boat and helicopter costs more than the wing on the ground during the rescue operation.

A WIG hovercraft would be clearly more efficient than identical aircrafts and faster than equivalent marine vehicles due to the ground effect. This creates the possibility for a faster vehicle to be adopted in search and rescue operations, allowing victims of maritime accidents to be saved more quickly.

Chapter 5: Conclusion

The thesis aimed to find the influence of WIG technology on a search and rescue hovercraft. It is found that the influence of the ground effect has significant effects on the lift and drag coefficient for the wing and hull of the WIG hovercraft vehicle, based on the variation of the aerodynamic performance of the wing. The introduction of wings to a hovercraft increases the lift coefficient and decreases the drag coefficient, while the lift-to-drag ratio increases due to increased lift. The study showed that a WIG hovercraft with a low aspect ratio, having the wing located closer to the ground, will increase the lift coefficient and reduce the drag of the craft.

The influence of ground effect on the wing of a WIG hovercraft has significant effects on the lift and drag coefficient based on the variation of the aerodynamic parameters of the wing. It was found that apart from the aspect ratio, angle of attack, and the aerofoil's height to chord ratio (h/c), the aerofoil's geometry also strongly influences the aerodynamic characteristics of the configuration when operating in ground effect. The decision to investigate different classes of aerofoil at a large range of angle of attack and h/c values was justified as this allowed for a more substantial analysis.

From this thesis, the hovercraft base model has been taken as a design model, and its size and performance have been studied. The base structure was designed, and its lift and drag have been determined. The NACA 4412 aerofoil was attached to the hovercraft to produce lift, which the fan had already produced. The wing-in-ground effect hovercraft model design was carried out at an optimized angle of attack of 5°. The NACA 0012 wing was used as the tail wing for the purpose of stability.

The lift and drag coefficient performance measures were calculated against the various angle of attack in ground effect using the SST k-ω turbulence model. The results indicated that the influence of the ground effect could be utilized for a higher amount of lift and lower induced drag to create a WIG hovercraft intended for search and rescue operations to save victims of maritime accidents at a quicker rate with better efficiency and good stability. The attached wing produces the speed required to provide the lift force as there is an increase in lift and reduction in drag from the initial result. In this wing-in-ground effect hovercraft, the most engine power will be delivered to propulsion alone. Thus, it is feasible for a wing-in-ground effect hovercraft to be used in search and rescue operations at sea state 2 at higher speeds with built-in lift wings.

Hence, this study provides a detailed procedure for the preliminary design of a wing-in-ground effect hovercraft. Considering that the craft is essentially a combination of a

hovercraft and a plane, many parameters must be considered. The ability of a WIG hovercraft to handle sea state opens the potential usage to coastal, interisland, and major rivers. There is a tremendous potential for this technology to be developed further using modern sustainable means of propulsion. Further developments in this technology may result in a faster means of saving lives in search and rescue operations, access to new routes, and long-distance oceanic transportation significantly less expensive than a plane while being faster than a regular ship.

Future Work

A further study on the optimisation approach to the WIG hovercraft should be carried out by the addition of flaps for improved performance of the craft. Furthermore, a comparison of the computational and experimental analysis of the optimised WIG hovercraft should be conducted to produce more accurate results and alternate findings.

References

1. Global report on drowning: preventing a leading killer. Who.int. (2021). Retrieved, from https://www.who.int/publications/i/item/global-report-on-drowning-preventing-a-leading-killer.
2. RNLI Search and rescue hovercraft. Retrieved, from https://rnli.org/what-we-do/lifeboats-and-stations/our-lifeboat-fleet/rescue-hovercraft?sf179885777=1 (Search and rescue hovercraft RNLI datasheet)
3. Doctors, L.J. (1997) “Analysis of the Efficiency of an Ekranoplan: A very high-speed Catamaran with Aerodynamic Alleviation”, Proc. International Conference on Wing-in-Ground-Effect Craft (WIGs '97), Royal Institution of Naval Architects, London, England, 16 pp Dec. 1997.
4. Chin Su Paek. (2006). *Core.ac.uk*. World maritime University. Retrieved February 18, 2023, from https://core.ac.uk/download/pdf/217238207.pdf
5. B Shah, N. (2011). Design of a Hoverwing Aircraft. Retrieved 18 August 2022, from https://pdp.sjsu.edu/people/nikos.mourtos/docs/Shah.S11.pdf.
6. Wright Flyer II. Wright-brothers.org. (1904). Retrieved 3 June 2022, from http://www.wright-brothers.org/Information_Desk/Just_the_Facts/Airplanes/Flyer_II
7. Mitra, P., Dewangan, A., & Ghose, P. (2014). Experimental study of Aero Foil with Wind Tunnel Setup. ResearchGate. Retrieved 3 June 2022, from https://www.researchgate.net/publication/259739000_Experimental_study_of_Aero_Foil_with_Wind_Tunnel_Setup
8. Search and rescue (SAR) operation Migration and Home Affairs. Available at: https://home-affairs.ec.europa.eu/pages/glossary/search-and-rescue-sar-operation_en.
9. Strahan (1998) *Air-Sea Rescue, Academic Dictionaries and Encyclopedias*. From https://en-academic.com/dic.nsf/enwiki/11669474 (Accessed: January 3, 2023).
10. Evans, C. (2003) Rescue at sea: An international history of lifesaving, Coastal Rescue Craft and organisations. London: Conway Maritime Press.
11. Sturdevant, A. (n.d.). *Neotric Hovercraft:* Neoteric Hovercraft: The World's Original Light Hovercraft Manufacturer. Retrieved February 18, 2023, from https://www.neoterichovercraft.com/hovercraft-resources/faq.php#:~:text=Depending%20upon%20the%20effects%20of,when%20there%20is%20a%20headwind.
12. Snooks, H. A., Nicholl, J. P., Brazier, J. E., & Lees-Mlanga, S. (1996). The costs and benefits of helicopter emergency ambulance services in England and Wales. Journal of Public Health Medicine, 18(1), 67–77. from http://www.jstor.org/stable/45160727

13. Chovatiya, G. (2015). Working model of Hovercraft. Uvpcemecharocks.blogspot.com. Retrieved, from https://uvpcemecharocks.blogspot.com/2012/03/working-model-of-hovercraft.html.

14. Hovercraft and the Air Cushion Principle. (1959), 31(8), 238-238. Retrieved, from, https://doi.org/10.1108/eb033146

15. John, C (2015). Working model of Hovercraft-How to make a hovercraft. Mechanical Engineering Projects-Ideas-PPT-PDF Reports. https://www.mechanicalengineeringprojects.net/working-model-of-hovercraft/

16. Lift Theory. (n.d.). Retrieved, from Incorrect Lift Theory website: https://www.grc.nasa.gov/www/k-12/airplane/wrong1.html

17. Aerofoil terminology. (2021, September 28). Retrieved from https://skybrary.aero/tutorials/aerofoil-terminology

18. Aerospaceweb.org. 2022. Aerospaceweb.org | Finite and Infinite Wing. Retrieved, from, <http://www.aerospaceweb.org/question/aerodynamics/q0167.shtml>

19. Engineering108.com. (2022). Retrieved, from http://www.engineering108.com/Data/Engineering/aeronautical_engineering/Basics-of-Aeronautics.pdf

20. Darnell, T., Farrar, C., & S. Kayser, Z. (2020). A2 Aero Micro - 20F12 Preliminary Proposal. Retrieved, from https://ceias.nau.edu/capstone/projects/ME/2021/20F12_SAEAeroMicro/ME_476C___Darnell_Tyler___Preliminary_Report.pdf (Four main aerofoil designs)

21. Hall, N. (2021). L/D Ratio. Retrieved, from https://www.grc.nasa.gov/WWW/k-12/airplane/ldrat.html (Lift and drag coefficients meaning)

22. Tahani, M., Masdari, M., & Bargestan, A. (2017). Aerodynamic performance improvement of WIG aircraft. Aircraft Engineering and Aerospace Technology, 89(1), 120-132. Retrieved, from, doi: 10.1108/aeat-05-2015-0139.

23. Signhal, A. (2015). Use of Magnetic Lifts in Fire Safety. IOSR Journal of Mechanical and Civil Engineering, 12(4), 41-43. Retrieved, from https://www.iosrjournals.org/iosr-jmce/papers/vol12-issue4/Version-6/J012468388.pdf

24. Spalart, P., & Allmaras, S. (1992b). A one-equation turbulence model for aerodynamic flows. 30th Aerospace Sciences Meeting and Exhibit, 1, 5–21. Retrieved, from doi:10.2514/6.1992-439

25. Menter, F. R. (1994). Two-equation eddy-viscosity turbulence models for engineering applications. AIAA Journal, 32(8), 1598-1605. Retrieved, from doi:10.2514/3.12149

26. Jakub Elcner, Frantisek Lizal, Jicha, Miroslav (2017). Retrieved, from DOI:10.1051/epjconf/201714302020 https://www.researchgate.net/publication/316892562_Comparison_of_turbulent_models_in_the_case_of_a_constricted_tube

27. Modelling Turbulent Flows introductory fluent training. (2006). Retrieved, from http://www.southampton.ac.uk/~nwb/lectures/GoodPracticeCFD/Articles/Turbulence_Notes_Fluent-v6.3.06.pdf

28. Jung et al (2008)"Experimental investigation of wing-in-ground effect with a NACA6409 section" P19

29. Abbott, I. H. (1995). Theory of wings section, including summary of airfoil data. Retrieved, from, <http://www.ijirset.com/upload/july/27_NUMERICAL.pdf> [Accessed 7 July 2020].

30. Reynolds number. (2021). Retrieved from https://www.grc.nasa.gov/www/BGH/reynolds.html

31. Rainer. (2018). Boundary layer separation and pressure drag – Aerospace engineering blog. Retrieved, from https://aerospaceengineeringblog.com/boundary-layer-separation-and-pressure-drag/

32. Jahanmiri, M. (2011). Boundary Layer Receptivity: A Retrospect. Retrieved, from https://www.researchgate.net/publication/277729464_Boundary_Layer_Receptivity_A_Retrospect

33. N. Moore, P. A. Wilson, A. J. Peters, "An Investigation into Wing in Ground Effect Airfoil Geometry", School of Engineering Sciences, University of Southampton, SO17 1BJ, UK

34. Bhopale, N., Chawathe, R., Potdar, S., & Magar, Y. (2021). Design and Analysis of Wing in Ground Effect Vehicle. Retrieved 18 August 2022, from https://www.ripublication.com/aasa/aasav11n1_02.pdf.

35. Maimun, A., Jamei, S., Priyanto, A., & Azwadi, N. (2010). Aerodynamic Characteristics of Wing of WIG Catamaran vehicle DuringGround Effect. WSEAS TRANSACTIONS on FLUID MECHANICS, 5.

36. Rozhdestvensky, K. V. (1997). Ekranoplans-the GEMs of fast water transport (Vol. 109). London.

37. Halloran M., O'Meara, S. (1999) Wing in Ground Effect Craft Review Apps.dtic.mil. (2022). Retrieved, from https://apps.dtic.mil/sti/pdfs/ADA361836.pdf.

38. Matdaud, Z., Zhahir, A., Pua'at, A., Hassan, A., & Ahmad, M. (2019). Stabilizing Attitude Control for Mobility of Wing in Ground (WIG) Craft - A Review. Retrieved 18 August 2022, from

https://www.researchgate.net/publication/336779717_Stabilizing_Attitude_Control_For_Mobility_Of_Wing_In_Ground_WIG_Craft_-_A_Review

39. Aerospaceweb.org | Ground Effect and WIG Vehicles. (2018). Retrieved 18 August 2022, from http://www.aerospaceweb.org/question/aerodynamics/q0130.shtml

40. Abramowski Tomasz. (2007). Numerical investigation of airfoils in ground proximity. Journal of Theoretical and Applied Mechanics, 45(2), 425-436. Retrieved from https://www.researchgate.net/publication/228651914_Numerical_investigation_of_airfoil_in_ground_proximity

41. WIG TECHNOLOGY. (2010). Retrieved, from http://transaquatisgb.free.fr/page6.html

42. B Shah, N. (2011). Design of a Hoverwing Aircraft" P6

43. Hovercraft - Product Range. (2020). Retrieved, from: https://www.griffonhoverwork.com/products/hovercraft/.

44. Hovercraft.com. 2021. UH-18SP | Universal Hovercraft. Retrieved, from: <https://www.hovercraft.com/content/index.php?main_page=index&cPath=5_34_221>

45. Tofa, M., Maimun, A., Ahmed, Y., Jamei, S., Priyanto, A., & Rahimuddin. (2014). Experimental Investigation of a Wing-in-Ground Effect Craft. The Scientific World Journal, 2014, 1-7. Retrieved, from, doi: 10.1155/2014/489308

46. Discoverhover.org. n.d. DiscoverHover: The Hovercraft Project. Retrieved, from: <http://discoverhover.org/>

47. Boat Trader Blog. 2021. Home | Boat Trader Blog. Retrieved, from: <https://www.boattrader.com/resources/>.

48. Yang, W. and Czysz, P.A. (2011) *WIG craft serves niche transportation needs*, *researchgate*. From: https://www.researchgate.net/publication/264436787_WIG_craft_serves_niche_transportation_needs (Accessed: January 3, 2023).

49. Koto, J. and Prayetno, E. (1970) Feasibility Study of wing-in-ground for Marine Rescue Operation, Semantic Scholar. From: https://www.semanticscholar.org/paper/Feasibility-Study-of-Wing-In-Ground-for-Marine-Koto-Prayetno/6715ed505f32082cdede8b1e63a230aab6667cf5.

50. Paek, C.S. (1970) The viability of commercializing wing-in-ground (WIG) craft in connection with technical, economic and Safety Aspects followed by Imo Legislation, Semantic Scholar. Available at: https://www.semanticscholar.org/paper/The-viability-of-commercializing-Wing-In-Ground-in-Paek/0f574774e25926b4f1e87b139bbd01cc5bc837b8#citing-papers (Accessed: January 3, 2023).

51. Flightboat (2012) FlightBoat. From: https://flighboat.webs.com/documents/Flightboat%20letter%20HW20-2.pdf.

52. Wdcs.org. 2021. Beaufort Sea States. Retrieved, from <https://www.wdcs.org/submissions_bin/WDCS_Shorewatch_Seastate.pdf>

53. Sizes.com. 2021. Sea state. Retrieved, from <https://www.sizes.com/natural/seastate.htm>.

54. Jung, K. H., Chun, H. H., & Kim, H. J. (2008). Experimental investigation of wing-in-ground effect with a NACA6409 section. Journal of Marine Science and Technology, 13(4), 317–327. Retrieved, from, doi:10.1007/s00773-008-0015-4

55. Ahmed, M., Takasaki, T., & Kohama, Y. (2006). Experiments on the aerodynamics of a cambered airfoil in ground effect. 44th AIAA Aerospace Sciences Meeting and Exhibit. Reston, Virigina: American Institute of Aeronautics and Astronautics.

56. N.Moore, Professor P A.Wilson, A J.Peters. (2002). An Investigation into Wing in Ground Effect Aerofoil Geometry. Retrieved, from, https://eprints.soton.ac.uk/51083/1/51083.pdf

57. Sarada, S., & Shankar, M. (2012). Numerical simulation of Viscous, Incompressible flow around NACA 64618 subsonic airfoil using Computational Fluid Dynamics. In Proceedings of National conference on advances in Mechanical Engineering. Allied Publishers Pvt Ltd.

58. Douvi C. Eleni, 2012. Evaluation of the turbulence models for the simulation of the flow over a National Advisory Committee for Aeronautics (NACA) 0012 airfoil. Journal of Mechanical Engineering Research, 4(3).

59. Dippold, V. (2005). Investigation of wall function and turbulence model performance within the wind code. 43rd AIAA Aerospace Sciences Meeting and Exhibit. Retrieved, from doi:10.2514/6.2005-1002

60. Sharma, S., & Clement, S. (2014). CFD simulation of the flow characteristics of NACA 0012, NACA 6409, and DHMTU airfoils in ground effect. Volume 1A, Symposia: Advances in Fluids Engineering Education; Turbomachinery Flow Predictions and Optimization; Applications in CFD; Bio-Inspired Fluid Mechanics; Droplet-Surface Interactions; CFD Verification and Validation; Development and Applications of Immersed Boundary Methods; DNS, LES, and Hybrid RANS/LES Methods. Retrieved, from doi:10.1115/fedsm2014-21131

61. Park, K., & Lee, J. (2008). Influence of endplate on aerodynamic characteristics of low-aspect-ratio wing in ground effect. Journal Of Mechanical Science and Technology, 22(12), 2578-2589. Retrieved from doi: 10.1007/s12206-008-0805-y

62. Yang, W., Yang, Z., & Ying, C. (2010). Effects of design parameters on longitudinal static stability for WIG craft. International Journal of Aerodynamics, 1(1), 97. Retrieved, from doi: 10.1504/ijad.2010.031705

63. Lex, E., & Kraker, P. (2015). A Critical Look at the ResearchGate Score as a Measure of Scientific Reputation. Retrieved from https://www.researchgate.net/publication/33076069

64. Rao S., Prakash V. S. S..(2014). Development of an integrated air cushioned vehicle (Hovercraft). Retrieved from https://www.academia.edu/7652543/Development_of_a_Integrated_Air_Cushioned_Vehicle_Hovercraft_

65. N. H. Saeid, E. Yunus and O. C. Fei, "CFD simulation of air flow around a hovercraft," 5th Brunei International Conference on Engineering and Technology (BICET 2014), 2014, pp. 1-7, doi: 10.1049/cp.2014.1071.

66. Nagaraju D., Urmila K. (2016). Modeling and structural Analysis of hovercraft Assembly - Anveshana's International Publication. Retrieved, from http://publications.anveshanaindia.com/sdm_downloads/modeling-structural-analysis-hovercraft-assembly/

67. Quah Yong Seng, Jonathan.2005. Stability, Performance & Control for a Wing in Ground Vehicle. Department of Mechanical Engineering. National University of Singapore.

68. Tofa, M., Maimun, A., Ahmed, Y., Jamei, S., Priyanto, A., & Rahimuddin. (2014). Experimental Investigation of a Wing-in-Ground Effect Craft. The Scientific World Journal, 2014, 1-7. Retrieved, from doi: 10.1155/2014/489308.

69. Ansys.com. 2020. Engineering Simulation & 3D Design Software | Ansys. [Retrieved, from <https://www.ansys.com/en-gb> [Accessed 1 April 2020].

70. ANSYS Fluent Theory Guide - [PDF Document]. (2022). Retrieved, from https://vdocuments.net/ansys-fluent-theory-guide.html

71. Schlemmer, H. (2012) *Hovercraft glides over land and water*, *Daily Mail Online*. Associated Newspapers. Available at: https://www.dailymail.co.uk/news/article-2140244/The-flying-hovercraft-hits-70-mph-50ft-air.html.

72. Antony Jameson., W, Schmidt & Eli Turkel (Ed.). (1981). Solutions of the Euler Equations by Finite Volume Methods Using Runge-Kutta Time-Stepping Schemes. AIAA Journal 1259. Retrieved, from https://www.researchgate.net/publication/247576565_Solutions_of_the_Euler_Equations_by_Finite_Volume_Methods_Using_Runge-Kutta_Time-Stepping_Schemes

73. Çakıcı, T. (2022). Production and characterization of GO:Se nanoparticles produced by biosynthesis method and current-voltage properties of Ag / GO:Se / p-Si device developed using GO: Se nanoparticles. Retrieved, from https://dergipark.org.tr/en/pub/ejosat/issue/48495/631135

74. Shatha Mardan, Zena K. Kadhim and Ali Arkan Alwan (2021) CFD Analysis for Different Types of Fins to Enhancement the Heat Transfer Rate Through A Cross Flow Heat Exchanger, Research Gate. Wasit University. From: https://www.researchgate.net/publication/349610842_CFD_Analysis_for_Dif

ferent_Types_of_Fins_to_Enhancement_the_Heat_Transfer_Rate_Through_A_Cross_Flow_Heat_Exchanger

75. School of Engineering Sciences, University of Southampton. 2002. AN INVESTIGATION INTO WING IN GROUND EFFECT AIRFOIL GEOMETRY. Retrieved, from, <https://eprints.soton.ac.uk/51083/1/51083.pdf>.

76. Engineering Simulation & Risk Management Software, Consulting, Training. Wilde Analysis Ltd. (2022). Retrieved, from https://wildeanalysis.co.uk/.

77. UIUC Applied Aerodynamics Group. Retrieved, from https://m-selig.ae.illinois.edu/

78. EPPLER 58 AIRFOIL (e58-il). Retrieved, from http://airfoiltools.com/airfoil/details?airfoil=e58-il

79. Pillai, N., Anil, Radhakrishnan, A., Vinod, R., Kumar E., S., Zaid, Z., Manojkumar. (2014). Investigation on airfoil operating in Ground Effect region. International Journal of Engineering & Technology, 3(4), 540. Retrieved, from doi:10.14419/ijet.v3i4.3245

80. Abbott, I. H. (1995) “Theory of wings section, including summary of airfoil data” P14

81. 2D NACA 0012 Airfoil Validation. Retrieved, from https://turbmodels.larc.nasa.gov/naca0012_val.html

82. University of Southampton “Investigation into wing in ground effect aerofoil” (2002) P33

83. Search and rescue hovercraft RNLI datasheet , P1

84. Mccune, J., Tavares, T., Lee, N., & Weissbein, D. (1988). Slender wing theory including regions of embedded total pressure loss. 26th Aerospace Sciences Meeting. Reston, Virigina: American Institute of Aeronautics and Astronautics. Retrieved, from https://citeseerx.ist.psu.edu/

85. Fraser-Mitchell, A. H. (2012). Fundamentals of aerodynamics — fifth edition, J. d. Anderson, McGraw-hill, shoppenhangers road, maidenhead, Berkshire, SL6 2QL, UK. 2011. 1098pp. ISBN 978-007-128908-5. The Aeronautical Journal, 116(1176), 222–223. Retrieved, from doi: 10.1017/s000192400000676x. https://www.sciencedirect.com/science/article/pii/S2092678216303776

86. Aşkan, A. and Tangöz, S., 2018. The impact of aspect ratio on aerodynamic performance and flow separation behavior of a model wing composed from different profiles. Retrieved, from <https://www.researchgate.net/publication/329917217_The_impact_of_aspect_ratio_on_aerodynamic_performance_and_flow_separation_behavior_of_a_model_wing_composed_from_different_profiles>

87. Average Weight of a Man | Onaverage.co.uk. Retrieved, from https://www.onaverage.co.uk/body-averages/average-weight-of-a-man#

88. Esakki, B., Ganesan, S., Mathiyazhagan, S., Ramasubramanian, K., Gnanasekaran, B., Son, B., Choi, J. S. (2018). Design of amphibious vehicle for unmanned mission in water quality monitoring using internet of things. Sensors (Basel, Switzerland), 18(10), 3318. Retrieved, from, doi:10.3390/s18103318

89. The ICARUS Project. N.d. Skirt design. Retrieved, from <https://icarushoverwing.wordpress.com/design/research/skirt-design/>.

90. Journal, S., (2014). Development of an Integrated Air Cushioned Vehicle (Hovercraft). Academia.edu. Retrieved, from <https://www.academia.edu/7652543/Development_of_a_Integrated_Air_Cushioned_Vehicle_Hovercraft_>.

91. Hovercraft Lift Calculator 4wings.com 956-943-5150. Retrieved, from http://4wings.com.phtemp.com/tip/tlift.html

92. Z series axial flow fans: Multi-Wing America. Retrieved, from https://www.multi-wing.net/products/z-series-fans/

93. CFD computational domain - IdealSimulations. Retrieved, from https://www.idealsimulations.com/resources/cfd-computational-domain/

94. MLTM (2010), "IMO WIG Craft Guidelines and International Cooperation," T. a. M. A. Ministry of Land, Republic of Korea, Ed., ed

95. Marc Reid (2020) The Piper Alpha Disaster: A Personal Perspective with Transferrable Lessons on the Long-Term Moral Impact of Safety Failures, ACS Publication. From: https://pubs.acs.org/doi/10.1021/acs.chas.9b00022.

96. Devon and Cornwall Police (no date) Helicopter faqs, Devon and Cornwall Police. From: https://www.devon-cornwall.police.uk/accessing-information/our-people/departments/helicopter-air-operations-unit/helicopter-faqs/.

97. RNLI rescue hovercraft - The rnli's lifeboat fleet. From: https://rnli.org/what-we-do/lifeboats-and-stations/our-lifeboat-fleet/rescue-hovercraft.

98. RNLI lifeboats – explore the lifeboats in the RNLI fleet (no date). From: https://rnli.org/what-we-do/lifeboats-and-stations/our-lifeboat-fleet.

99. Flexible Moorings For Marine Turbines. Retrieved, from https://www.esru.strath.ac.uk//EandE/Web_sites/11-12/MORE/hydrofoil/introduction.html

100. Frére, A., Sørensen, N. N., Hillewaert, K., & Winckelmans, G. (2016). Discontinuous Galerkin methodology for Large-Eddy Simulations of wind turbine airfoils. Journal of Physics. Conference Series, 753, 022037. doi:10.1088/1742-6596/753/2/022037. Retrieved, from https://www.researchgate.net/publication/308803450_Discontinuous_Galerkin_methodology_for_Large-Eddy_Simulations_of_wind_turbine_airfoils

Appendices

Appendix A: Gap in Literature

Author/Scope	Profile	Variables	Approach	Target Improvements
S. Sharma, M.R. Ahmed	ResearchGate: CFD Simulation of the Flow Characteristics of NACA 0012, NACA 6409, and DHMTU Aerofoils in Ground Effect	2D Aerofoils, Angle of Attacks, Ground Effect, WIG Crafts Aerodynamic performance	Computational & Experimental	3D wing analysis
R. Ranzenbach, and Barlow, J	SAE Mobilus: Two-Dimensional Aerofoil in Ground Effect, an Experimental and Computational Study	2D Aerofoils, Angle of Attacks, Ground Effect	Computational & Experimental	3D wing analysis
Moore et al.	ResearchGate: Investigation into Wing in Ground Effect Aerofoil Geometry	NACA 0012 and DHTMU 12 Angle of Attacks, Ground Effect	Experimental	Wig craft
Douvi,	ResearchGate: Evaluation of the turbulence models for the simulation of the flow over a National Advisory Committee for Aeronautics (NACA) 0012 aerofoil	2D Aerofoils, Angle of Attacks, Ground Effect, Turbulence Model	Computational	3D wing analysis, WIG Crafts
Park and Lee	Springer: Influence of endplate on aerodynamic characteristics of low-aspect-ratio wing in ground effect	3D wings, Endplates, Low Aspect Ratio, Ground effect	Computational	Hovercraft, WIG Craft
BE Okafor	ResearchGate: Development of a Hovercraft Prototype	Hovercraft	Analytical	Computational and experimental
Nawaf H. Saeid	ResearcGate: CFD simulation of air flow around a hovercraft	Hovercraft	Computational	Experimental
Siva Nagaraju Dasari	Anveshanaindia: Modelling and structural analysis of hovercraft assembly	Hovercraft, Stress Analysis	Computational	Experimental
NB Shah	SJSU: Design of a Hoverwing Aircraft	Wig Craft, 3D wings, Aerodynamic performance	Computational and analytical	Experimental
Universal Hoverwing	Commercial WIG Hovercraft	Recreational WIG Hovercraft	Not Available	Computational and experimental
Current Research	Feasibility study of an Integrated Wing-In-Ground Effect Hovercraft	2D aerofoil, 3D wings, Angle of Attack, Aerodynamic performance, Ground Effect, Hovercraft	Computational	Experimental

Appendix B: Aerofoil Terminology

- **Leading edge:** The point at the front of the aerofoil that has maximum curvature (minimum radius).

- **Trailing edge:** It is the edge of the aerofoil which is pointed in nature. It is located at the back side of the aerofoil.

- **Chord length:** This is the length of the chord line.

- **Chord line:** This is a line that connects the leading and trailing edges of the aerofoil.

- **Angle of attack:** It is the angle formed when relative wind hits an aerofoil. It is the angle formed by the chord line of the aerofoil and the direction of the relative wind, it is an important parameter which affects the coefficient of lift and drag.

- **Chamber line**: This is a line that connects the leading and trailing edges of an aerofoil, dividing it into two symmetrical parts. It could be a straight line or not.

- **Stall angle of attack:** This is the angle of attack at which the lift coefficient is at its maximum and then begins to decrease.

- **Maximum Thickness:** The thickest part of the wing expressed as a percentage of chord thickness [99].

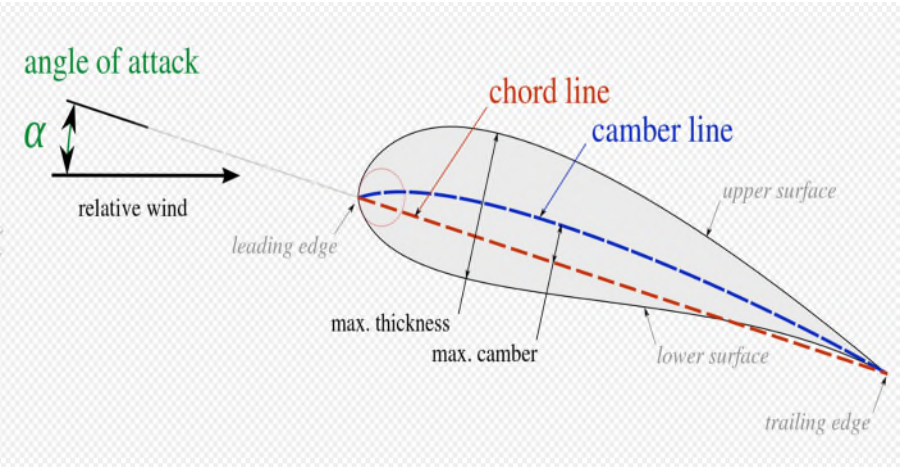

Figure 81: Aerofoil Terminology [99]

Appendix C: Pressure Coefficient

The pressure coefficient of the lower surface is always higher than the pressure coefficient on the upper surface. On the lower surface, it remains almost constant, whereas the upper surface gradually rises from the leading edge to the trailing edge of the aerofoil, as shown in figure 82. Since the pressure coefficient on the lower surface of the aerofoil was greater than the pressure coefficient of the incoming flow stream, the aerofoil was forced upward, normal to the incoming flow stream. The CFD plot shows a similar trend to that of the experimental data plot [100].

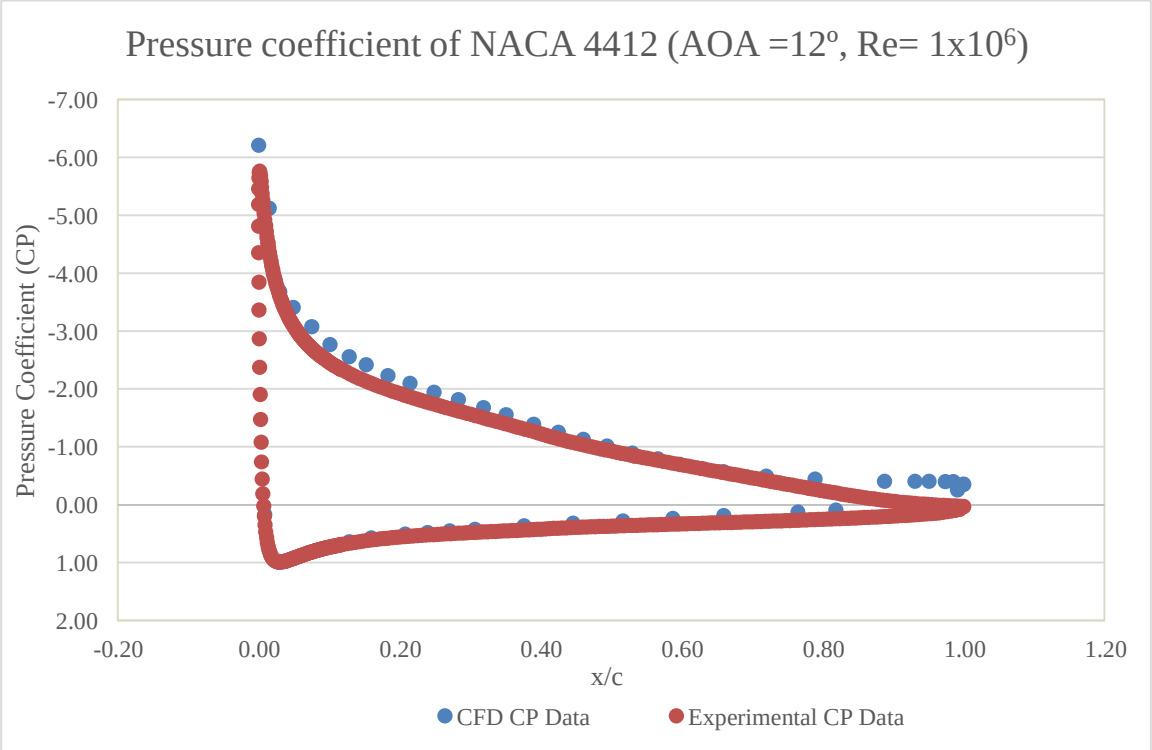

Figure 82: NACA 4412 Pressure coefficient graph of 12 degrees AOA at 30m/s